

AD-A126 845

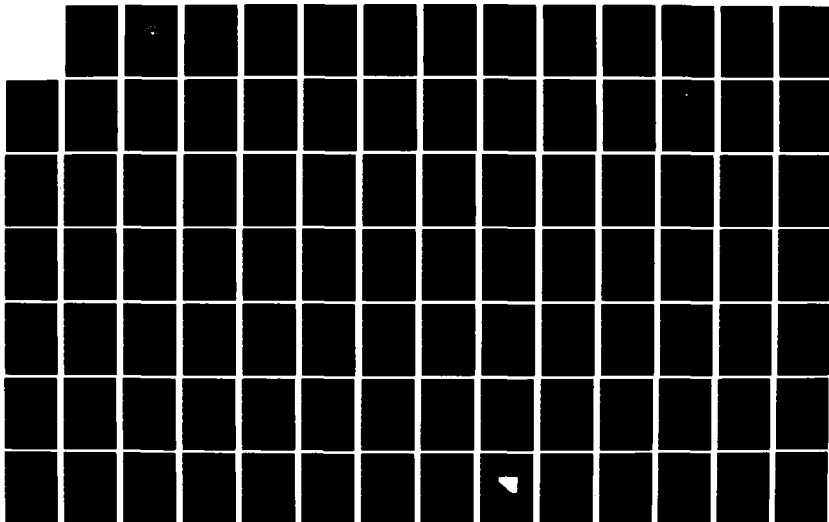
ESTIMATION AND MAPPING OF CLOUDS AND RAINFALL AREAS
WITH AN INTERACTIVE COMPUTER(U) NAVAL POSTGRADUATE
SCHOOL MONTEREY CA C A NELSON DEC 82

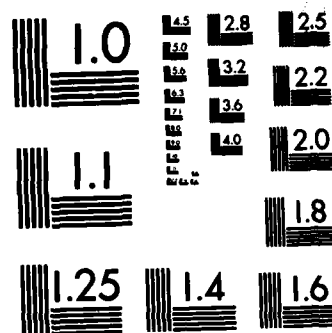
1/2

UNCLASSIFIED

F/G 9/2

NL





MICROCOPY RESOLUTION TEST CHART
NATIONAL BUREAU OF STANDARDS-1963-A

AD A 126845

DTIC FILE COPY

②

NAVAL POSTGRADUATE SCHOOL

Monterey, California



THESIS

ESTIMATION AND MAPPING OF CLOUD AND RAINFALL AREAS
WITH AN INTERACTIVE COMPUTER

by

Cynthia Ann Nelson

December 1982

Thesis Advisor :

C.H. Wash

Approved for public release; distribution unlimited.

DTIC
ELECTE
APR 15 1983
S D E

REPORT DOCUMENTATION PAGE		READ INSTRUCTIONS BEFORE COMPLETING FORM
1. REPORT NUMBER	2. GOVT ACCESSION NO. AD-A126845	3. RECIPIENT'S CATALOG NUMBER
4. TITLE (and Subtitle) Estimation and Mapping of Cloud and Rainfall Areas With an Interactive Computer		5. TYPE OF REPORT & PERIOD COVERED Master's Thesis; December 1982
7. AUTHOR(s) Cynthia Ann Nelson		6. PERFORMING ORG. REPORT NUMBER
9. PERFORMING ORGANIZATION NAME AND ADDRESS Naval Postgraduate School Monterey, California 93940		8. CONTRACT OR GRANT NUMBER(s)
11. CONTROLLING OFFICE NAME AND ADDRESS Naval Postgraduate School Monterey, California 93940		10. PROGRAM ELEMENT, PROJECT, TASK AREA & WORK UNIT NUMBERS
14. MONITORING AGENCY NAME & ADDRESS (if different from Controlling Office)		12. REPORT DATE December 1982
		13. NUMBER OF PAGES 136
		15. SECURITY CLASS. (of this report) Unclassified
		15a. DECLASSIFICATION/DOWNGRADING SCHEDULE
16. DISTRIBUTION STATEMENT (of this Report) Approved for public release; distribution unlimited.		
17. DISTRIBUTION STATEMENT (of the abstract entered in Block 20, if different from Report)		
18. SUPPLEMENTARY NOTES		
19. KEY WORDS (Continue on reverse side if necessary and identify by block number) Automated Nephanalysis Precipitation Intensity Satellite Processing Cloud Top Height Interactive Computer Cloud Top Temperature Cloud Typing Cloud Amount		
20. ABSTRACT (Continue on reverse side if necessary and identify by block number) An automated cloud analysis program was developed and established on the SPADS computer system at the Naval Environmental Prediction Research Facility (NEPRF). The program evaluates GOES visual and infrared imagery simultaneously. The analysis method produces information on cloud types, cloud amount, precipitation intensity, and cloud top height and temperature through use of threshold tests of radiance, texture, and temperature. A review of current work on the evaluation of satellite information by		

(20. ABSTRACT Continued)

computer and by manual analysis is included.

A Maritime region 460 X 460 nautical miles in size was selected for test analysis. The satellite imagery was manually evaluated and compared to the computer generated output. Reasonably good patterns of cloud types, precipitation and cloud amount were produced by the computer, although further testing and verification is needed.

Accession For	
NTIS GRA&I	<input checked="" type="checkbox"/>
DTIC TAB	<input type="checkbox"/>
Unannounced	<input type="checkbox"/>
Justification	
By	
Distribution/	
Availability Codes	
Dist	Avail and/or Special
A	



Approved for public release; distribution unlimited

Estimation and Mapping of Cloud and Rainfall Areas
with an Interactive Computer

by

Cynthia Ann Nelson
Lieutenant, United States Navy
B.S., Indiana University, 1971
M.S., State University of New York, Geneseo, 1972

Submitted in partial fulfillment of the
requirements for the degree of

MASTER OF SCIENCE IN METEOROLOGY AND OCEANOGRAPHY

from the

NAVAL POSTGRADUATE SCHOOL
December 1982

Author:

Cynthia Ann Nelson

Approved by:

Curtis P. Ward
Thesis Advisor

James P. Munk
Second Reader

Robert J. Munk
Chairman, Department of Meteorology

William M. Colles
Dean of Science and Engineering

ABSTRACT

→ An automated cloud analysis program was developed and established on the SPADS ^(Satellite Data Processing and Display System) computer system at the Naval Environmental Prediction Research Facility (NEPRF). The program evaluates ^(Geostationary Operational Environmental Satellite) GOES visual and infrared satellite imagery simultaneously. The analysis method produces information on cloud types, cloud amount, precipitation intensity, and cloud top height and temperature through use of threshold tests of radiance, texture, and temperature. A review of current work on the evaluation of satellite information by computer and by manual analysis is included.

A maritime region 460 X 460 nautical miles in size was selected for test analysis. The satellite imagery was manually evaluated and compared to the computer generated output. Reasonably good patterns of cloud types, precipitation and cloud amount were produced by the computer, although further testing and verification is needed.

↑

TABLE OF CONTENTS

I.	INTRODUCTION	14
II.	CLOUD CLASSIFICATION TECHNIQUES	17
A.	INTRODUCTION	17
B.	CLOUD TYPING	18
1.	Cloud Index	19
2.	Three-Dimensional Nephanalysis (3DNEPH)	26
3.	Spectral Cross-correlation	31
4.	Two-dimensional Histogram	37
C.	CLOUD HEIGHT AND AMOUNT	40
1.	Cloud Index	40
2.	Three-Dimensional Nephanalysis (3DNEPH)	43
3.	Bispectral	52
D.	PRECIPITATION	58
1.	Cloud Index	61
2.	Life History	63
3.	Bispectral	66
4.	Cloud Model	73
III.	SPADS CLOUD MODEL DESCRIPTION	78
A.	INTRODUCTION	78
B.	CLOUD TYPING	78
C.	CLOUD TOP TEMPERATURES	83
D.	PRECIPITATION INTENSITY	87

E.	FLOW CHART	88
IV.	THE MODEL TEST AND RESULTS	93
A.	INTRODUCTION	93
B.	DATA	93
C.	TEST PROCEDURES	94
D.	RESULTS	101
1.	Run 1	102
a.	Cloud Typing	102
b.	Precipitation	103
c.	Cloud Amount	105
d.	Cloud Top Temperatures and Heights .	105
e.	Cloud Texture (Standard Deviation) .	110
2.	Run 2	112
a.	Cloud Typing	112
b.	Cloud Amount	112
c.	Cloud Top Temperature and Height . .	112
V.	SUMMARY	116
A.	DISCUSSION	116
1.	Accomplishments	116
2.	Problems	117
3.	Recomendations	118
	LIST OF REFERENCES	120

APPENDIX A. SPADS CLCUD MODEL COMPUTER PROGRAM	122
INITIAL DISTRIBUTION LIST	135

LIST OF FIGURES

Figure 1.	Manual Nephanalysis Flow Chart	21
Figure 2.	VIS Key to be Used in Manual Nephanalysis . .	22
Figure 3.	IR Key to be Used in Manual Nephanalysis . .	23
Figure 4.	Flow Chart for Automated Objective Nephanalysis	26
Figure 5.	Graph of Vector Dispersion Technique. (a) represents	27
Figure 6.	Decision Space Using Two Texture Measurements, Standard Deviation and Vector Dispersion . .	29
Figure 7.	The Decision Space of the 3DNEPH Program. . .	32
Figure 8.	An Additional Decision Space of the 3DNEPH Program.	32
Figure 9.	Parallelepipedon Classification of Cloud Types by IR and VIS Digital Counts	34
Figure 10.	Two Dimensional Decision Space for Typing Clouds	35
Figure 11.	Two-dimensional Histogram Plot of Albedo Versus Temperature	39
Figure 12.	Ideal Histograms of Cloud Types	39
Figure 13.	Detailed Nephanalysis of an IR Satellite Picture	42
Figure 14.	The 3DNEPH Program Flow Chart for the VIS Satellite Processor	45
Figure 15.	Graph Used by 3DNEPH VIS Processor to Make a Cloud or No-cloud Decision	46
Figure 16.	3DNEPH Flow Chart of the IR Satellite Data Processor Program	48
Figure 17.	An IR Bias Correction Curve Used by the 3DNEPH Computer Program	49

Figure 18.	An Example of an IR Frequency Distribution at a Single point	50
Figure 19.	A Cloud Cutoff Curve Used to Limit Low Clouds Over Bright Areas	51
Figure 20.	The Relationship Between Albedo and Blackbody Radiation	59
Figure 21.	The relationship between albedo and IR emissivity	60
Figure 22.	Flow Chart for a Recent Version of the Manual Nephanalysis	62
Figure 23.	Regression Diagram Used to "Float" Rainfall Estimates	64
Figure 24.	VIS (top) and IR (bottom) Satellite Data Cloud (Ac) and Echo (Ae) Area Relationships .	65
Figure 25.	The Griffith/Woodley Technique Flow Chart Used for GATE	67
Figure 26.	Frequency Distribution of VIS and IR Data Pairs for the No-rain Case	71
Figure 27.	Frequency Distribution of IR and VIS Data Pairs for the Rain Case	71
Figure 28.	Probability of Rain in Percent	72
Figure 29.	The Resulting Satellite Rain Map	72
Figure 30.	Rain Rates Averaged Over Cloud Areas Measured on IR Images	75
Figure 31.	Two Dimensional Cloud Typing Graph Using GOES IR and VIS Satellite Digital Data	81
Figure 32.	Graph of SPADS Cloud Model Precipitation Intensities.	90
Figure 33.	The SPADS Cloud Model Generalized Flow Chart.	92
Figure 34.	Infrared Satellite Image, Center Point is at Latitude 44°N, Longitude 141°W	96

Figure 35.	Infrared Satellite Image Selected from Fig. 34	97
Figure 36.	Visual Satellite Image with the Same Area and Center Fig. 35	98
Figure 37.	Manual Cloud Analysis of Fig. 35 and 36 . .	100
Figure 38.	Cloud Types as Analyzed by the SPADS Cloud Model in Run 1	104
Figure 39.	Qualitative Precipitation Intensity from Run 1 of the SPADS Cloud Model	106
Figure 40.	Cloud Top Temperature (K) from Run 1 of the SPADS Cloud Model.	108
Figure 41.	Cloud Top Heights (mb) from Run 1 of the SPADS Cloud Model.	109
Figure 42.	Cloud Texture (standard deviation of the digital counts) from Run 1 of the SPADS Cloud Model	111
Figure 43.	Cloud Types as Analyzed by the SPADS Cloud Model, Run 2	113
Figure 44.	Cloud Amount (in 100ths) from Run 2 of the SPADS Cloud	114

LIST OF TABLES

TABLE I.	Algorithms for the Objective Nephanalysis . .	28
TABLE II.	3DNEPH Statistical Equations for the Average Grayshade and Variance	31
TABLE III.	Cloud Classification to be Used with Fig. 10.	36
TABLE IV.	Algorithms for Cloud Top Temperature and Cloud Amount	55
TABLE V.	The Errors in Cloud Amount (with Hs = 5%) and in Cloud Temperature	56
TABLE VI.	Comparison of cirrus correction and VTPR results	60
TABLE VII.	Empirically Derived Rainfall Probabilities and Intensities from Satellite Pictures . . .	63
TABLE VIII.	Applications of the Griffith/Woodley Technique	68
TABLE IX.	The Error Statistics from the Applications Listed in Table VIII	68
TABLE X.	Threshold Values Describing Precipitation Intensity Levels as Applied in Fig. 10 . . .	74
TABLE XI.	Estimated and Observed Precipitation and Stability Adjustment Factors	76
TABLE XII.	SPADS Cloud Model's Cloud Types, Least Squares Fit Equations, and Standard Deviation Values (SIG _i)	84
TABLE XIII.	SPADS Cloud Model Precipitation Intensity Categories	91
TABLE XIV.	FNOC Temperature Profile for 1200 GMT, November 9, 1982 at latitude 44°N, longitude 141°W	99

TABLE XV. Definitions of Symbols Used in Fig. 37 . . 101

TABLE XVI. Standard Deviation (SIGI) Values Used for
Run 1 and 2 101

ACKNOWLEDGMENTS

I would like to take this opportunity to express my sincere gratitude to Dr. Carlye H. Wash for his time , guidance, and patience. I also wish to express my deepest thanks to my husband, LCDR Craig S. Nelson (NOAA), for his guidance in editing and computer programming. Without both of these gentlemen's expert assistance and encouragement, this thesis would not have been completed. Additionally, I would like to thank Dr. James Mueller for his guidance in editing the manuscript.

Special thanks is given to the staff at the Naval Environmental Prediction Research Facility for their assistance in modifying computer code. Especially, I would like to thank Ms. Linda Rodriguez, Supervisor of Computer Operations, for her patience and persistence in data collection. Also, I wish to thank Mr. Lang Chou for his assistance. Ms. Kyong H. Lee also deserves thanks for her assistance in preparation of the graphics.

Finally, I would like to express my deepest appreciation to Craig and Becky for their support, encouragement and understanding.

I. INTRODUCTION

The personnel operating Naval ships, aircraft and weapon systems need near real-time subsynoptic and mesoscale maritime weather information to operate effectively and safely. Current conventional observational data (from surface, rawinsonde, and aircraft observations) do not adequately cover the maritime region or provide for mesoscale analysis of weather phenomena. Specifically needed are detection and monitoring of any adverse weather conditions. This need pertains to phenomena ranging from mesoscale (10-100 km) to synoptic scale (100-1000 km) which are poorly resolved by conventional observations. Satellite observations can solve this problem through the acquisition of global high density data which are available regardless of local influences of geography, surface conditions, or local politics.

Another problem is the need to provide an analyzed product to the user in a short (1-3 hour) time frame. Manual analysis of satellite data is time consuming and tedious, and it does not provide the information in a real-time fashion. An interactive computer system, on the other hand, can collect, analyze, and produce the required products within the required time limit.

This research effort concentrated on the development of techniques to specify cloud types, cloud amount, cloud height, and precipitation intensity with an emphasis on the maritime regions from satellite images. Information on critical weather parameters such as low visibilities, ceilings, precipitation presence, and intensity can be derived from these cloud characteristics. This work uses Geostationary Operational Environmental Satellite (GOES) Visual-Infrared Spin Scanned Radiometer (VISSR) digital satellite data from visual and infrared channels which have a one-half hour temporal and 0.5 to 4 nautical miles (n mi.) spatial resolution. The data were received and processed at the Naval Environmental Prediction Research Facility (NEPRF) in Monterey, California using the Satellite Data Processing and Display System (SPADS). This interactive computer system was developed at NEPRF for use by the operational Navy to give real-time information about weather phenomena. One system is now operational at the Naval Eastern Oceanography Center (NEOC) at Norfolk, Virginia.

The objective of this thesis is to establish and evaluate a computer program on the SPADS to analyze GOES images to derive cloud types, precipitation intensity, cloud height, and cloud amounts. To accomplish this, an in-depth

study of previous research and analysis techniques was initiated, and, from this study, useful algorithms and techniques were gleaned. These algorithms and techniques were combined to produce the desired computer program. Preliminary tests of the computer program were completed on the SPADS system at NEPRF.

Chapter II begins with a review of previous studies. This includes discussions of four techniques of cloud type classification: (1) cloud index (Harris and Barrett, 1975, 1978), (2) spectral analysis (Liljas, 1981a, 1981b), (3) 3-dimensional nephanalysis (Fye, 1978), and (4) two-dimensional histogram (Platt, 1981). A discussion of the techniques for determining cloud height and cloud amounts used by Reynolds and Vonder Haar (1977) and others, and of procedures for identifying precipitation areas and their associated intensities is also covered. Chapter III describes the set of algorithms selected for implementation on SPADS. Chapter IV presents an outline of the test procedures used and reports the results of these tests (including detected problem areas). Chapter V summarizes the research efforts and problems and provides suggestions for future changes and additional research.

II. CLOUD CLASSIFICATION TECHNIQUES

A. INTRODUCTION

Satellite visual (VIS) and infrared (IR) imagery can provide a wide variety of weather information, including estimates of cloud type, cloud height, cloud amount, and precipitation intensity. In fact, a satellite nephanalysis can produce a spatial summary of these important cloud features. An analyst examines the visual brightness to derive estimates of thickness of the cloud and the cloud texture to differentiate between cumulus and stratus type clouds. By using the IR imagery, cloud top heights can be estimated; the brighter the cloud image, the colder; therefore, the higher it is. With combined visual and infrared, one has a greater ability to pick out the cloud types and, furthermore, to estimate the probability of precipitation.

One of the main problems encountered in the 1960's and early 1970's was the lack of standardization of rules governing the nephanalysis construction. Each country, and sometimes each analyst, has used subjective methods for producing cloud analyses. Some of the specific problems arising from lack of standardization, as discussed in Harris and

Barrett (1975), have been: no minimum size is established as reference for inclusion or exclusion from analysis; cirrus clouds are rarely identified in middle latitudes; significant cloud areas are subjectively delineated at the discretion of the analyst; only four cloud categories are assigned (which consisted of unequal percents of areas); and no standard nephanalysis construction rules have been published.

With these problems in mind, Harris and Barrett (1975, 1978), Barrett and Martin (1981), Platt (1981), Fye and Logan (1977) and Liljas (1981a), to name a few, have been working toward the goal of producing a recommended standard for objective nephanalysis of satellite VIS and IR imagery through manual and computer analysis. The following sections review these representative research efforts in this endeavor. The discussions are divided into three areas of concern to this thesis; cloud typing, cloud height and amounts, and precipitation.

B. CLOUD TYPING

Basically four distinct approaches to effective cloud typing have been proposed in the literature. They are: (1) cloud index (Harris and Barrett, 1975, 1978; Barrett and

Harris,1977), (2) the U.S. Air Force 3DNEPH program (Fye and Logan,1977; Fye,1978), (3) spectral cross-correlation (Liljas,1981a, 1981b), and (4) two-dimensional histogram (Platt,1981). These methods are reviewed below.

1. Cloud Index

Harris and Barrett (1975) recognized the need for standardization and for increased information content. As a result, they developed a cloud indexing system which provided specific guidance and rules for analyzing satellite visual imagery manually. For clarity and understanding, they proposed the analysis be composed of three separate layers of analyses; two descriptive and one interpretive. Fig. 1 is the flow chart of the stages in the construction of this nephanalysis. The authors developed a key (Fig. 2) which includes details on the following cloud features: (1) percent of cloud, (2) cloud type (e.g. cumulus), (3) cloud structure (including size, shape, and pattern), and (4) height of cloud tops. The key also gives interpretive weather phenomena.

The first analysis layer contains information on geography and cloud cover. The cloud cover is divided into five equal percent categories with a minimum size reported of a 2 1/2 degree square.

The second descriptive layer includes cloud type and cloud structure. They are classified in the following order: major cloud systems, definite boundaries and finally indefinite boundaries. The analyst uses cloud brightness and texture to discern six types of clouds (see Fig. 2).

The final analysis layer produced is the interpretation of the cloud features using the information from the first two layers. The types of cloud features considered important are displayed in Fig. 2. All three analysis layers combined were designed to be completed within one hour by a skilled analyst.

Barrett and Harris (1977) extended this procedure to include infrared imagery for the purpose of supplementing the visual analysis. This added capabilities for nighttime and high latitude analyses. They mention three possibilities for analyzing IR imagery: (1) use longstanding internationally accepted codes and symbols, (2) follow the visual procedures previously outlined, or (3) use a new procedure which recognizes and represents the special properties of the IR images. The first two methods would be directly comparable to the visual analysis. The third approach would offer additional information to allow identification of

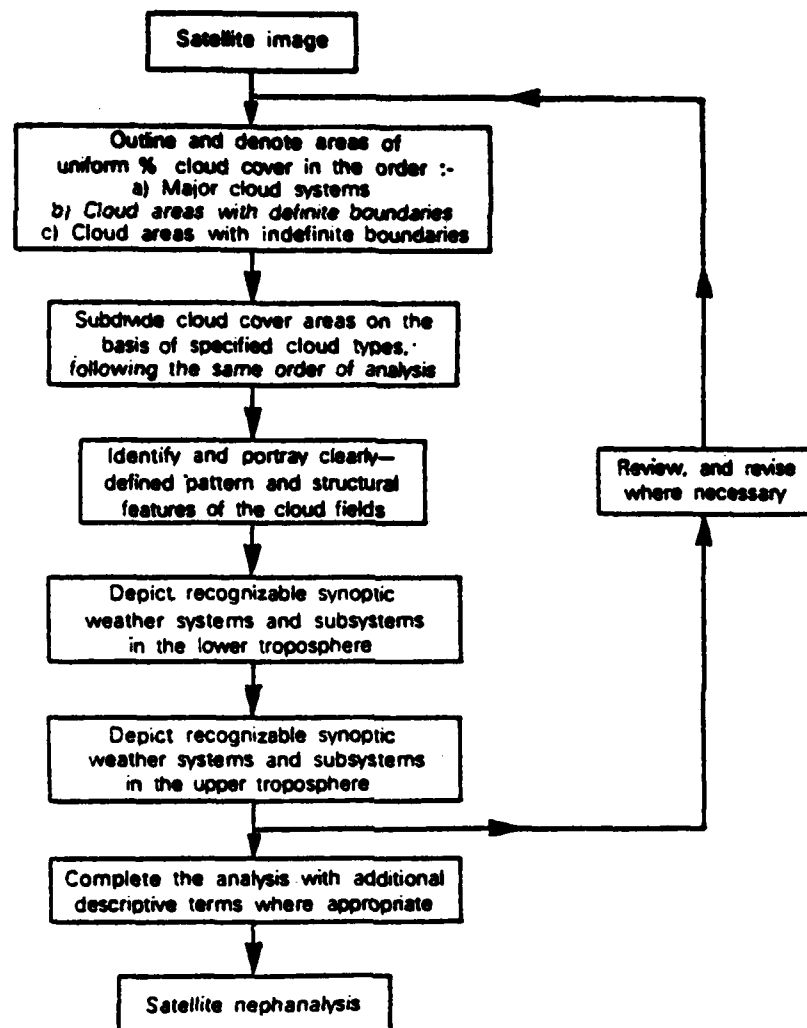


Figure 1. Manual Nephanalysis Flow Chart (from Harris and Barrett, 1975).

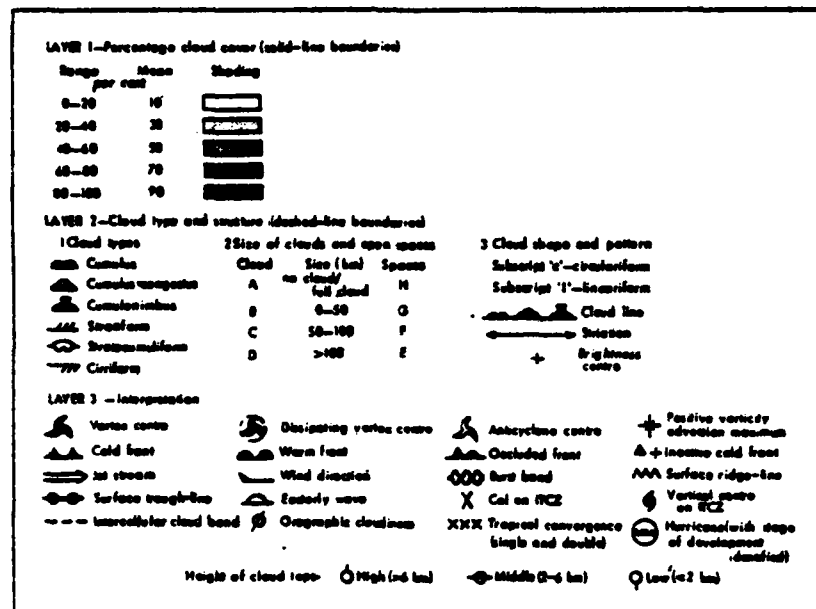


Figure 2. VIS Key to be Used in Manual Nephanalysis (from Harris and Barrett, 1975).

cloud height through cloud brightness evaluation and a more specific identification of cloud texture.

The IR analysis technique identifies the following cloud features (see Fig. 3): (1) percent of cloud cover (same as VIS technique), (2) brightness of cloud, (3) cloud texture, and (4) size of clouds (same as VIS), plus interpretive categories with eighteen of them the same as VIS (heights and three cloud descriptions are not included). Barrett and Harris (1977) felt that any of the three methods could produce an analysis in a single hour if done by a trained analyst.

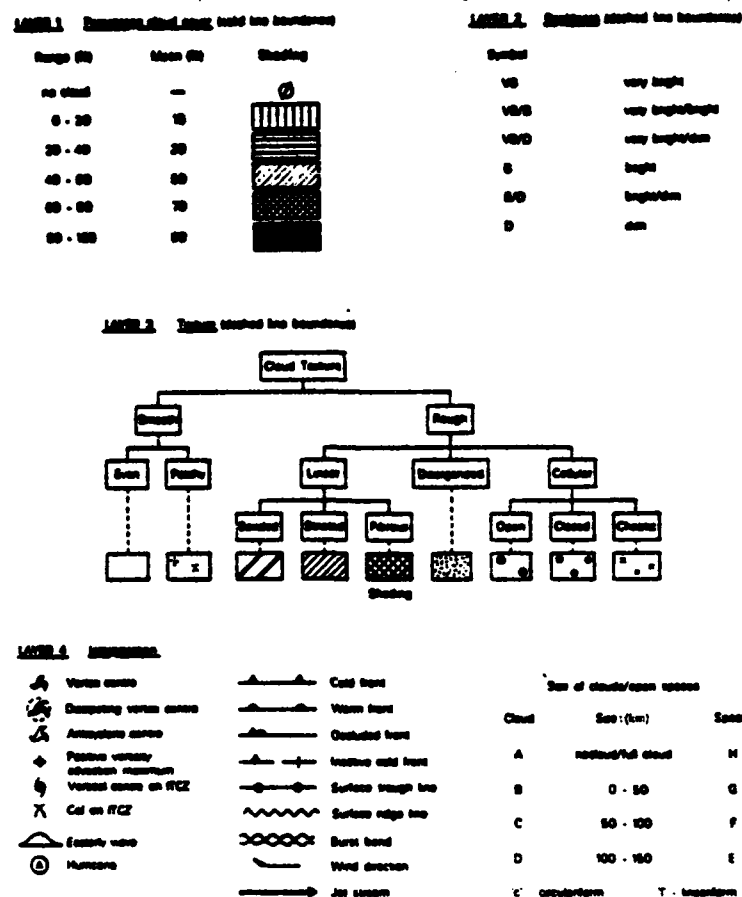


Figure 3. IR Key to be Used in Manual Nephanalysis (from Barrett and Harris, 1977).

After establishing a manual method for both VIS and IR satellite nephanalysis, Harris and Barrett(1978) developed an automated objective nephanalysis through a cloud recognition scheme. They used an approach which examined quantitative cloud brightness and texture within a small area of the whole picture. The flow chart in Fig. 4 outlines their approach. Cloud brightness was assessed in each

subarray by summing the brightness counts of only cloud pixels and then dividing by the number of cloud pixels (Eq. 1 and 2, Table I). Cloud amount was calculated in each subarray by summing the number of cloud pixels and then dividing by the total number of pixels per subarray. This number was then multiplied by 100 to obtain a percent of cloud cover (Eq. 3 in Table I).

Their assessments of cloud texture used statistical, instead of structural, measures of local variation in image density. One measure they employed was the standard deviation of each subarray (5x5 pixel array) of density values, as calculated with Eq. 4 (Table I).

Their other criterion was vector dispersion, which required that the density values be treated as a set of adjacent triangular planes. The dispersion in three dimensions of the normal to these planes gave another measure of texture. Fig. 5 shows a graphical representation of this method. Eq. 5, 6, and 7 in Table I were used to calculate these estimates of texture.

Once all these values were calculated, boundaries between cloud types had to be established. Three categories were selected; (1) sheet or layered clouds (stratiform),

(2) cellular/tower clouds (cumulus) and (3) broken/mottled cloud (stratocumulus or mixed) (Harris and Barrett, 1978). A three-dimensional decision space was set up using two texture measurements and one brightness value. Those areas that had a brightness above the threshold were included in further analyses; those below were not. Fig. 6 shows the decision space based on the two texture measurements. The discriminant lines were developed through analysis of a training set of Defense Military Satellite Program (DMSP) sample brightness and texture measurements of each cloud category.

In assessing the accuracy of this method, Harris and Barrett (1978) found several problem areas. For example, towering cumulus in post frontal areas (especially) were not identified because of the field of view (FOV) size and snow areas were included as clouds. But the overall accuracy was still good with a greater than 72% correct classification. Harris and Barrett (1978) felt that several procedures would improve the output of the model. Among these were increasing the resolution of the data by decreasing the size of scanning spot, decreasing the subarray size, normalizing the image brightness for changes in sun viewing angle, and

increasing the texture parameters to permit identification of more cloud classes.

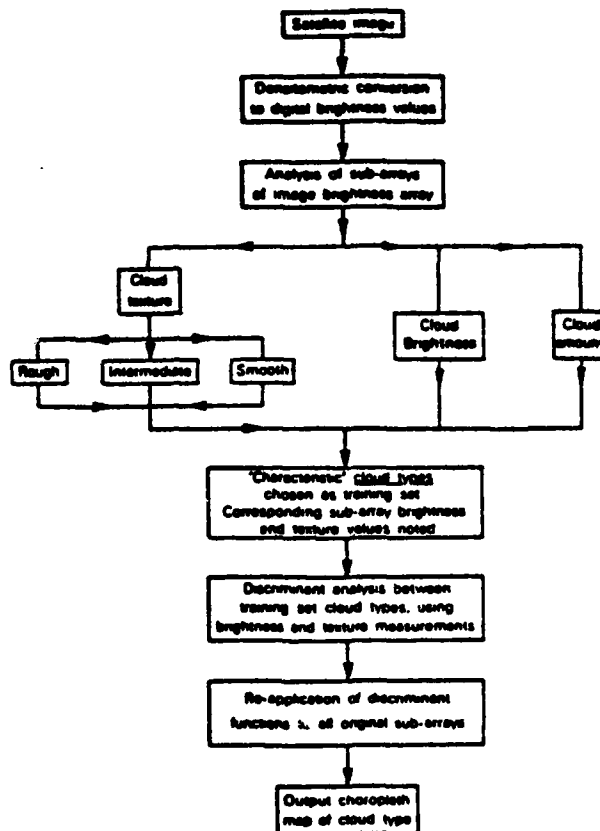


Figure 4. Flow Chart for Automated Objective Nephanalysis (from Barrett and Harris, 1978).

2. Three-Dimensional Nephanalysis (3DNEPH)

The United States (U.S.) Air Force developed an automated three-dimensional cloud analysis called the "3DNEPH model". It uses satellite imagery from the DMSP and TIROS-N satellite series together with conventional in situ

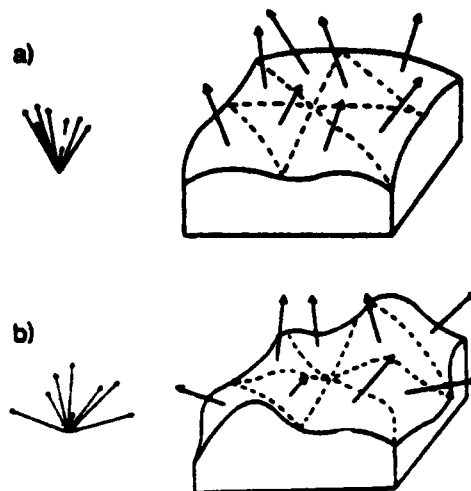


Figure 5. Graph of Vector Dispersion Technique. (a) represents a smooth surface (stratiform clouds) and (b) represents a rough surface (cumulus clouds). Normal vectors for each case are included to the left of the diagrams (from Harris and Barrett, 1978).

data from aircraft, surface, and upper air observations. A cloud analysis is produced in a real-time fashion regardless of ice, snow, desert, or other geographical anomalies (Fye and Logan, 1977). The satellites provide high density data over the entire world, thus permitting a global analysis of clouds. The horizontal resolution of the output is 25 n mi.

The data array has a pixel resolution of 3 n mi. The satellite data are first formatted, rectified, mapped, and stored on a computer storage device before running the 3DNEPH program. The rectification corrects for the effects

TABLE I

Algorithms for the Objective Nephanalysis (from Harris and Barrett, 1978)

$$(1) \quad B = \frac{\sum_{i=1}^N \sum_{j=1}^N X_{ij} \delta_{ij}}{M}$$

B = cloud brightness

N = number of rows/columns

 X_{ij} = density at each point
$$\delta_{ij} = \text{step function} \begin{cases} = 1 & X_{ij} \geq \dagger \\ = 0 & X_{ij} < \dagger \end{cases}$$
 \dagger = density threshold defining the boundary between cloud/no cloud

$$(2) \quad M = \sum_{i=1}^N \sum_{j=1}^N \delta_{ij}$$

$$(3) \quad A = 100 (M/N^2)$$

A = average cloud amount

$$(4) \quad \sigma = \left[\sum_{i=1}^N \sum_{j=1}^N (X_{ij} - \bar{X})^2 / N^2 - 1 \right]^{1/2}$$

 σ = standard deviation of each subarray density values \bar{X} = mean of the subarray density values

$$(5) \quad l = \frac{1}{R} \sum l_i$$

 (l_i, m_i, n_i) = direction cosines of the i th plane

$$m = \frac{1}{R} \sum m_i$$

 (l, m, n) = max likelihood of true polar vector (λ, μ, γ)

$$n = \frac{1}{R} \sum n_i$$

$$(6) \quad R^2 = (\sum l_i)^2 + (\sum m_i)^2 + (\sum n_i)^2$$

$$(7) \quad k = \frac{N-1}{N-R}$$

N = the sample size

k = estimate of the texture of the surface

where:

k=1 = smooth surface (stratiform)

k=0 = uneven surface (cellular cumulus)

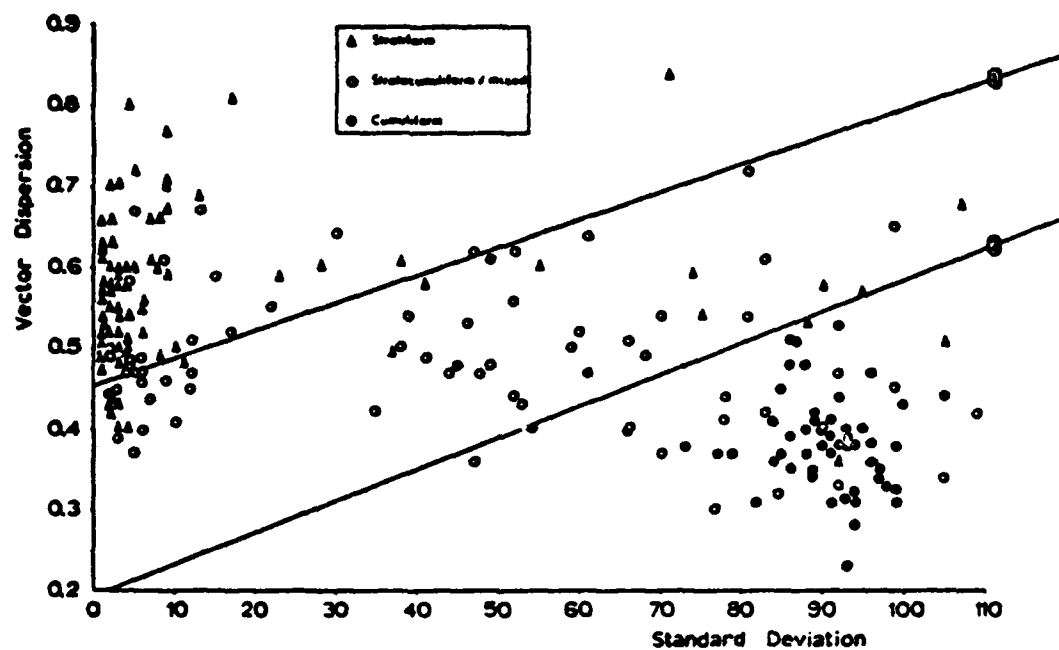


Figure 6. Decision Space Using Two Texture Measurements, Standard Deviation and Vector Dispersion. Line (1) separates stratiform from mixed stratocumulus and line (2) separates mixed from cumulus clouds (from Harris and Barrett, 1978).

of limb darkening before storage. Limb darkening is the effect of a decrease in brightness as the edges or "limbs" of the earth scan are approached. The data are not normalized with respect to light (VIS) or longwave radiation (IR) (Fye and Logan, 1977). Each visual and infrared pixel is represented by a single grayshade value in the range from 1 to 63. In the visual, 1 is dark and 63 is white. Infrared pixels represent temperature in degrees Kelvin (K) from 210 K for a value of 1 to 310 K for 63; each grayshade represents a 1.6 degree change (Fye, 1978). The preliminary processor calculates the average grayshade value per 25 n mi. square using Eq. 1 (Table II) and then uses this to get the variability within the square using Eq. 2 (Table II) (Fye, 1978). Both these calculations are performed separately for IR and VIS images. The VIS and IR grayshade values and variabilities are used to identify the various cloud types. Fig. 7 and 8 represent the cloud typing algorithms used. They were constructed empirically by comparing many grayshades and variabilities to corresponding satellite imagery and surface data (Fye, 1978). The operational algorithms were derived from the figure and then modified to obtain optimum results. One obvious problem with electing

to use the model (given the available documentation) is the lack of graduated values on the axes of these two figures. Only relative values of warm/cold or light/dark are included in the report. Also lacking in the Fye(1978) report are any details of the current algorithms used for cloud typing.

TABLE II
3DNEPH Statistical Equations for the Average Grayshade and Variance (from Fye, 1978)

(1) $\bar{G} = 1/N \sum_{i=1}^N G_i$, $G>0, N>0$	\bar{G} = average gray shade G_i = individual 3 nmi area grid gray shade N = total number of G_i per 25 nmi grid space
(2) $V = 1/N \sum_{i=1}^N G_i - \bar{G} $, $G>0, N>0$	V = variability within the 25 nmi grid space

3. Spectral Cross-correlation

The third classification method is the spectral cross-correlation method developed by Erik Liljas (1981a) for use on an interactive computer. Liljas used TIROS-N and National Oceanic and Atmospheric Administration (NOAA) 6 satellite data from three spectral channels; channel 1 (VIS), channel 2 (near-IR) and channel 4 (IR). During the summer time, different cloud types, land and water surfaces

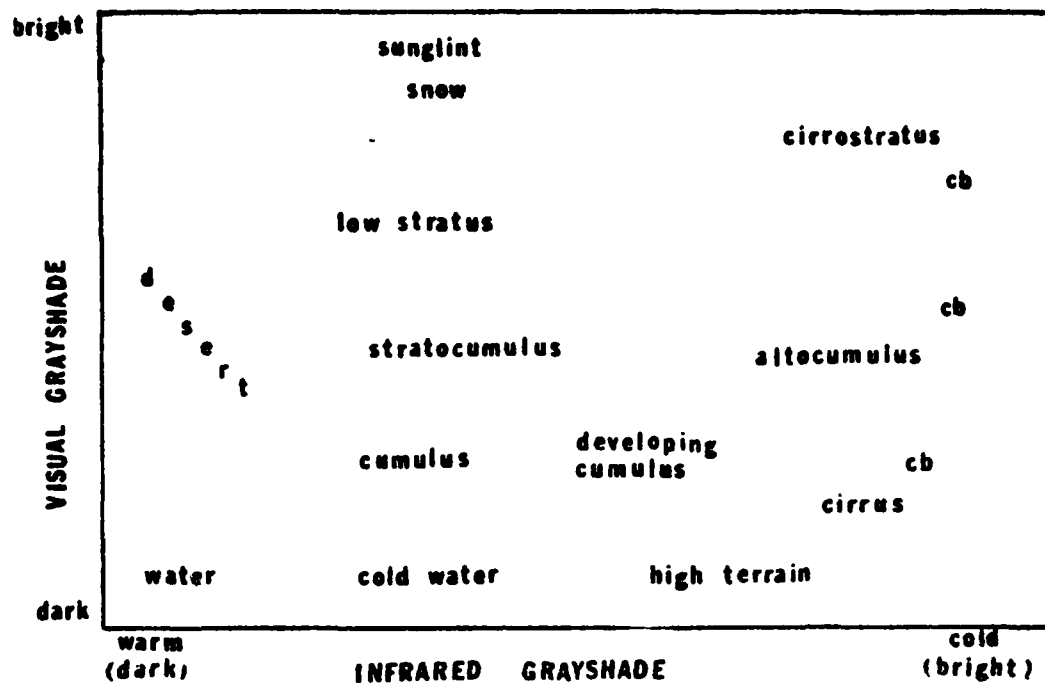


Figure 7. The Decision Space of the 3DNEPH Program. IR and VIS grayshades are used to determine the cloud type (from Fye, 1978).

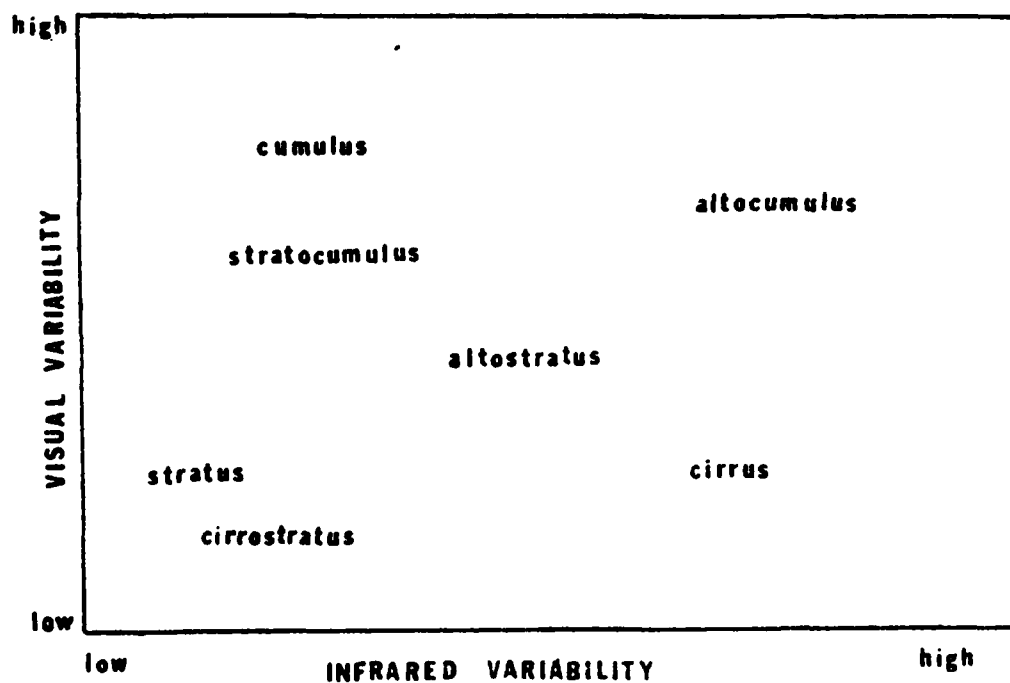


Figure 8. An Additional Decision Space of the 3DNEPH Program. IR and VIS variabilities are used for cloud typing (from Fye, 1978).

were analyzed to detect their unique spectral signatures. The results were used to build a three dimensional parallelepipedon classification, Fig. 9.

Two satellite types were used for the test of the model; polar orbiting (TIROS-N and NOAA-6) and geostationary (Meteosat). The satellite data used for the test of the model were geometrically corrected, but they did not need to be normalized because the mid-day pass of the satellite was used (approximate sun elevation of 45 degrees). Normalization corrects for the radiance variation caused by the sun location (elevation). Also the amount of data was reduced from 1,024 digital levels to 256 levels, which was considered adequate resolution for the study. Data from channel 2 were primarily used to separate land and water areas. Channels 1 and 4 were the principal cloud type identifiers.

Comparison of the spectral cross-correlation method with synoptic observations showed that the computer method gave correct indication of cloud types, and also an improved cloud division. As shown in Fig. 10 (see Table III for symbol definitions of cloud types), several cloud types are in the same boxes; Liljas recommends the use of texture

observation to discern between these cloud types. This was done manually and entered interactively. Liljas (1981b) also reports that good information on cloud structure of weather systems can be retrieved. He recommends the use of multiple parallelepipedon classifications, each classification associated with a different sun elevation instead of normalization of the reflected imagery.

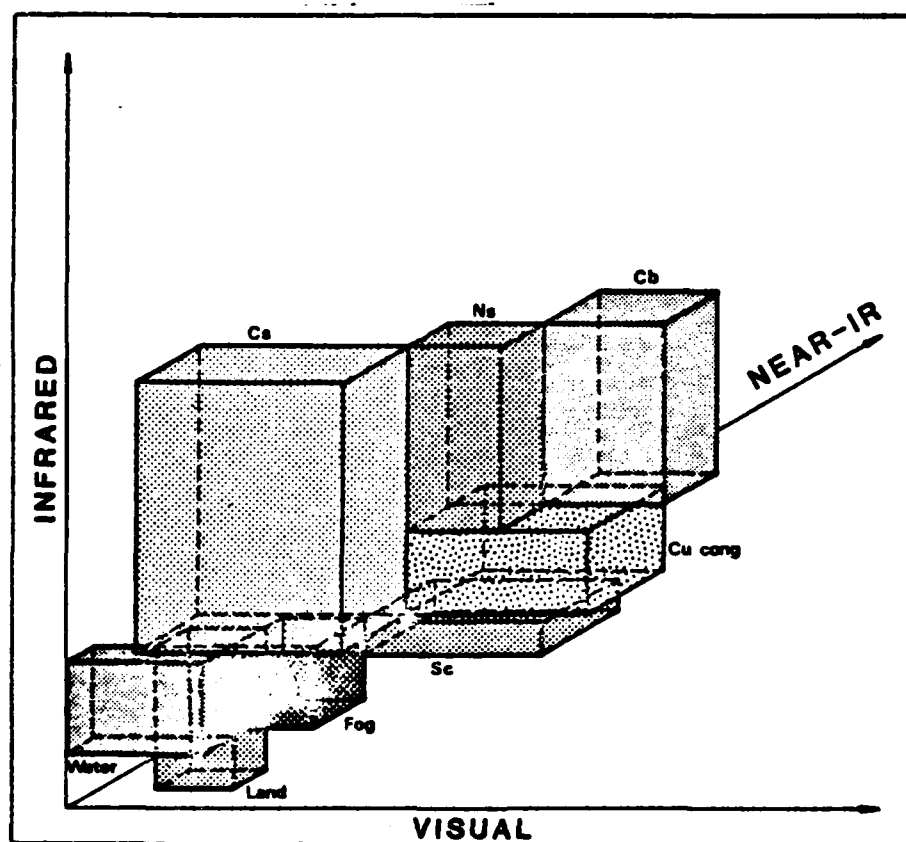


Figure 9. Parallelepipedon Classification of Cloud Types by IR and VIS Digital Counts (from Liljas, 1981a).

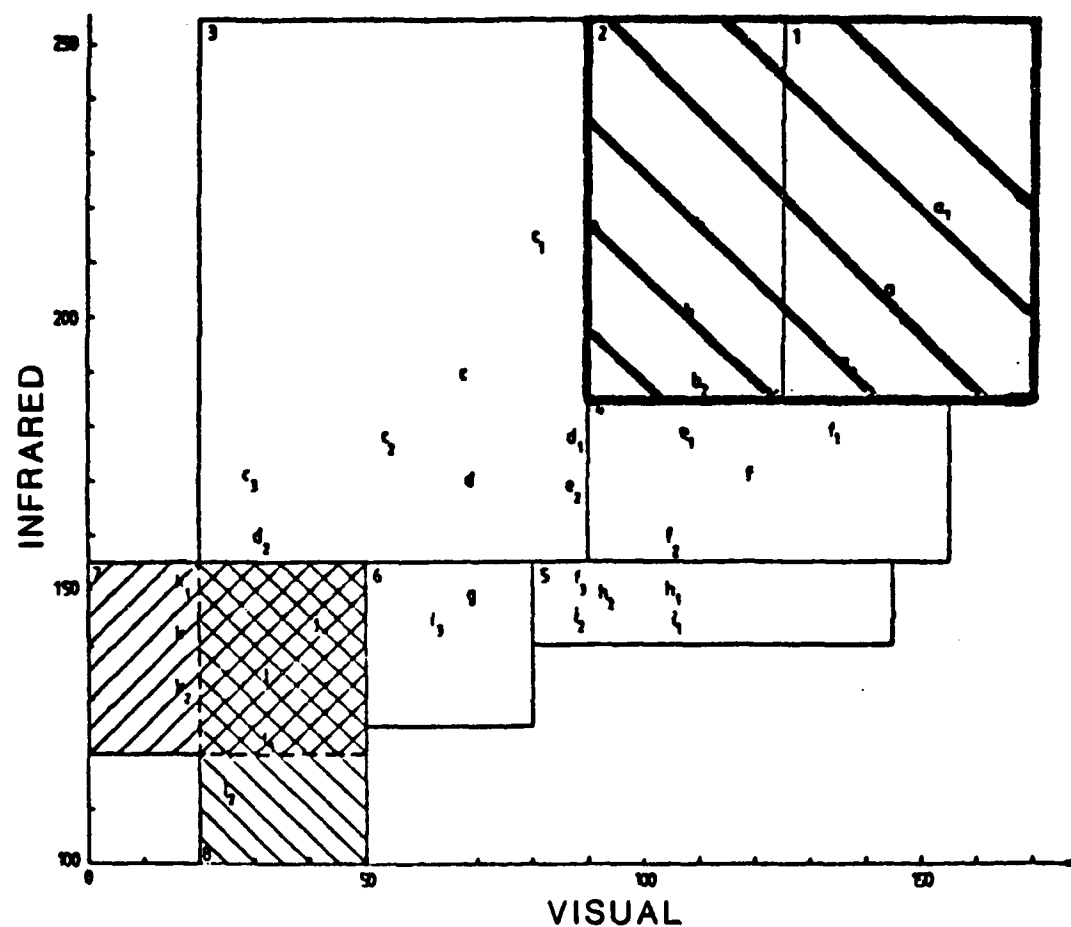


Figure 10. Two Dimensional Decision Space for Typing Clouds (Table III defines the symbols for clouds) and Precipitation Intensity. It is represented by the area with dark diagonal lines (see Table I for the mathematical description of the intensity areas) (from Liljas, 1981a).

TABLE III
Cloud Classification to be Used with Fig. 10 (from Liljas, 1981a)

Main and Cloud Types:

1. Cumulonimbus	a a ₁ Storm cloud with high top a ₂ Squall cloud with scattered showers
2. Nimbostratus	b b ₁ Large vertical thickness b ₂ Rather low topside
3. Cirrostratus	c c ₁ Dense cirrostratus c ₂ Cirrus c ₃ Thin cirrus over water d ₁ Dense altostratus d ₂ Thin altostratus over water e ₂ Thin altostratus
4. Cumulus congestus	f e ₁ Dense altocumulus f ₁ Large piled up cumulus f ₂ Rather small and flat cumulus
5. Stratocumulus	h h ₁ Dense stratocumulus h ₂ Ordinary f ₃ Slightly piled up cumulus with clear areas in between i ₁ Very dense haze/stratus i ₂ Dense haze/stratus
6. Haze/Stratus	i i ₃ Ordinary haze/stratus g Cumulus humilis
7. Land	l j Haze over water l ₁ Planting season spring or autumn l ₂ Warm green season
8. Water	k k ₁ Cold k ₂ Warm

4. Two-dimensional Histogram

Another spectral method was developed by Platt (1981) using a two-dimensional histogram representation of cloud types. He selected satellite data with typical cloud fields to develop a histogram decision space representation of cloud types. Platt concentrated on evaluating cloud systems instead of isolated clouds and therefore his results are biased toward synoptic features.

The measured visual radiances were compared with the direct radiance from the solar disk on the satellite to produce a calculated isotropic albedo per 2.5 km. These albedoes are expressed as a fraction from 0 to 1. The infrared radiances are converted to blackbody brightness temperatures ranging from 193.3 to 301.5 K. A histogram was then constructed by sorting these data into 988 different bins of temperature and albedo. Each area evaluated was approximately 500 X 500 km, with roughly 40,000 values per histogram. The total bin counts were plotted on a two-dimensional grid and then contoured by same bin count (see Fig. 11). This cloud histogram representation could then be used to classify cloud types by matching plots of the satellite data. After classifying various types of

clouds, Fig. 12 was compiled to give an idealized depiction of the location of cloud types by albedo and temperature.

Platt (1981) discussed several factors that tend to reduce the usefulness of Fig. 12. One cloud problem arises when there are either breaks in a cloud deck, or partially filled field of view (FOV) in the satellite view area. Additionally, clouds of the same optical depth, but exhibiting breaks will have a different albedo measurement than an unbroken cloud of the same optical depth (stratocumulus in Fig. 14 demonstrates this). Another factor that changes the albedo and temperature values is variation in cloud top height. All of these factors create ambiguity in determining the cloud type, amount, optical depth, and cloud top temperature. As a result, the author recommends that additional work should be done with these results before using the two-dimensional histogram approach to identify clouds.

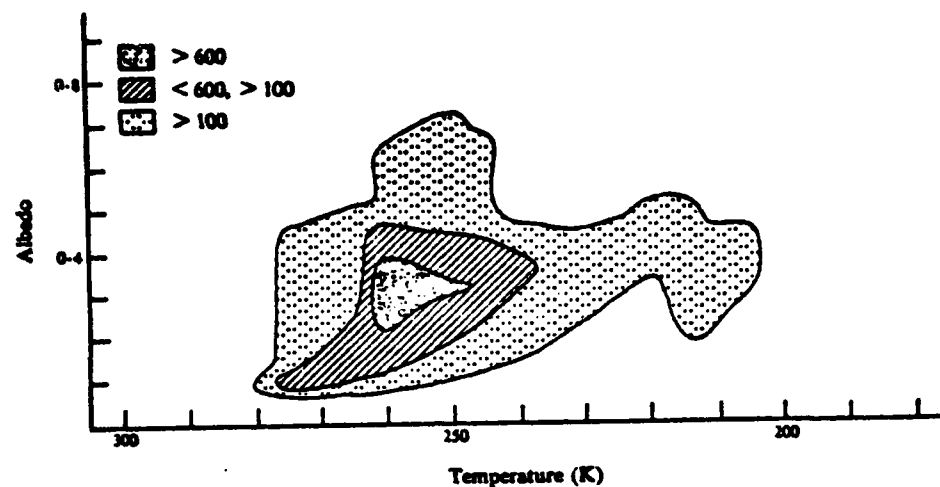


Figure 11. Two-dimensional Histogram Plot of Albedo Versus Temperature (representing cumulus clouds) (from Platt, 1981).

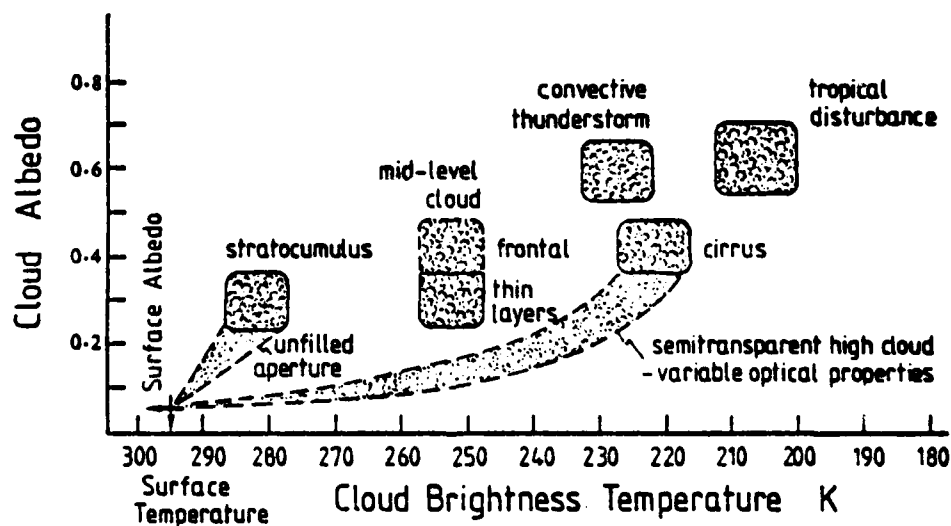


Figure 12. Ideal Histograms of Cloud Types (from Platt, 1981).

C. CLOUD HEIGHT AND AMOUNT

Three methods of deriving cloud height and amount have been proposed in current research. Two methods are an extension of those reviewed in the cloud typing section; cloud index (Harris and Barrett, 1975, 1978; Barrett and Harris, 1977) and the U.S. Air Force 3DNEPH (Pye and Logan, 1977; Pye, 1978). In addition, a new bispectral technique (Reynolds and Vonder Haar, 1977) is discussed.

1. Cloud Index

In two separate studies, Barrett and Harris (1977; Harris and Barrett, 1975) developed a recommended standard cloud height and amount determination procedure for manual analysis of satellite visual and infrared images. The visual method combined brightness, cloud type, and synoptic situation to determine qualitative estimates of cloud height (low, middle, or high level). Later, they developed a system for identifying cloud levels through the degree of cloud brightness in the IR image. IR cloud information specifically lends itself to this task since the radiation temperature of the cloud is a function of the cloud-top altitude (Barrett and Harris, 1977).

Some problems arose with cirrus and cloud elements smaller than the field of view. In this instance, satellite measured temperatures can appear warmer than actual cloud temperature, because the satellite is also receiving the radiation temperature of the surface or lower clouds. This problem can be minimized by using IR and VIS together to identify cirrus clouds and by using higher resolution data, e.g., data from the Advanced Very High Resolution Radiometer (AVHRR) on NOAA satellites.

Fig. 3 is the key for the IR nephanalysis and includes the cloud brightness steps and Fig. 13 is an example of how these are applied. This analysis can be interpreted in terms of qualitative heights, low (dim) to high (very bright) (Barrett and Harris, 1977). Cloud amount determination categories are also delineated in Fig. 2 for VIS and Fig. 3 for IR. It is done in categories of size of cloud element, e.g., 100-150 km. Harris and Barrett's (1978) objective automated method does not specifically address cloud height, but does calculate an average cloud amount for each subarray size (5x5 pixels) using Eq. 3 (Table I).

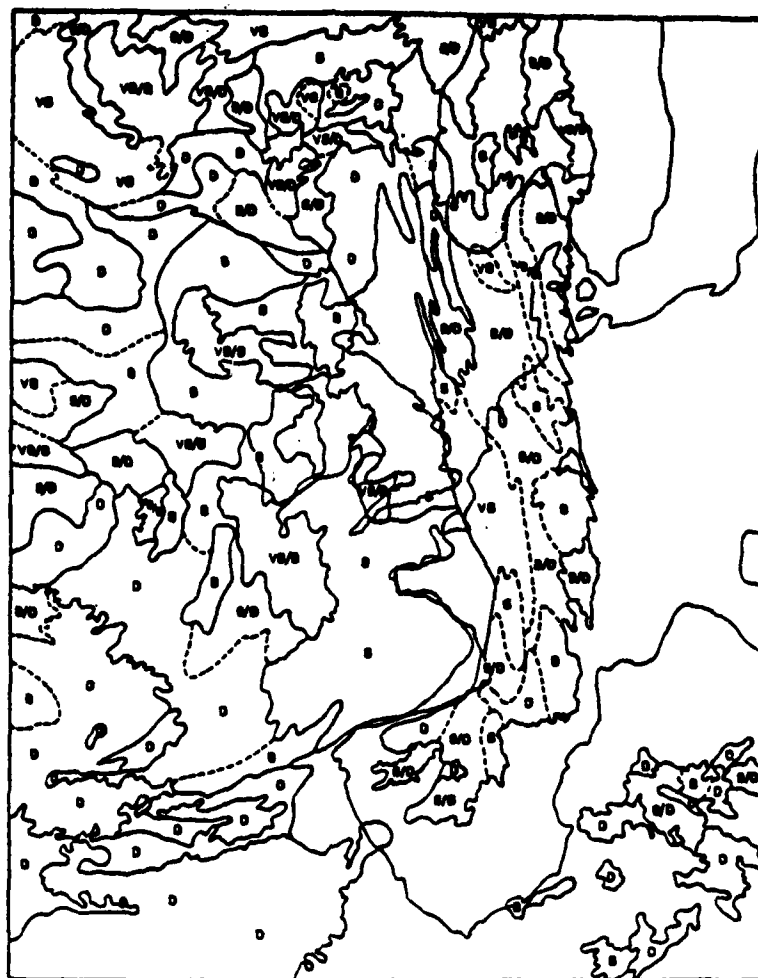


Figure 13. Detailed Nephanalysis of an IR Satellite Picture. The symbols are defined in Fig. 3 (from Barrett and Harris, 1977).

2. Three-Dimensional Nephanalysis (3DNEPH)

The U.S. Air Force 3DNEPH program's main objective is to produce information on cloud height and cloud amount. It uses a standard vertical grid of 15 layers, which range from the surface to 100 millibars (mb). The IR image is used to determine height and element cloud amounts, and the visual and infrared are used together to determine total cloud amount. This information is then combined with surface, aircraft and rawinsonde data to determine the final cloud height and cloud amount analyses.

The preliminary processor, as described in the cloud type section, prepares the satellite data for height determination. In addition, it sorts, screens, and combines the conventional data received from the Air Force's global weather data base to produce a vertical and horizontal 3DNEPH gridded layered format.

Next, the satellite data goes to the visual and infrared processors. The VIS processor steps are outlined in Fig. 14. Each pixel grayshade is directly compared to a grayshade (background/surface brightness) specified for each 25 n mi. square. This value represents a clear sky earth radiance for each square. The difference between each pixel

grayshade and the background brightness is used in Fig. 15 to decide if there is a cloud or not. The curve in Fig. 15 represents the brightness threshold for clouds; any variability greater than this is a cloud area. This curve incorporates the background brightness and the varying brightness associated with different surfaces (e.g., desert). The total number of cloud decisions divided by the total number of available pixels represents the amount of cloud cover in the square.

The infrared processor incorporates a slightly different analysis method. The major steps of the processor are included in Fig. 16 as a flow chart. The first step is to construct a frequency distribution of the 64 raw grayshades for each 25 n mi. area to detect significant modes (maxima) of 6 or more grayshades or 12 or more adjacent shades. If more than 2 modes are identified, the modes are combined on the basis of relative amplitude (strongest modes are retained) and the differences between modes. If there is no apparent mode, then the processor defaults to a cloud threshold temperature determined from appropriate surface temperatures. Before any cloud decision is made, a correction is applied to the IR temperatures to compensate for

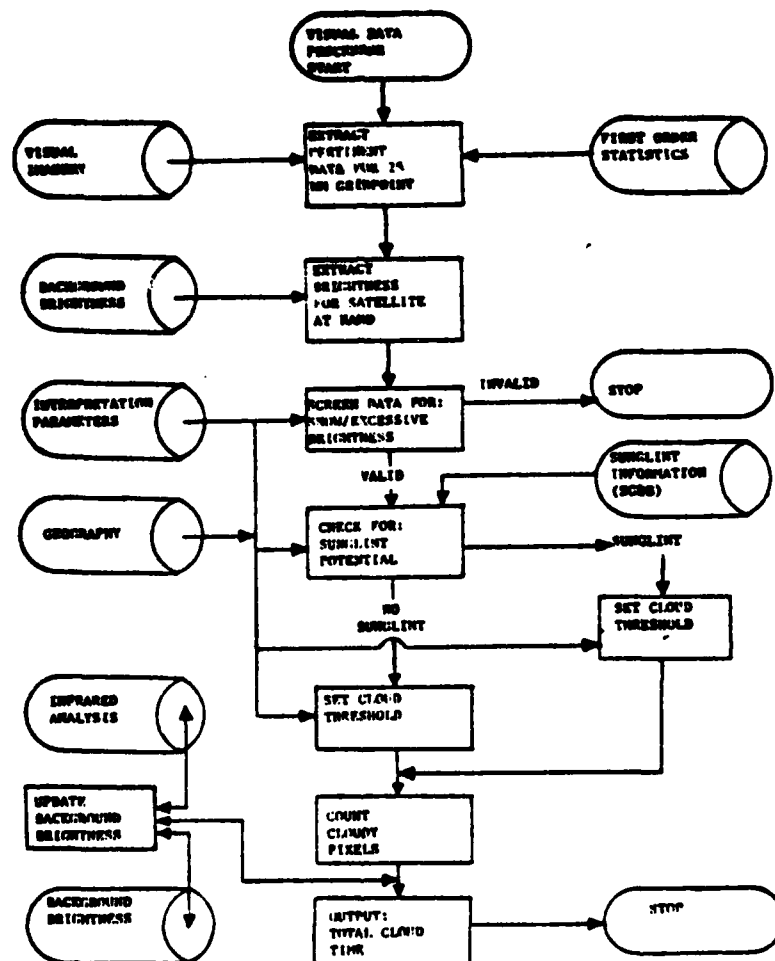


Figure 14. The 3DNEPH Program Flow Chart for the VIS Satellite Processor (from Fye, 1978).

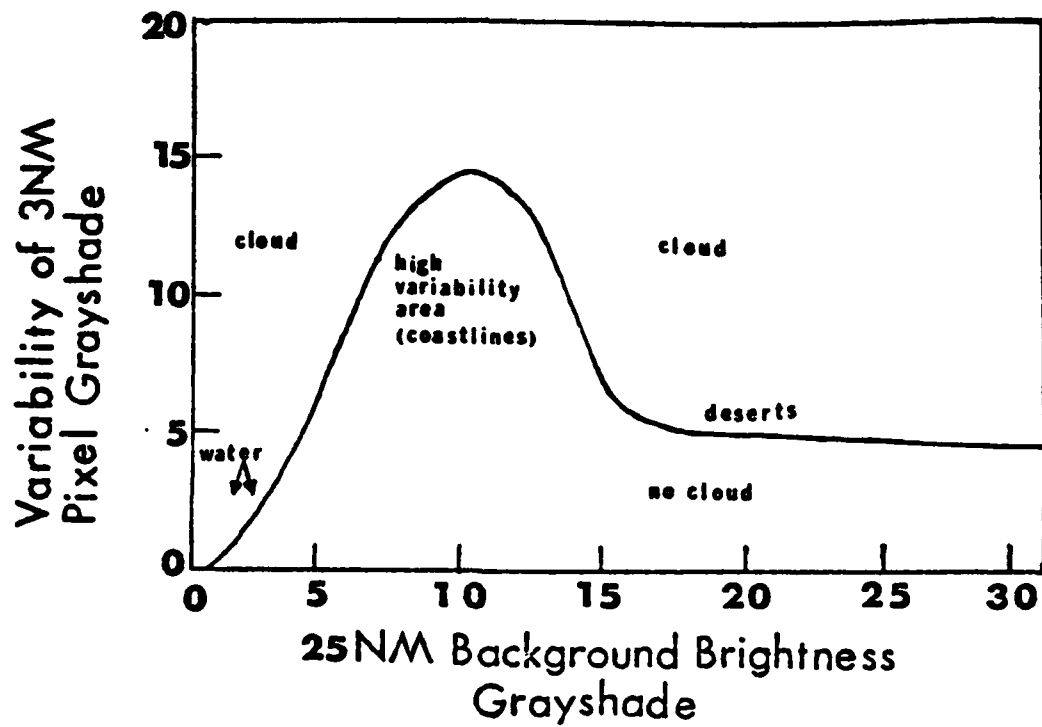


Figure 15. Graph Used by 3DNEPH VIS Processor to Make a Cloud or No-Cloud Decision (from Pye, 1978).

atmospheric absorption and other effects such as zenith and local angle which create biases in the IR data. Fig. 17 is an example of a curve used to derive bias correction for a particular satellite. The actual bias correction is the difference between the best fit curve and the diagonal line of perfect correlation. Next a representative temperature is selected for each mode (usually the coldest in the mode) and these data are compared to a gridded, conventionally derived surface temperature data base to make a cloud/no cloud decision. Fig. 18 graphically represents this decision process. The final cloud decision is made by using Fig. 19. This compensates for irregularities in the surface temperature data base which limit the reliability of the cloud/no cloud decision. The cloud amount is determined by the number of pixels in the cloudy mode (Fye and Logan, 1977). Additionally, the IR processor determines the cloud height by comparing the coldest temperature in the cloudy mode to a real-time upper air data base.

Other processors include the conventional data processor, the data integration processor, and the manual data processor. The conventional data processor takes the surface, aircraft, and upper air reports and produces a

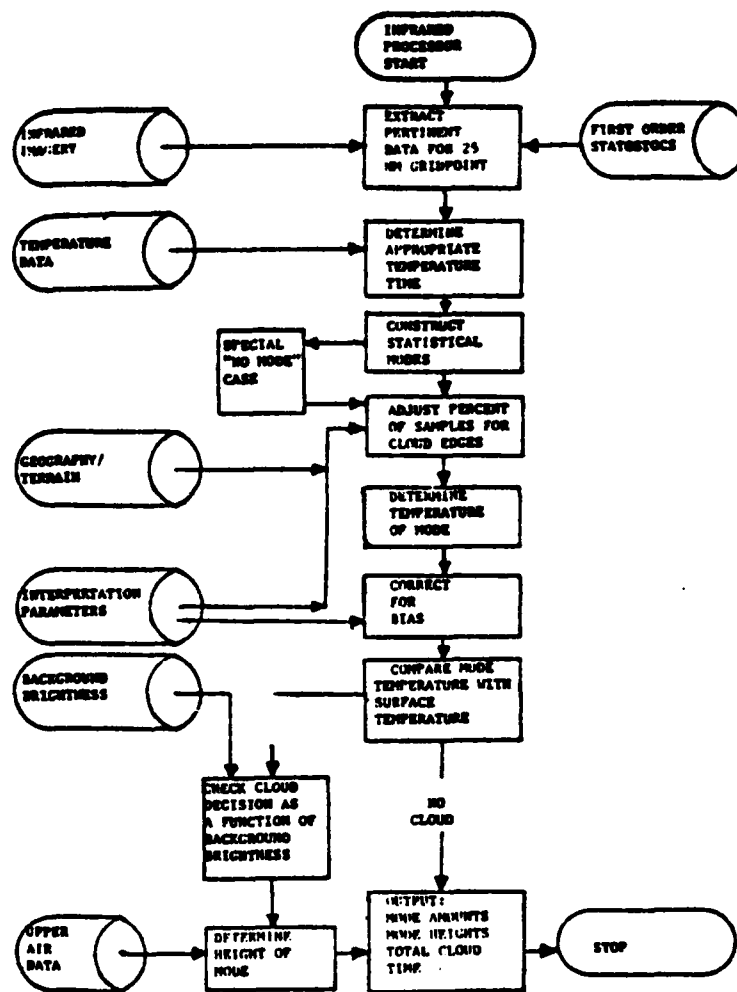


Figure 16. 3DNEPH Flow Chart of the IR Satellite Data Processor Program (from Pye, 1978).

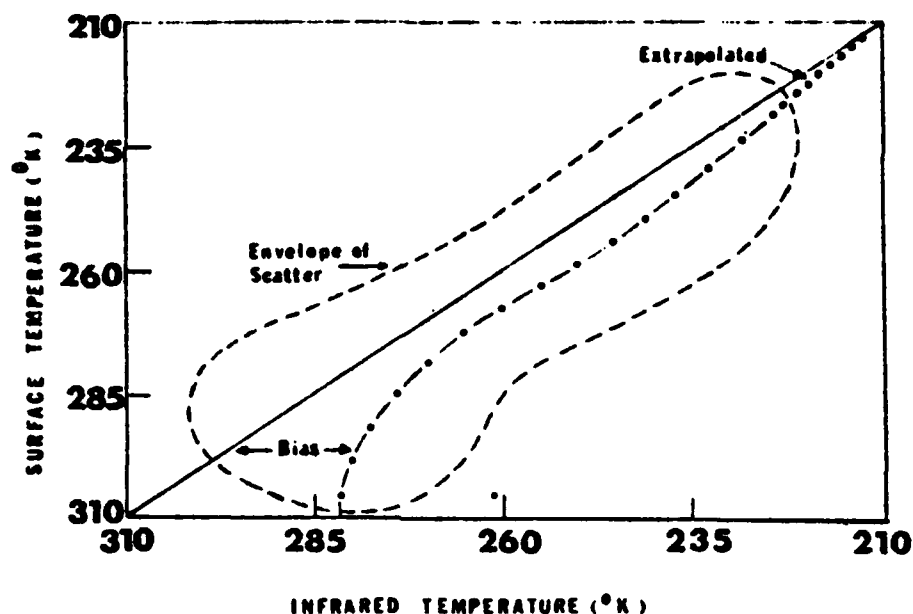


Figure 17. An IR Bias Correction Curve Used by the 3DNEPH Computer Program (from Fye, 1978).

horizontally gridded, eight mesh data base of cloud information for 15 vertical layers. These layers of data and the output of VIS and IR processors are merged by the data integration processor. The processor also performs meteorological consistency checks. The cloud amounts, heights, and types from VIS and IR data are converted to specific cloud layer amounts and heights. Conflicts are also resolved by this processor by checking age of data, greatest cloud cover, layer amount, and cloud top height. Next, the

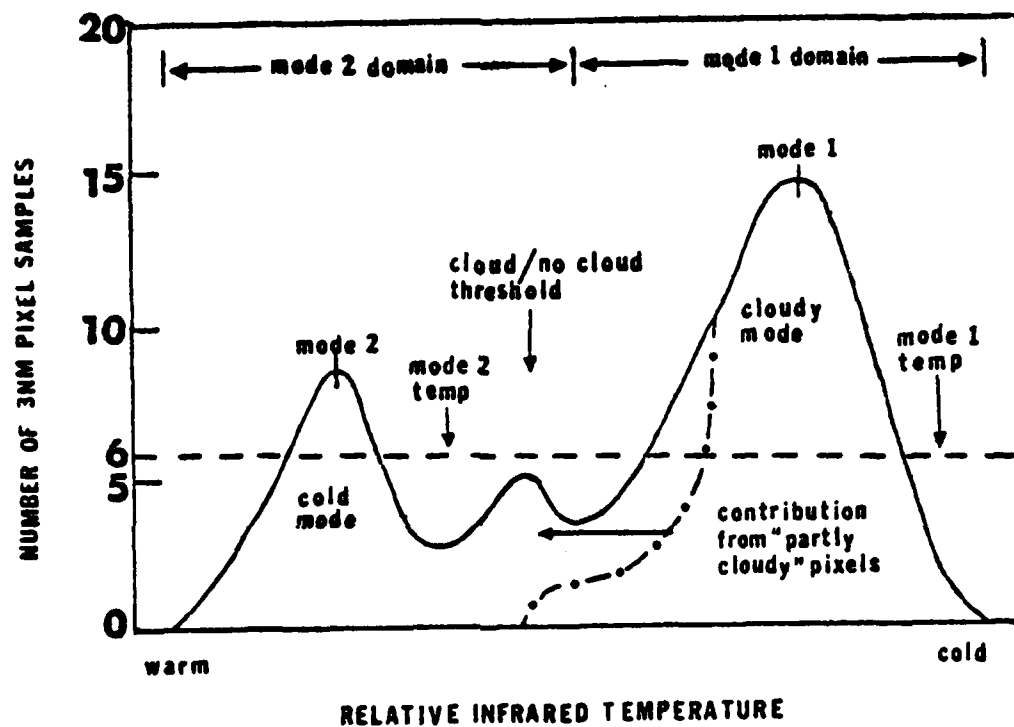


Figure 18. An Example of an IR Frequency Distribution at a Single Point (from Pyle, 1978).

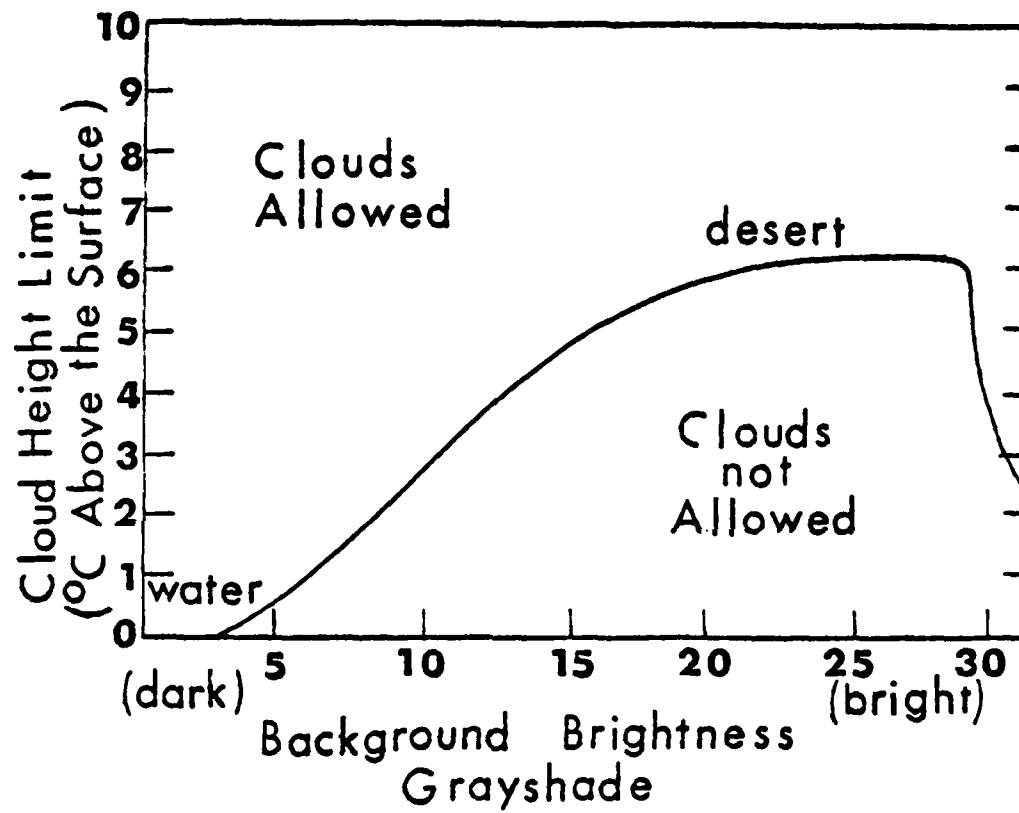


Figure 19. A Cloud Cutoff Curve Used to Limit Low Clouds Over Bright Areas (from Fye, 1978).

satellite and conventional data are compared and integrated with a continuity field to complete the cloud analysis (Fye, 1978). The continuity field is the previous or latest 3DNEPH analysis which fills in missing data and parameters.

The analyst next enters manually encoded input to alter the 3DNEPH data base as necessary. The manual data processor takes this information and incorporates it into the overall data base. This provides an avenue for quality control, correction of errors and improvement of the overall analysis.

3. Bispectral

A bispectral method for determining cloud height and amount was developed by Reynolds and Vonder Haar (1977). Visual and infrared data were each analyzed quantitatively over an array of scan spots. This analysis yielded cloud amount and cloud top temperature, from which cloud height was derived by comparison to a nearby vertical temperature sounding.

The method was based on manipulation and solution of two equations (Eq. 1 and 2, Table IV). These equations are basically comprised of adjustments for the fraction of cloud-covered and clear-sky areas in a single field of view and for backbody emissivity of the clouds. One was the

satellite visual radiance equation (Equation 1, Table IV) and the other was the satellite infrared radiance equation (Eq. 2, Table IV). The equations related the amount of cloud (A_{cld} in tenths) to either cloud albedo ($\rho_{cld} \times H_s$) in the visual or cloud radiances (N_{cld}) in the infrared channels (note that A_{cld} plus the amount of clear area, A_{clr} in tenths, equaled 1.0). The IR radiance equation also accounted for the effect of emissivity (ϵ) of clouds on cloud and surface (N_{clr}) radiances. In both equations, A_{clr} was replaced by $1.0 - A_{cld}$. The rest of the terms in the equations except two (A_{cld} and N_{cld}) were available. Average values of the cloud and surface albedoes were known and more exact values can be obtained in practice "from the actual array of satellite measurements" (Reynolds and Vonder Haar, 1977). Measured surface temperatures were converted to IR radiances and used for the surface radiance. The emissivity was initially assumed to be 0.9 for all clouds. This left only the two unknowns to be determined. Eq. 1 (Table IV) was then solved for A_{cld} and Eq. 2 (Table IV) for N_{cld} radiance which resulted in Eq. 3 and 4 (Table IV). The A_{cld} value was derived first from the visual satellite data. Next, A_{cld} was used with the simultaneously received IR data to obtain

the cloud radiance value. The resulting radiance was then converted to cloud top temperature via Plancks' equation. The final step was to use a local upper air sounding and the cloud temperature to obtain the cloud top height.

Reynolds and Vonder Haar (1977) performed an uncertainty analysis on this technique to determine on what the uncertainty (Δ) of the cloud amount (A_{cld}) and cloud temperature (ΔN_{cld}) measurements depend and how large an uncertainty (Δ) is allowable. It was shown that ΔA_{cld} depends on the magnitude and precision of H_s , M_s , ρ_{cld} , and ρ_{clr} , where ΔH_s and $\Delta \rho_{clr}$ will be less than 10% of the error. N_{cld} depends on the magnitude and uncertainty of M_l , A_{cld} , N_{clr} and ϵ .

The two quantities ΔA_{cld} and ΔN_{cld} were evaluated using typical mid-latitude values obtained from satellites. Table V gives the absolute ΔA_{cld} error for given ΔH_s , M_s , and ρ_{cld} . These results show that the "uncertainties must stay below the 10% level if reasonable accuracy is to be maintained" (Reynolds and Vonder Haar, 1977). This accuracy is possible through use of ground and cloud truth measurements along with improvements in instrument calibration. At present there is approximately a 3 degree Celcius ($^{\circ}C$)

TABLE IV

Algorithms for Cloud Top Temperature and Cloud Amount (after Reynolds and Vonder Haar, 1977)

- | | |
|--|--|
| (1) $m_s = A_{clr} \rho_{clr} H_s + A_{cld} \rho_{cld} H_s$ | $cld = \text{cloud}$ |
| (2) $m_L = A_{clr} N_{clr} + A_{cld} N_{cld} \epsilon$
$+ A_{cld} (1.0 - \epsilon) N_{clr}$ | $clr = \text{clear}$ |
| (3) $A_{cld} = \frac{m_s - \rho_{clr} H_s}{H_s (\rho_{cld} - \rho_{clr})}$ | $A_{cld} = \text{area of array covered with cloud}$ |
| (4) $N_{cld} = \frac{m_L - N_{clr}}{\epsilon A_{cld}} + N_{clr}$ | $m_s = \text{measured visible radiance}$
$\rho_{cld} = \text{bi-directional reflectance cloud areas}$ |
| (5) $A_{cld} + A_{clr} = 1.00$ | $H_s = \text{solar irradiance reaching the surface } (.5 < \lambda < .8 \mu m)$ |
| (6) $\epsilon = \frac{m_L - N_{clr}}{N_{cld} - N_{clr}}$ | $\rho_{clr} = \text{bi-directional reflecting of clear areas}$
$N_{cld} = \text{spectral IR } (10 < \lambda < 12 \mu m)$
$N_{clr} = \text{spectral IR radiance from clear area}$
$m_L = \text{measured IR radiance}$
$\epsilon = \text{IR emissivity}$
$A_{clr} = \text{area of array clear of clouds}$ |

error in satellite derived temperature which is equivalent to approximately 5% Δ in N_{clr} . N_{cld} will have a 16°C error if the A_{cld} has 24% error (Table V). This error can be reduced by better A_{cld} determination using higher resolution data and through use of ground truth measurements.

TABLE V

The Errors in Cloud Amount (with $\Delta H_s = 5\%$) and in Cloud Temperature ($N_{cld} = 265$ K, after Reynolds and Vonder Haar, 1977)

Uncertainty	5% ρ_{clr} , ρ_{cld} , Ms	10% ρ_{clr} , ρ_{cld} Ms	15% ρ_{clr} ρ_{cld} , Ms
ΔA_{cld} ($A_{cld} = 0.26$)	0.09	0.14	0.20
ΔA_{cld} ($A_{cld} = 0.53$)	0.13	0.21	0.30
ΔA_{cld} ($A_{cld} = 0.83$)	0.17	0.29	0.40
	5% ML, N_{clr} , ϵ 24% in A_{cld}	10% ML, N_{clr} , ϵ 40% in A_{cld}	
ΔN_{cld}	16°	30°	
ΔZ	3 km	4.2 km	

The bispectral method was tested with NOAA satellite coverage in an area that had cloud observations and upper air data available. Three locations were chosen; White Sands Missile Range (WSMR), Denver, and Oklahoma City. A 75 X 75

km area was used because it best corresponded to surface and upper air data. Average values of ρ_{cld} , ρ_{clr} , and H_s were assumed initially and then changed as sun angle and satellite viewing angles varied (Reynolds and Vonder Haar, 1977). The results showed a rms error of 0.2 in cloud amount with a slight underestimation bias. The cloud height error with cirrus included was 4.6 km with a -4.2 km bias. Without cirrus cloud, the rms error improved to 0.5 km with overestimation of 0.27 km.

This problem with cirrus is linked to the use of 0.9 for the emissivity of all clouds. Because of the ice crystals in cirrus, its emissivity is less than the 0.9 value. Two approaches were considered by Reynolds and Vonder Haar (1977) to correct this problem.

One approach was to correlate the visible spectral albedo of a cloud to its emissivity through the blackbody temperature. Fig. 20 shows the scatter diagram of the relationship between the albedo and the blackbody temperature and a second order fit which was used to determine the cloud top temperature for a specific albedo. Once this cloud top temperature is known the emissivity can be calculated using Eq. 4, Table IV (derived from Eq. 2 of Table IV).

Fig. 21 is the resulting curve which relates albedo to emissivity. The curve is a second order equation of the best fit curve measured in the bispectral method along with a slight adjustment to p_{clr} and p_{cld} . This cut the error of the old method in half (Reynolds and Vonder Haar, 1977).

The second procedure for determining cirrus cloud height was to compare channels 4 and 8 of the Vertical Temperature Profile Radiometer (VTPR) on the NOAA-4 satellite. This led to a reduction by one half in the apparent error of the old method. Table VI lists the results of using a cirrus correction and the VTPR approach compared with non-adjustment for cirrus.

D. PRECIPITATION

Four approaches for estimating precipitation from satellites are reviewed in this section. They are cloud index (Barrett and Martin, 1981; Barrett, 1981), life history (Barrett and Martin, 1981; Griffith and Woodley, 1981), bi-spectral (Liljas, 1981a, 1981b; Austin and Lovejoy, 1981), and cloud modeling (Wylie, 1979; Simpson and Wiggert, 1969).

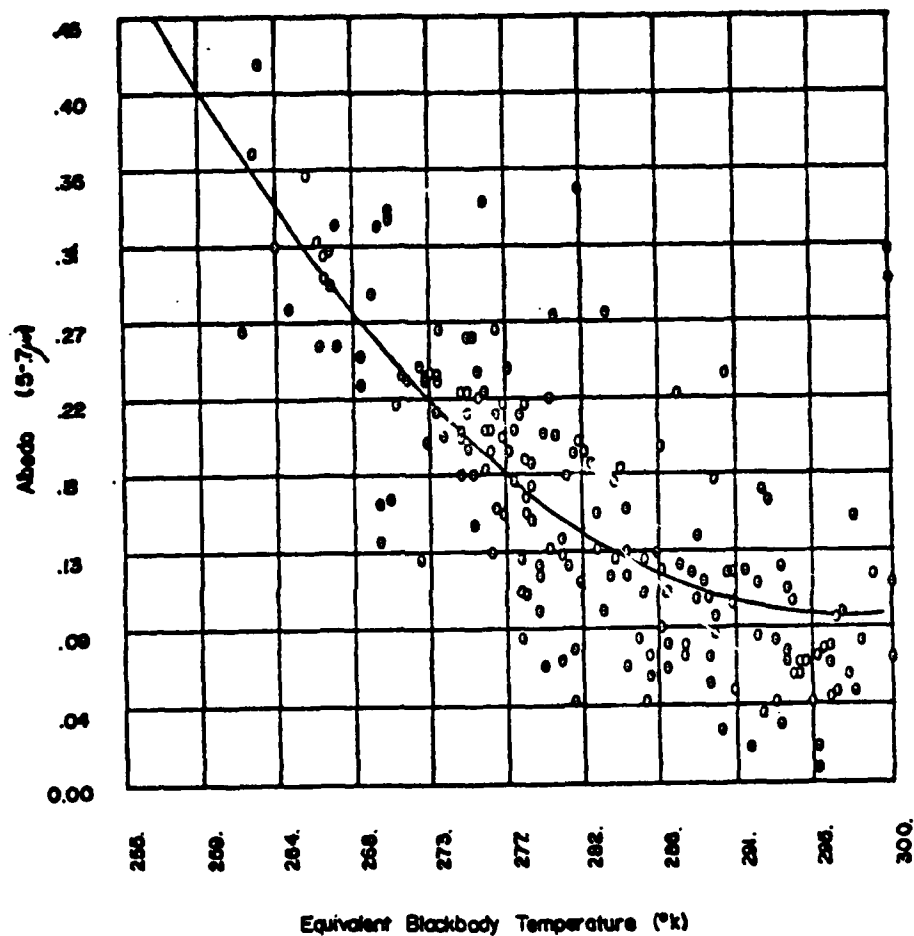


Figure 20. The Relationship Between Albedo and Blackbody Radiation. This was derived from NOAA satellite measurements of cirrus clouds over the Gulf of California (from Reynolds and Vonder Haar, 1977).

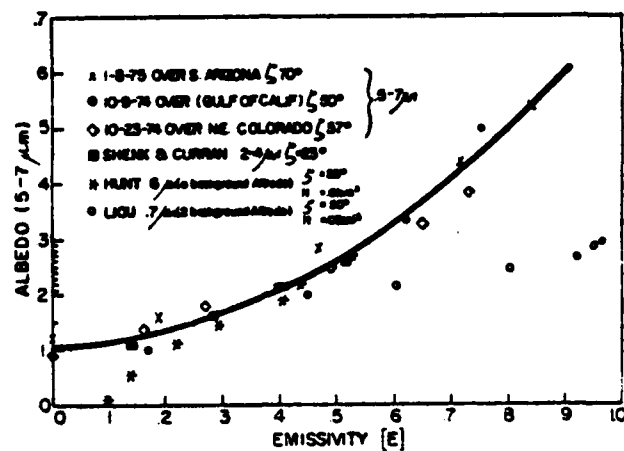


Figure 21. The Relationship Between Albedo and IR Emissivity from Empirical Studies (from Reynolds and Vonder Haar, 1977).

TABLE VI

Comparison of cirrus correction and VTPR results (from Reynolds and Vonder Haar, 1977)

CIRRUS CORRECTION RESULTS					
Date	Uncorrected Bi-Spectral Cloud Top Temp. (K)	Cloud Height Error (Km)	Bi-Spectral Cloud Top Temp. with Cirrus Correction (K)	Cloud Height Error (Km)	Observed Cloud Top Temp. (K)
8 Jan 75	298	+3.2	248	+1.7	233
8 Jan 75	261	+3.3	242	+1.1	233
23 Oct 75	256	+2.2	229	- .5	233
9 Oct 75	250	+1.6	231	- .4	236
RMS Error = 2.6 km		RMS Error = 1.1 km			
Bias = +2.6 km		Bias = +.48 km			

VTPR RESULTS					
Date	Spot	VTPR Determined Cloud Height (Km)	SR Determined Cloud Amount	Observed Cloud Height (Km)	Error (Km)
8 Jan 75	33N 114W	8.2	.7	8.7	+ .5
8 Jan 75	33.2N 114.3W	8.6	.7	8.7	+ .1
8 Jan 75	33.5N 116.3W	5.7	.6	8.7	+3.0
RMS Error = 1.75 km		Bias = +1.2 km			

1. Cloud Index

Barrett (1981) developed a cloud index method of determining rainfall (called the 'Bristol Method'). It is a manual method which uses observed rain gage data and the cloud index system (see Section B) to predict the amount of rainfall accumulated over a specified time period (usually 12 hours) in grid squares of a selected size ($1/6^\circ$ to 1° grid squares). Cloud area and altitude are also taken into account (Barrett and Martin, 1981). Fig. 22 presents the flow diagram of a recent version of the Bristol Method with two stages, preparatory and operational. Both IR and VIS are used whenever possible to identify cloud types. Next, the cloud types of each grid square are assigned an index (see Table VII). The cloud index is generally "evaluated differently for ranges of chosen cloud types and for different regions" (Barrett and Martin, 1981). Then mean cloud indices are calculated along with mean observed rainfall amounts for each cloud field unit. Subsequently, regression techniques are used to relate the observed rainfall to the cloud type, and these help establish rainfall estimates for areas of satellite cells where conventional data are sparse (see Fig. 23). Tests show that the accuracy of this method

is approximately 75% for all cases belonging to a specific category (Barrett and Martin, 1981).

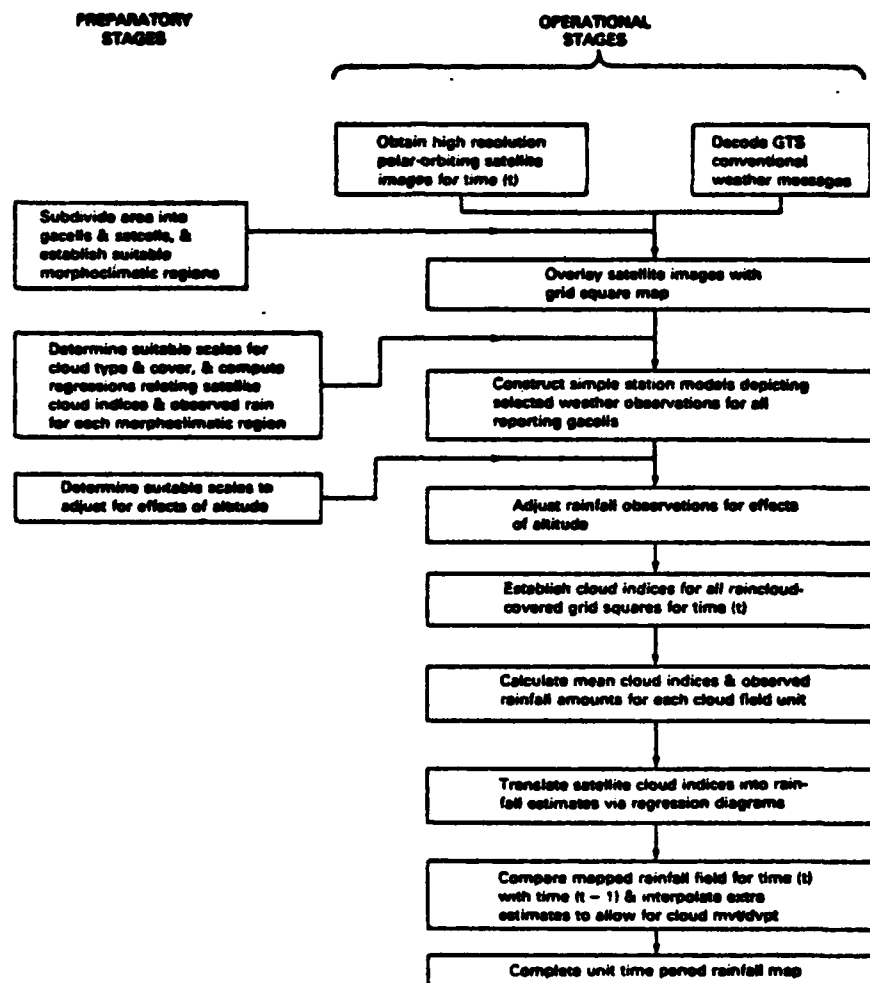


Figure 22. Flow Chart for a Recent Version of the Manual Nephanalysis (from Barrett and Martin, 1981).

TABLE VII

Empirically Derived Rainfall Probabilities and Intensities
from Satellite Pictures (from Barrett and Martin, 1981)

1	2	3
States of the sky (nephanalysis cloud categories)	Assigned probabili- ties of rainfall (relative scale range 0 - 1.00)	Assigned intensities of rainfall (rela- tive scale range 0 - 1.00)
Cumulonimbus	0.90	0.80
Stratiform	0.50	0.50
Cumuliform	0.10	0.20
Stratocumuliform	0.10	0.01
Cirriform	0.10	0.01
Clear skies	--	--

2. Life History

The Griffith/Woodley (Griffith and Woodley, 1981; Griffith et al., 1978) technique for estimating convective precipitation was developed using a cloud life history model in which satellite imagery is compared to radar echo life history of the cloud area (Griffith and Woodley, 1981; Barrett and Martin, 1981). The basis of the technique is the hypothesis that in the tropics rain occurs with cold (bright) clouds and the intensity of the rain is a function of the stage of development of cumulonimbus clouds. In a study of clouds over Florida, Griffith and Woodley (1981) found that the cumulonimbus cloud area is related to radar

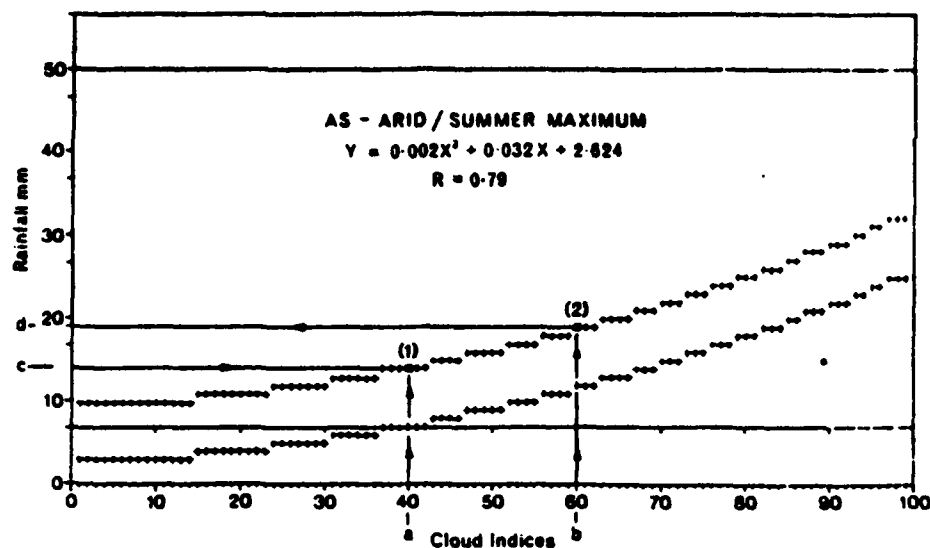


Figure 23. Regression Diagram Used to "Float" Rainfall Estimates for Satellite Pictures (from Barrett and Martin, 1981).

echo area (see Fig. 24). Cloud areas (A_c) are evaluated in either VIS or IR satellite imagery and then compared to the radar echo area (A_e). Fig. 24 is a plot of the relationship between cloud and echo areas (Griffith et al., 1978). It was empirically derived using measurements and comparisons of Florida clouds viewed by radar and geosynchronous satellites. The rain cloud threshold (IR) used in the approach was 253 K.

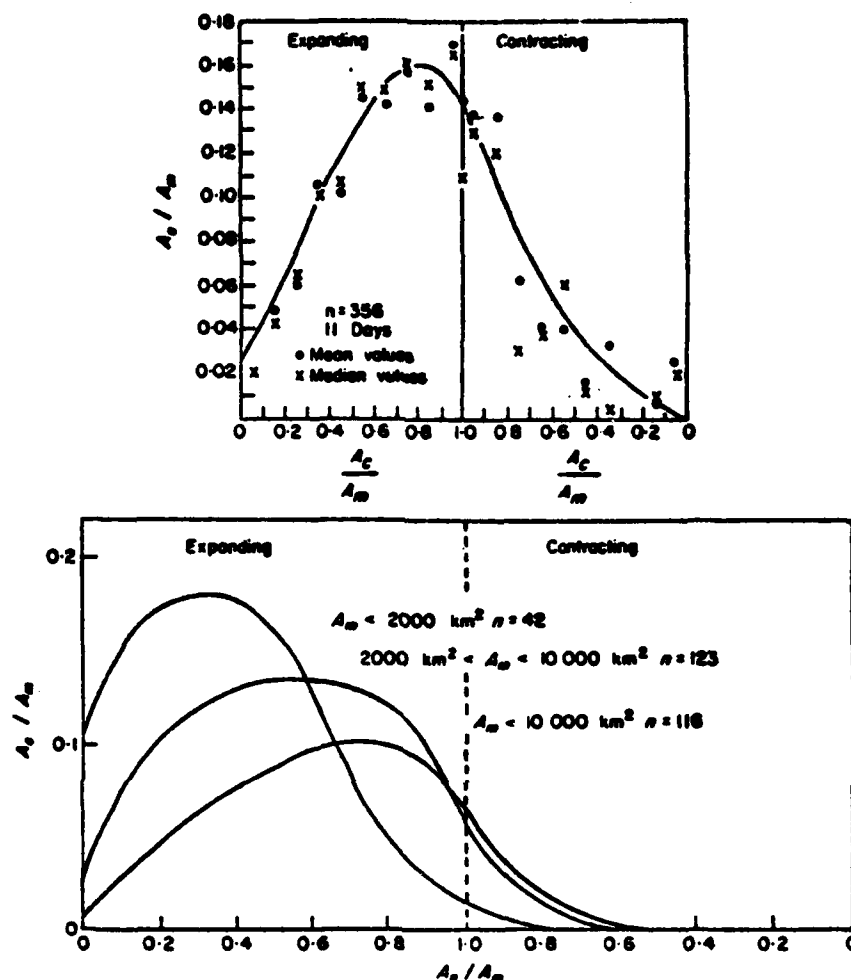


Figure 24. VIS (top) and IR (bottom) Satellite Data Cloud (A_c) and Echo (A_e) Area Relationships for Florida. Both cloud and echo area values are normalized to relative maximum cloud area (A_m) (from Griffith et al., 1978).

This technique is fully automated (Figure 25) and has been tested in the Florida area and in extra-tropical convective areas (Barrett and Martin, 1981). There are four major computer modules that together produce a rain map. The

programs are navigation, cloud isolation and tracking, cloud life history compilation and volumetric calculation of rain, and rain mapping (Griffith and Woodley, 1981; Barrett and Martin, 1981).

This model has been applied on several time scales and in different regions as shown in Table VIII. The error statistics (bias (B), root mean square error (Erms), and linear least squares fit (R, slope, and intercept)) for these applications (Table IX) show that on average the model results agree fairly well with the ground truth data (Griffith and Woodley, 1981). The Erms is small except for two locations, with an overall average of 0.85 millimeters per hour. The bias is close to 1.00 which is the value of perfect correspondence. In the linear fits, all correlations (R) are greater than or equal to 0.78, where 1.0 is perfect correlation.

3. Bispectral

Lovejoy and Austin (1979) developed a technique in which visual and infrared wavelength patterns are used to identify clouds with a high probability of rain. These clouds have large optical and physical thickness "as measured by the visible albedo in comparison with their

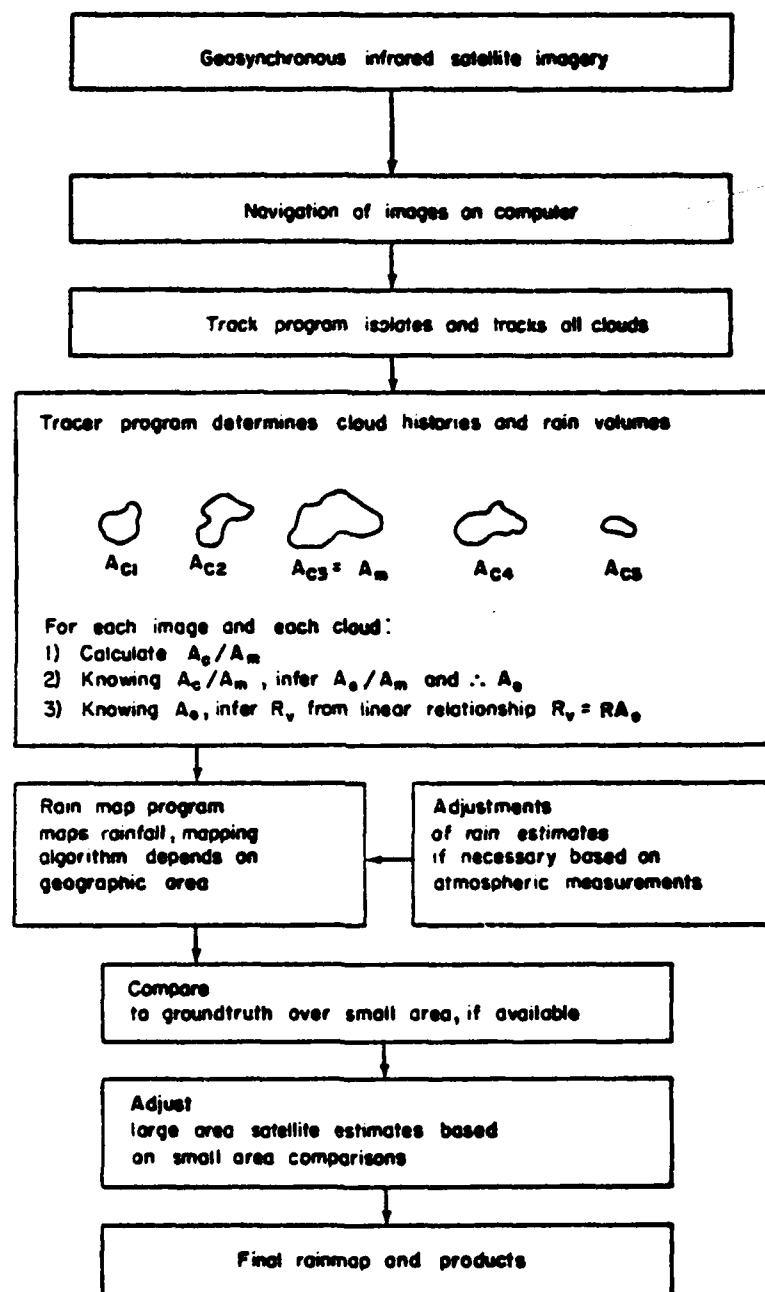


Figure 25. The Griffith/Woodley Technique Flow Chart Used for GATE (from Barrett and Martin, 1981).

TABLE VIII
Applications of the Griffith/Woodley Technique (from
Griffith and Woodley, 1981)

AREA	PERIOD
Global Atmospheric Research Project's Atlantic Tropical Experiment (GATE)	June 27 to Sept. 28, 1974
Florida Area Cumulus Experiment (FACE)	Selected days June to September 1972 to 1980
Equatorial Pacific Ocean Climate Studies (EPOCS)	2-1/4 days November, 1978 30 days November, 1979
High Plains Experiment (HIPLEX)	Selected days, May to July 1976 to 1978
Hurricanes	Selected storms 1969 to present
Flash floods	Big Thompson, CO 7/31 - 8/1, 1976 Johnstown, PA July 19-20, 1977

TABLE IX
The Error Statistics from the Applications Listed in Table
VIII (from Griffith and Woodley, 1981)

LOCATION	N	B	E_{RMS}	R	SLOPE	INTERCEPT
GATE	53	0.84	0.79	0.87	0.97	-1.47
HIPLEX (dense)	15	0.77	2.81	0.90	0.62	0.07
FACE	11	0.88	0.42	0.95	1.18	-0.23
HIPLEX (sparse)	9	0.90	0.55	0.78	1.81	-0.27
HURRICANES	3	1.00	0.06	1.00	0.89	0.18
FLASH FLOOD	2	1.39	0.48	0.99	0.89	23.93
PERFECT CORRESPONDENCE		1.00	0.00	1.00	1.00	1.00

height, determined by the intensity of the IR emission" (Austin and Lovejoy, 1981). Liljas (1981a, 1981b) followed this with a similar type of bispectral identification of precipitation area based on VIS and IR imagery. This subsection will first review Austin and Lovejoy's (1981) technique and then Liljas' (1981a, 1981b) technique.

Austin and Lovejoy (1979) first addressed the question, "How well can rain areas be delineated in coincident visible and infrared satellite images?" They felt that the problem was to find boundaries between rain and no rain. Estimation of rain amount is assumed to depend on two steps, the delineation of the rain areas and estimation of rain rate once the area is known. The authors used three statistics to characterize errors and from these were able to estimate rain area and rain rate. The first step in rain estimation was to map a frequency matrix for both rain areas and non-rain areas (see Fig. 26 and 27). The ratio of rain to non-rain was found and plotted (see Fig. 28) along with a line of greater than 50% probability of rain. From this, a rain map (see Fig. 29) was produced. The next step was to try to quantitatively estimate the rain rate. Austin and Lovejoy (1981) tried several techniques to do this but met

with little success. They believe this was due to "...the visible and IR wavelengths primarily responding to the relative abundance of cloud droplets and not to precipitation sized particles" (Austin and Lovejoy, 1981). They concluded that a good or even passable quantitative estimate of rainfall rate is not realistic or practical using visual and infrared data. The authors felt their study supported the hypothesis that visual and infrared satellite images are good for estimating rain areas but not for estimating quantitative rain rates.

Liljas' (1981a) main objective was to apply an approach similar to that used by Lovejoy and Austin (1979) for identifying precipitation areas and intensity using TIROS-N satellite imagery, but without using radar to calibrate it. He decided not to try quantifying intensity, but to instead define it qualitatively by categories of light to heavy rain. This follows the work of Muench and Keegan (1979) on the relation of cloud reflectance and intensity of rain. Pursuing their concepts, Liljas (1981a, 1981b) developed a relative precipitation intensity identification technique which relies on his cloud typing model (see Section B, Chapter II). It can be applied quickly to both frontal and convective type precipitation and gives the

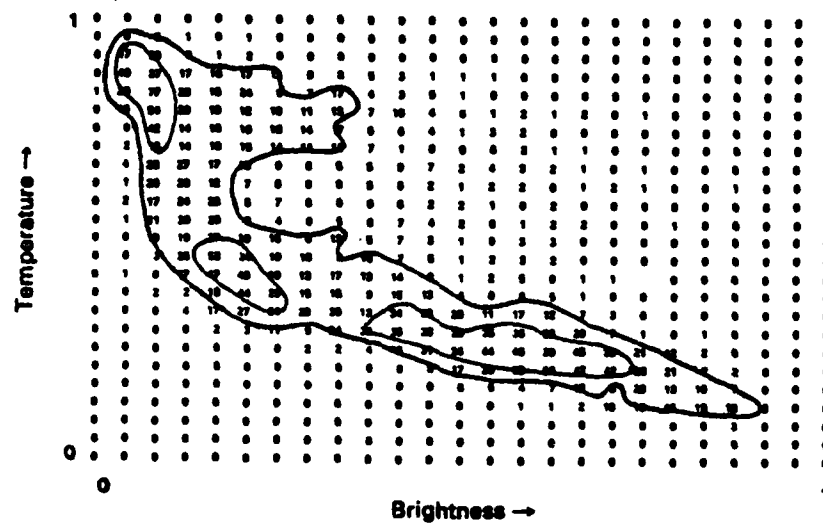


Figure 26. Frequency Distribution of VIS and IR Data Pairs for the No-rain Case (from Barrett and Martin, 1981).

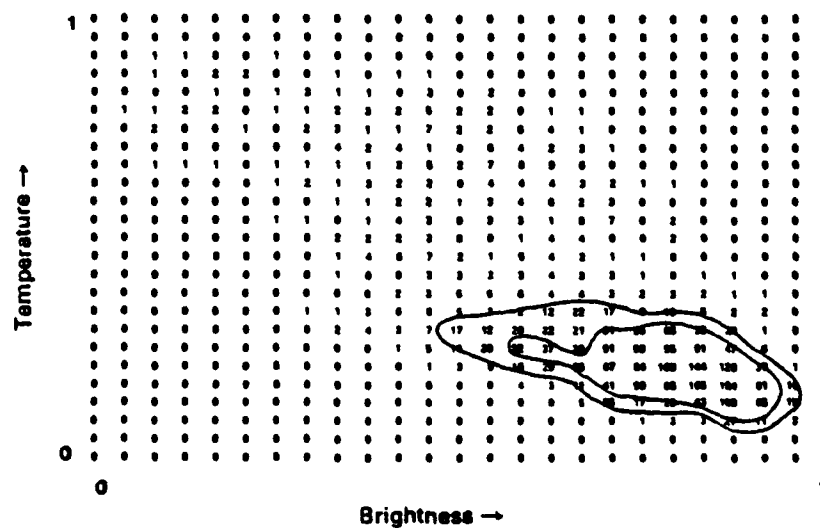


Figure 27. Frequency Distribution of IR and VIS Data Pairs for the Rain Case at the Same Location as Fig. 26 (from Barrett and Martin, 1981).

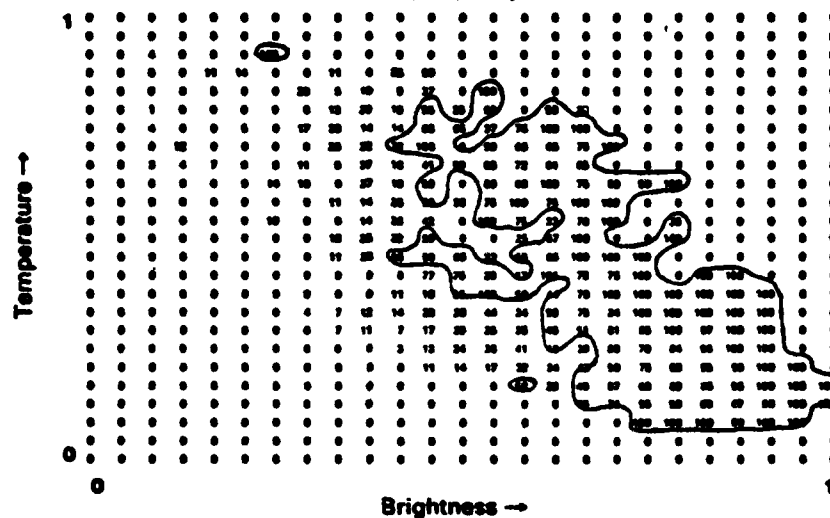


Figure 28. Probability of Rain in Percent from the Arrays of Fig. 26 and 27 with the 50% Boundary Sketched (from Barrett and Martin, 1981).

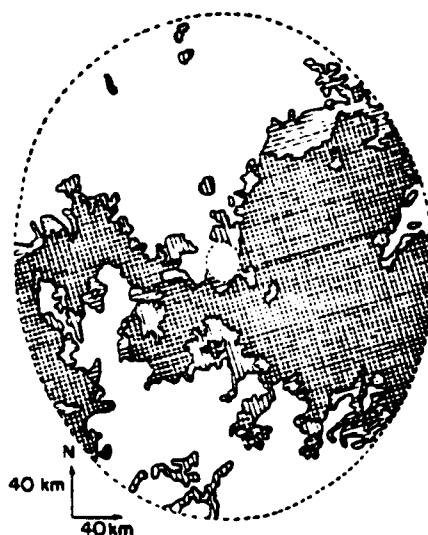


Figure 29. The Resulting Satellite Rain Map from the Use of the Same Data as Fig. 26 and 27. The vertical lines are radar rain areas and horizontal lines are satellite rain areas (hatched areas are the agreement areas) (from Barrett and Martin, 1981).

information in a real-time fashion. The first step is to identify the cloud types (see Fig. 9). Next, the area on the graph representing cumulonimbus and nimbostratus is sectioned (see Fig. 10) based on the premise that cold, high and dense clouds give the highest precipitation rate. An additional requirement for the cloud top temperature to be colder than -22°C was established (Liljas, 1981a) and supported by investigations of Muench and Keegan (1979). Table X gives the thresholds determined by summing the infrared and visual digital values that correspond to the precipitation intensity levels. The method gave good information on the distribution of precipitation areas and the relative intensity within the areas for both frontal and scattered showers. In addition, the method detected "intense precipitation in mesoscale cloud clusters between synoptic" observations (Liljas, 1981a).

4. Cloud Model

Wylie (1979) compared tropical and mid-latitude cloud area and rain rates to see if the Griffith/Woodley (Griffith et al., 1978) and other techniques could be applied to non-tropical cloud features, instead of the tropical cloud systems for which they were developed. Six days

TABLE X
Threshold Values Describing Precipitation Intensity Levels
as Applied in Fig. 10 (from Liljas, 1981a)

Ch1 + Ch4	291-310	light rain
	311-330	
	331-350	
	351-370	
	371-390	
	> 390	very strong rain

of two different types of rain clouds (frontal convective and frontal stratiform) in the Montreal, Quebec, Canada area were chosen for comparison to the 1979 GATE data set of Stout et al. (1979) (see Table VII).

The rain rates of the two areas are shown in Fig. 30. The GATE rain rates are higher than the rain rates of Montreal, even at the colder thresholds. The Montreal rain rates tend to vary considerably, especially the convective cases (June cases). This shows that a scheme based on the GATE data would overestimate rain rate in the midlatitudes, and additionally, if one uses a constant adjustment, there would be a large variance in the rain amounts. Table XI

shows the comparison for GATE and Montreal rates of precipitation. Wylie (1979) found that the precipitable water alleled the difference in the average rain rate with some minor exceptions when the troposphere was exceptionally stable. He decided to use Simpson and Wiggert's (1969) one-dimensional cloud model to assess the effects of stability and to possibly improve his results in the mid-latitudes.

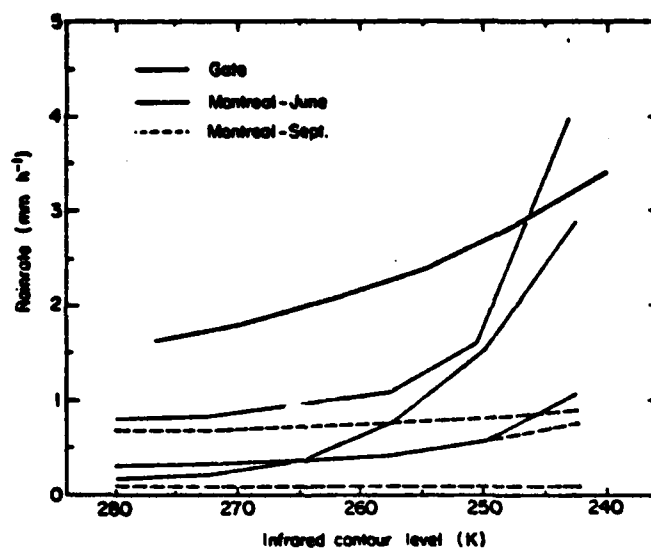


Figure 30. Rain Rates Averaged Over Cloud Areas Measured on IR Images for Various Cloud Threshold Temperatures (from Wylie, 1979).

This model simulates cloud growth by using an ascending 2 km bubble. The model incorporates cloud physics processes in the development of precipitation (Simpson and

TABLE XI
Estimated and Observed Precipitation and Stability Adjust-
ment Factors (after Wylie, 1979)

Case	Observed rainrate ^a (mm h ⁻¹)	Precipi- table water (mm)	(Montreal/GATE)		Precipitation		Bias	Error factor
			Precipi- table water	Model precipi- tation	Adjusted satellite (10 ⁶ m ²)	Radar		
GATE	2.2	54	—	—	—	—	—	—
<i>Montreal</i>								
29 June	1.0	38	0.7	0.5	24.6	25.5	0.9	1.1
2 June	0.9	22	0.4	0.3	8.9	8.8	1.0	1.0
26 Sept.	0.9	27	0.5	0.3	30.8	48.3	0.8	1.3
1 June	0.4	27	0.5	0.3	10.4	7.4	1.4	1.4
20 Sept.	0.4	27	0.5	0.0	3.2	14.6	0.2	4.6
16 Sept.	0.1	22	0.4	0.0	7.0	7.2	1.0	1.0
Average					14.1	17.5	0.9	1.7

Wiggert, 1969). Only one bubble ascent was used although normally the bubble would ascend many times. As a result, the rainfall prediction could not be used directly, but was nevertheless used as an adjustment to correct the Montreal data for stability.

Table XI shows the results of Wylie's (1979) study: the corrected precipitation of the satellite closely matches the radar measured amount of rain. He noted that the overall bias was small, and therefore by using a stability correction (calculated from the one-dimensional cloud model), the technique to measure precipitation by satellite in the tropics could be applied to mid-latitude areas.

III. SPADS CLOUD MODEL DESCRIPTION

A. INTRODUCTION

The cloud analysis model adapted for the SPADS interactive computer is a combination of procedures drawn from several previously tested techniques. The mainstay of the model is Liljas' (1981a) parallelepipedon (Fig. 9 and 10) classification. Added to this are a texture test for discriminating some cloud types, a non-linear least squares curve fit to discern cirrus and altostratus, Harris and Barrett's (1978) cloud amount calculation, part of Reynolds and Vonder Haar's (1977) cloud top temperature calculation, and Liljas' (1981a) qualitative precipitation intensity model. The following sections describe these parts of the SPADS model and explain why they were selected. The last section of the chapter summarizes with the flow chart of the model's computer program.

B. CLOUD TYPING

The approach selected for cloud typing was developed and tested by Liljas (1981a). It is a multispectral method that uses three channels to type clouds and differentiate

between land and water. The SPADS cloud model uses two channels, thereby becoming bispectral (the near-IR channel was not used due to non-availability in GOES VISSR data). Fig. 10 depicts the bispectral model incorporated in the SPADS Cloud Model. Both the visual and infrared thresholds shown in Fig. 10 were converted from Tiros-N Advanced Very High Resolution Radiometer (AVHRR) to GOES VISSR data counts. Liljas' visual data brightness counts ranged from 0 to 255 while the SPADS counts range from 0 to 63. A four to one linear relationship exists in the VIS channel and therefore a direct conversion of thresholds was performed. The IR thresholds were converted to temperatures (K) using an August 1980 TIROS-N AVHRR temperature calibration table. This gave a rain cloud threshold of about 251 K which is in agreement with the Griffith/Woodley (Griffith and Woodley, 1981) and the Liljas (1981a) rain cloud thresholds. These temperature thresholds were converted to GOES IR brightness counts. The transformed thresholds used in the SPADS cloud model are depicted in Fig. 31.

One of the reasons for selecting the Liljas model is that it was tested on an interactive computer similar to SPADS. In addition, the test area selected by Liljas (1981a) included land and ocean areas along with many types of clouds associated with mesoscale and synoptic scale features. A complete description with color pictures is in Liljas' (1981a) technical report. In addition, a combined approach using texture and bispectral counts was suggested by Liljas (1981a), Harris and Barrett (1978) and Reynolds and Vonder Haar (1977). The U.S. Air Force's 3DNEPH program used both these approaches, but documentation of thresholds and tests was not available to us. Thus, the 3DNEPH program could only be used as a qualitative guide.

The GOES IR resolution is approximately 4 n mi. at the subsatellite point, but for the visual channel a higher resolution of 0.5 n mi. is available. This VIS resolution affords an opportunity to get a better estimate of cloud cover. All the studies reviewed highly recommended the use of an array of brightness counts to give an improved representation of the cloud picture. The 0.5 n mi. resolution allowed an 8X8 array of visual pixels per IR pixel. For each grid space an average visual brightness count is calculated (Eq. 1, Table II).

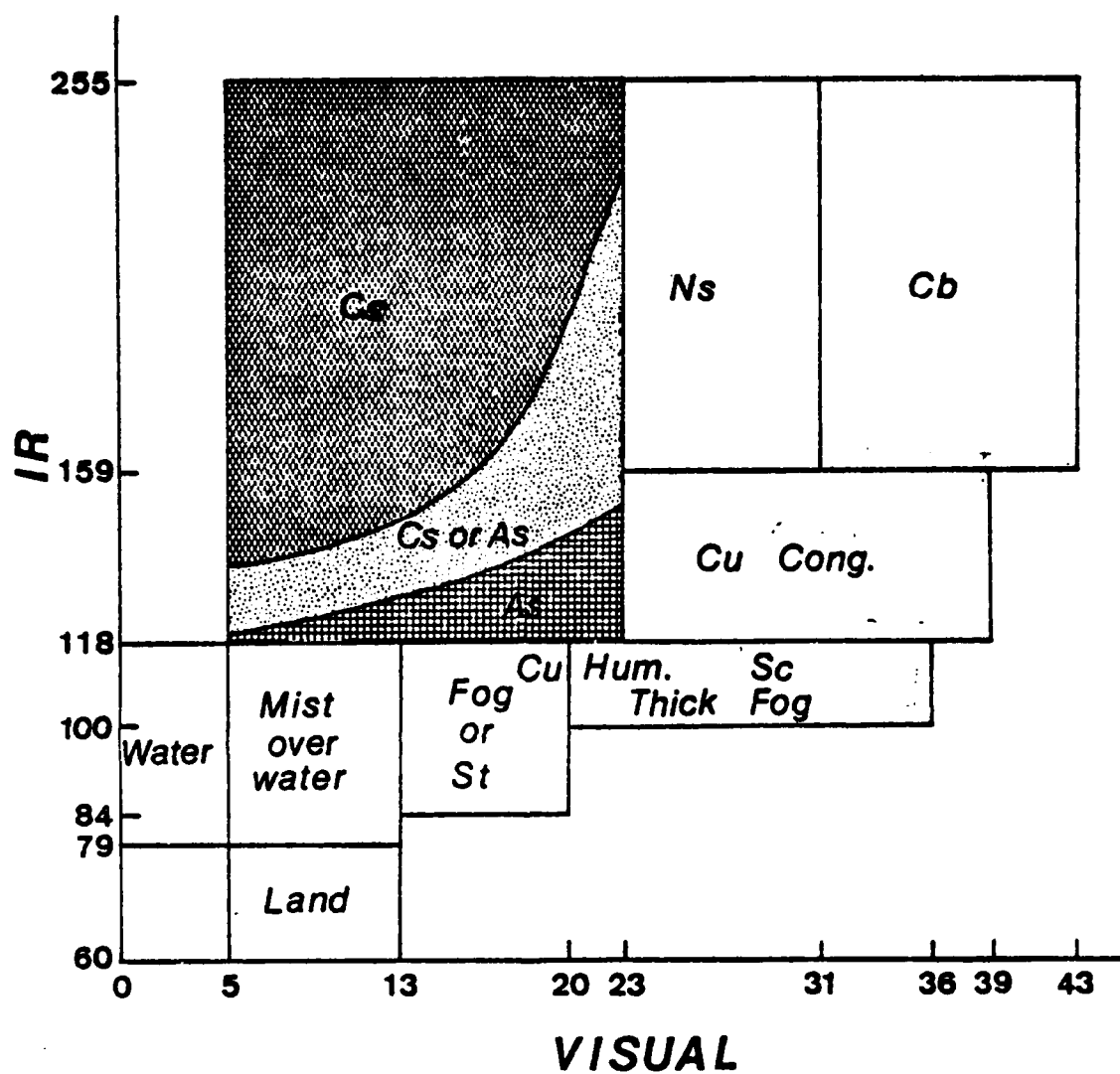


Figure 31. Two Dimensional Cloud Typing Graph Using GOES IR and VIS Satellite Digital Data (after Liljas, 1981a).

At the same time as the visual average brightness is being calculated, the standard deviation of the cloudy visual counts per grid space is determined. The standard deviation (Eq. 4, Table I) is the statistic used to represent texture. As suggested and tested by Harris and Barrett (1978), the standard deviation is used to discriminate between stratiform and cumulus humulus, small and large cumulus congestus, and altostratus and cirrus. The initial standard deviation threshold values for this discriminant analysis were approximated by using information in Fig. 6 and 8. An additional test was used first for the cirrus/altostratus decision. A second order polynomial least squares fit was applied to the cirrus (c) points and also to the altostratus (d) points in Fig. 10. The calculated curves are depicted in Fig. 31, with the associated equations in Table XII. Entering the equations with the average visual brightness, the resulting IR value is compared to the actual IR to determine cloud type. If the calculated value falls between the two curves then an additional test, using the standard deviation threshold, is used to discriminate cloud type.

C. CLOUD TOP TEMPERATURES

The Reynolds and Vonder Haar (1977) study is used as a basis for estimating cloud top temperatures. Their calculation is based on two equations (Eq. 1 and 2, Table IV), one for cloud amount and the other for the cloud top temperature. The resolution of the data used was 4 n mi. but the authors' analysis suggested an improved resolution would give better results. As mentioned above, this led to the choice of 0.5 n mi. visual data in this study.

The first step in determining the cloud top temperature is to calculate the amount of cloud per IR pixel. The cloud decision was based on comparing the visual digital count of each pixel in the 8X8 grid to a no cloud threshold. This threshold value (initially 5 VIS counts) was derived from Fig. 31 (after Liljas, 1981a) where it is the lowest VIS count to have clouds. A cloud threshold test was also used by Harris and Barrett (1978). Their threshold value was derived by comparing the visual image with a computer produced density slice, but neither the value nor the formula to obtain the value were included in their report. The U.S. Air Force's 3DNEPH program based the cloud decision on the amount of visual grayshade difference between a 3 n mi.

TABLE XII

SPADS Cloud Model's Cloud Types, Least Squares Fit Equations, and Standard Deviation Values (SIGi)

Cirrus (1)* - Cs

a. $y \geq 158.094 - 6.6076 x + 4.159 x^2$ **

b. $\sigma \leq \text{SIG3}$

Altostratus (2) - As

a. $y \leq 115.24 + .5246 x + .0395 x^2$ **

b. $\sigma > \text{SIG3}$

* The number in the parens is the computer cloud type identifier.

**{ y = IR digital value
x = average Visual digital value

Fog/stratus (3) - ST

Thick Fog/stratocumulus (4) - Sc

$\sigma \leq \text{SIG 1}$

Cumulus humilis (5) - CuHu

$\sigma > \text{SIG 1}$

Small cumulus congestus (6) - CuCong

$\sigma \leq \text{SIG 2}$

Large cumulus congestus (7) - CuCong

$\sigma > \text{SIG 2}$

Nimbostratus/multilayered (8) - Ns

Cumulonimbus (9) - Cb

pixel and a background brightness (Fig. 15, refer to Chapter II for more complete details). This program uses an extensive global background brightness file that is updated regularly (Fye, 1978). The development and maintenance of such a file for SPADS is not feasible at this time.

The average cloud amount is determined by summing the number of cloud decisions in the grid space and dividing by the total number of pixels per grid space. This calculation followed the Harris and Barrett (1978) Eq. 3 (Table I). This cloud amount fraction is then used in the Reynolds and Vonder Haar (1977) equation for cloud top IR radiance (Eq. 2, Table IV). One of the reasons this cloud amount calculation is used instead of Reynolds and Vonder Haar's equation was that, in the latter, three additional constants would have to be calculated and verified, which is beyond the scope of this thesis. The authors felt that it was essential in using their cloud amount equation that these constants be well determined (Reynolds and Vonder Haar, 1977).

The next parameter of the cloud top radiance equation to be determined is the clear area IR spectral radiance. Fleet Numerical Oceanography Center (FNOC) analyses of surface

temperatures (K) are obtained and a representative temperature profile matching the location of the IR image center point is selected. These temperatures are converted to IR radiances via Planck's function and used in the cloud top temperature equation.

Emissivity of the clouds also must be determined. Reynolds and Vonder Haar (1977), among others, found that the emissivity is nearly constant (approximately equal to 0.9) for all clouds except cirrus, for which it is approximately 0.55. In the program, cirrus clouds are identified by the cloud typing and standard deviation modules so that the lower emissivity can be used in the cloud top temperature equation. In addition, an emissivity of 1.0 was used for cumulonimbus and nimbostratus based on the assumption that these clouds do not allow any surface radiance through.

The cloud top radiance (N_{cld}) is calculated using Reynolds and Vonder Haar's (1977) equation (Eq. 2, Table III) which consists of the surface temperature field obtained from FNOC (converted to an IR radiance via Planck's law), the emissivity (cirrus or non-cirrus), the satellite IR radiance (M_1) value, and the fractional amount of cloud (f_{cld}). Once N_{cld} is calculated, a conversion to a cloud top

temperature is made via the inverse of Planck's function. This temperature can then be compared to the latest FNOG upper air data analyses to find the corresponding height in millibars (mb) of the cloud top. The upper air data are available at ten standard levels consisting of 1000, 900, 850, 700, 500, 400, 300, 250, 150, and 100 mb.

D. PRECIPITATION INTENSITY

The precipitation intensity identification technique selected is the Liljas' (1981a) method. It is an extension of his cloud typing method (see Chapter II) and therefore easily fits into the overall SPADS cloud model without adding much time to the process. Wylie's (1979) cloud model, as discussed in Chapter II, used the Griffith/Woodley (Griffith *et al.*, 1978) technique with a stability correction which gave good indication of rain rates. One problem with it is that the Griffith/Woodley technique is based on the development and identification of convective cloud systems' life history through use of radar echoes not available to this study. Another problem with using this scheme is the computer run time it would add to the SPADS cloud model.

Although time is an important factor, it is not the only reason for selecting the Liljas method. Liljas (1981a) reported good success with this technique, obtaining good

indications of relative precipitation over land and sea areas as verified by synoptic reports. He felt that this technique would be useful for sea areas where no synoptic observations were available. In addition, relative precipitation from mesoscale cloud clusters was detected between synoptic observations. This identification scheme was modified for use in the SPADS cloud model by reducing the number of precipitation intensity categories from six (see Fig. 9) to three. Fig. 32 depicts the new categories of precipitation types representing light, moderate, and heavy rainfall and Table XIII includes the equation for the lines separating the categories. The light rainfall category includes the requirement that cloud top temperatures be less than 251 K.

E. FLOW CHART

The SPADS Cloud Model (Fig. 33) begins with obtaining the initial infrared and visual data fields from the GOES satellite and conventional surface and upper air data from FNOC. The IR and VIS satellite data are collocated both in space and time. The upper air and surface temperatures are selected to correspond to the I,J position closest to the center point of the image from the latest FNOC analysis on

the same date as the satellite pictures. Next, the SPADS cloud model computer program (see Appendix A) is run.

As shown in Fig. 33, the first step of the program is to calculate three values based on the 8X8 grid of VIS pixels; the average VIS brightness, standard deviation, and cloud amount as discussed in Section B of this chapter. Once the values are obtained, the cloud typing module (based on Liljas, 1981a) is called. Two tests are performed within this module; one is based on comparison of the IR and average VIS counts and the other supplements the first by using texture (standard deviation) to complete the cloud typing task. If nimbostratus or cumulonimbus clouds are identified; the precipitation module is called and it determines the intensity (qualitatively) of the precipitation.

The cloud top temperature module, in which the temperature and the height of the clouds are calculated, is called for all cloud cases. The FNOC surface temperature value is used in the cloud top temperature calculation, while the FNOC upper air data are used in the height calculation.

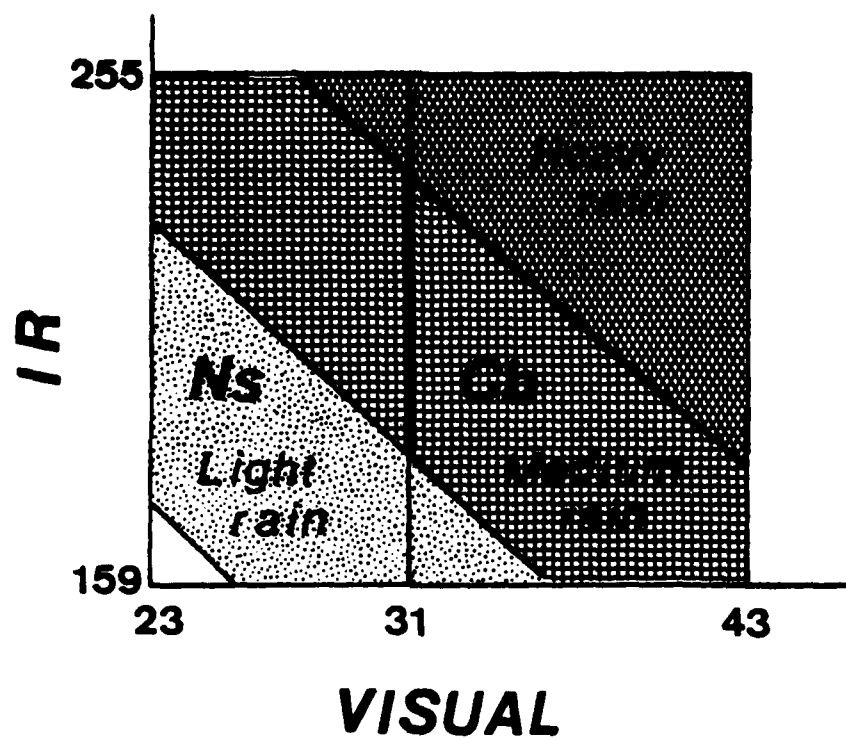


Figure 32. Graph of SPADS Cloud Model Precipitation Intensities.

TABLE XIII
SPADS Cloud Model Precipitation Intensity Categories

Equation	$\text{suml} = \text{IR radiance} + \text{average VIS brightness}$
No rain (ϕ)	$\text{suml} < 184$
Light rain (1)	$184 < \text{suml} \leq 195$
Moderate rain (2)	$195 < \text{suml} \leq 224$
Heavy rain (3)	$224 < \text{suml}$

The final step is processing the results. Cloud types (Table XII), precipitation intensities (Table XIII), cloud top temperatures (K), and cloud top heights (mb) are stored in a permanent file for future display. The average visual brightness, standard deviation, and the amount of cloud that correspond to each IR pixel are printed for reference and validation purposes.

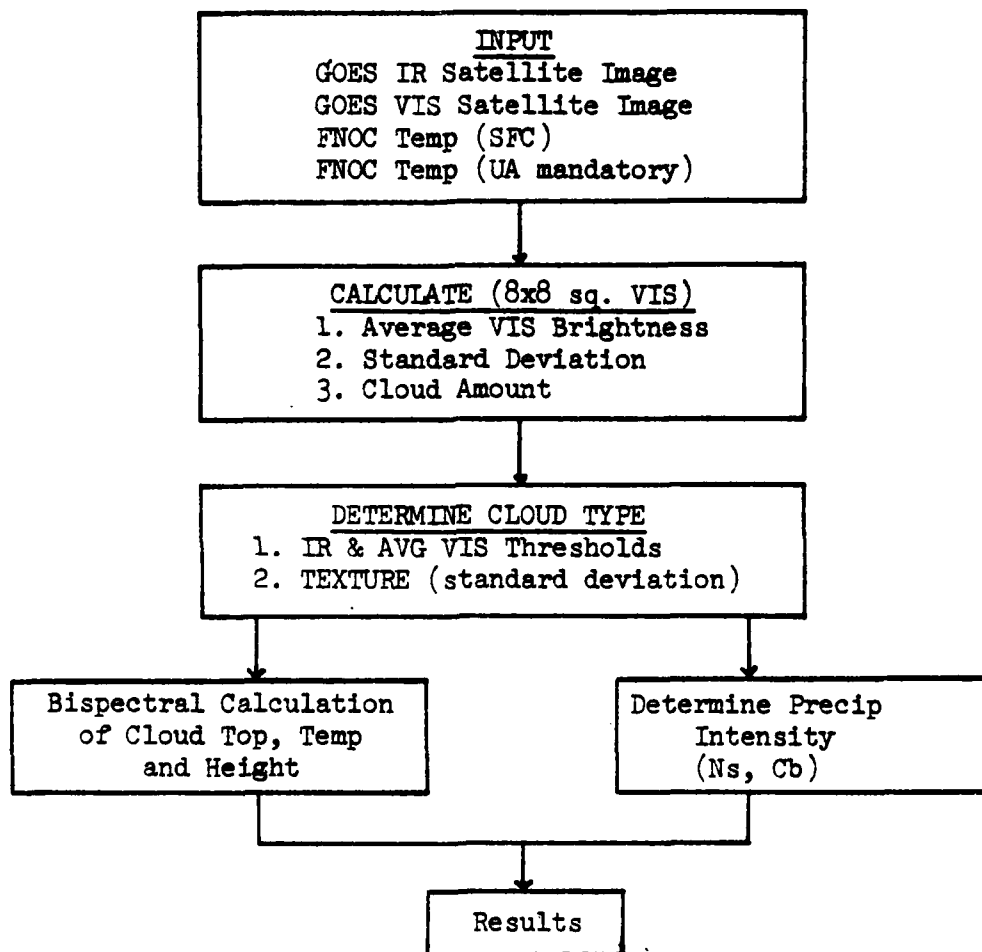


Figure 33. The SPADS Cloud Model Generalized Flow Chart.

IV. THE MODEL TEST AND RESULTS

A. INTRODUCTION

A test was conducted to determine if the SPADS Cloud Model concepts were valid. The test was designed: (1) to capture a small area of coincident IR and VIS satellite data in the mid-latitudes and to obtain FNOC fields for the same date-time group and location as the satellite data, (2) to run the SPADS Cloud Model using these data, and (3) to analyze the results of the model to determine the validity of the model's analyses. The following sections describe the input to this test, test procedures, results, and subsequent iterations and adjustments made to improve the model's performance.

B. DATA

GOES IR and VIS data were captured and archived on November 9, 1982 at 1315 local time, for a site centered at location latitude 44°N , longitude 141°W . The corresponding FNOC data fields were also saved for the same date from 1200 GMT data. Fig. 34 is the GOES IR image from which an area of approximately 460×460 n mi. was selected for analysis. This afforded 4096 IR pixels for evaluation. Fig. 35 is the

IR satellite picture of the selected area with the center point matching that in Fig. 34. The IR data resolution was approximately 7 n mi. at this latitude and 4 n mi. at the subsatellite point. The visual data resolution used was 0.9 n mi. (0.5 n mi. at subsatellite point). The visual area (see Fig. 36) is the same area as the infrared giving an 8X8 visual grid of pixels (64 points) per IR pixel.

The FNOG vertical temperature profile was obtained to match the center point of the satellite pictures and the corresponding heights (mb) are listed in Table XIV. Only one set of temperatures was used because the resolution of the FNOG fields (63 X 63 field with 381 km mesh length) is approximately the same as the area of the satellite pictures used in this test.

C. TEST PROCEDURES

The following list is the set of procedures for this test of the SPADS Cloud Model. The steps taken were to:

1. Capture coincident VIS and IR satellite images.
2. Receive surface and upper air temperatures from FNOG.
3. Manually analyze images for cloud boundaries and types.
4. Select the temperature profile closest to satellite image.

5. Run SPADS Cloud Model computer program.
6. Output results in a format for analysis.
7. Compare manual to computer output.
8. Adjust computer model as appropriate.
9. Repeat steps 5, 6, and 7.

The manual nephanalysis was completed by Dr. C.H. Wash, Assistant Professor in Meteorology at the Naval Postgraduate School. He used both the IR and Visual images (Fig. 34, 35, and 36) to discern the cloud boundaries and types seen in Fig. 37 (see Table XV for symbol definition)

During the first computer run, a cloud threshold of 5 visual digital counts was used. This value corresponded to the lowest visual threshold that could have clouds (see Fig. 33). After analysis of the first run, however, a threshold of 20 counts was selected. This adjustment accounts for our uncertainty in the GCES VISSR visible channel calibration, as compared to that for the TIRDS AVHRR visible channel. In normal use, VISSR is a relatively qualitative radiometer, and the engineering data needed to convert values to high-quality calibrated radiances were not readily available. Two sets of standard deviations were used and are presented in Table XVI.

AD-A126 845

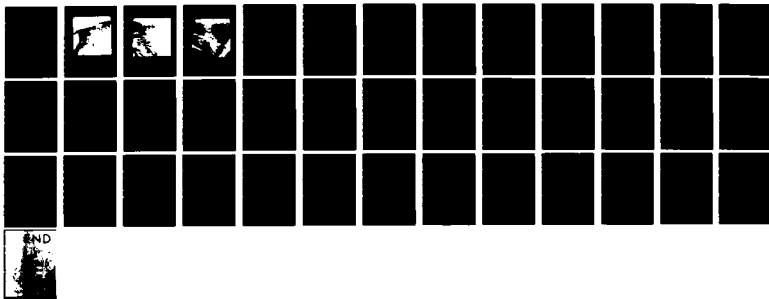
ESTIMATION AND MAPPING OF CLOUDS AND RAINFALL AREAS
WITH AN INTERACTIVE COMPUTER(U) NAVAL POSTGRADUATE
SCHOOL MONTEREY CA C A NELSON DEC 82

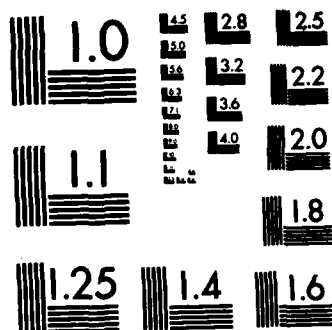
2/2

UNCLASSIFIED

F/G 9/2

NL





MICROCOPY RESOLUTION TEST CHART
NATIONAL BUREAU OF STANDARDS-1963-A

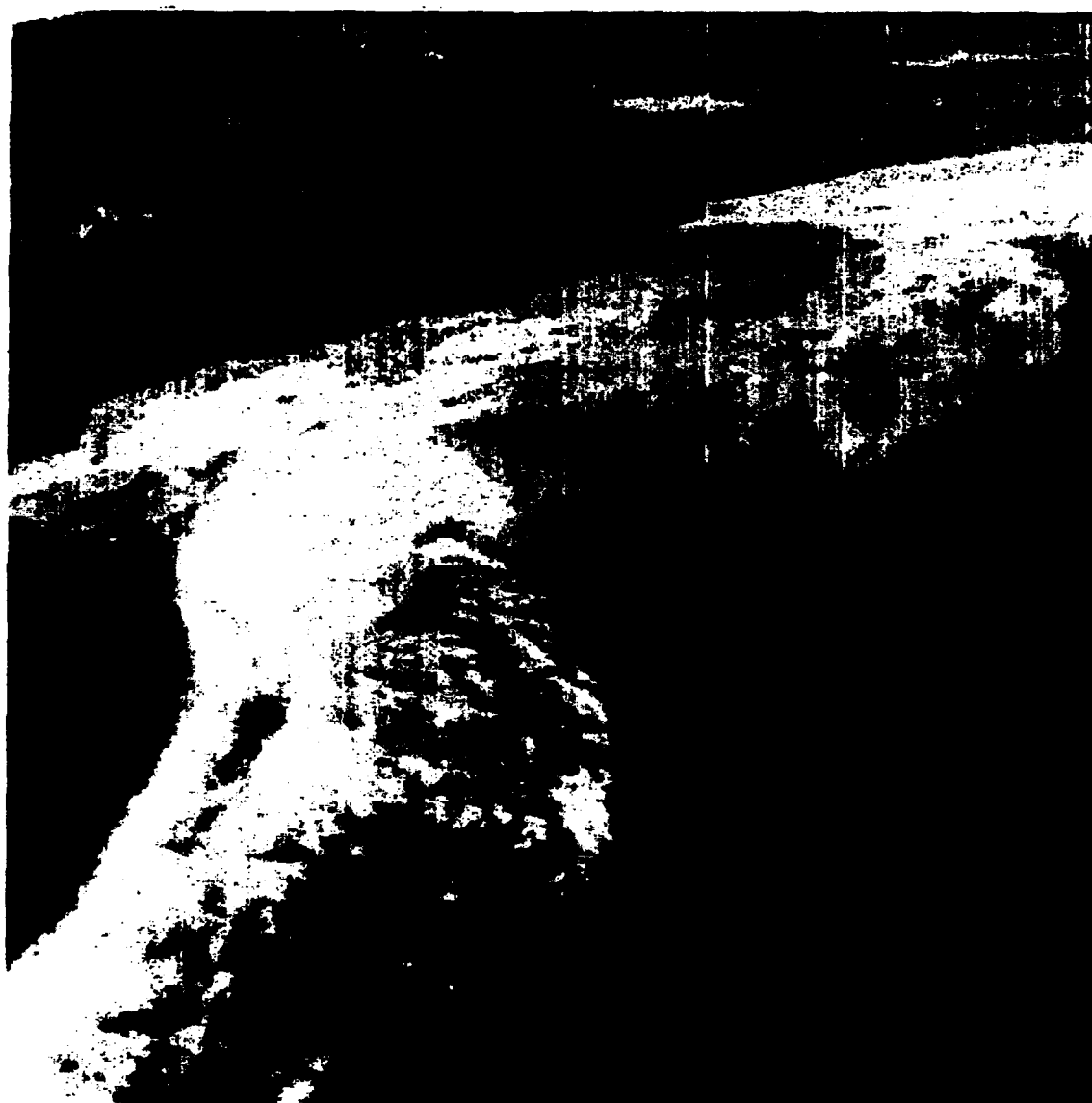


Figure 34. Infrared Satellite Image, Center Point is at Latitude 44°N , Longitude 141°W .

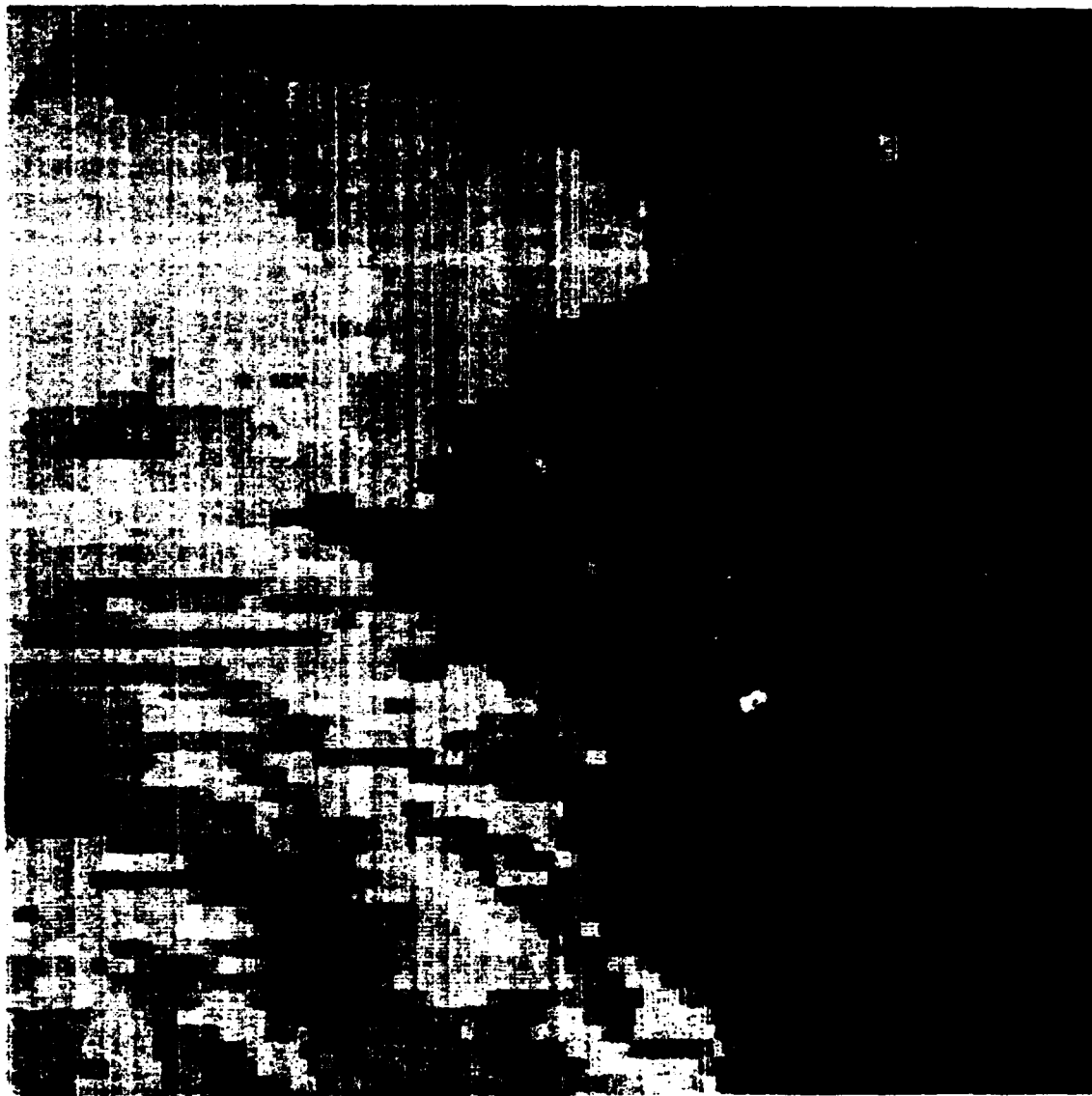


Figure 35. Infrared Satellite Image Selected from Fig. 34, with an Area of 460 X 460 n mi. (center point is at latitude 44°N, longitude 141°W).

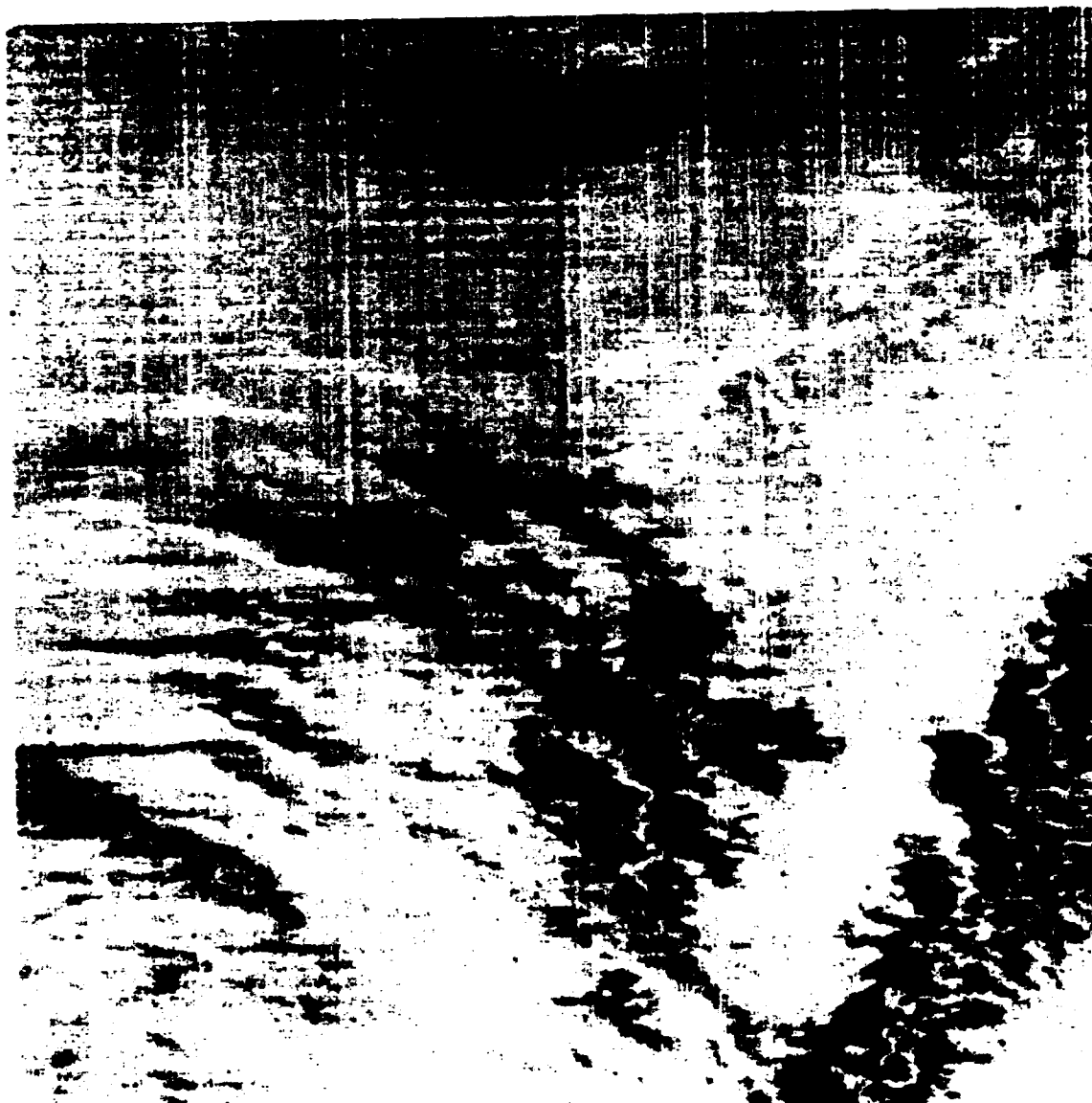


Figure 36. Visual Satellite Image with the Same Area and Center Point as Fig. 35.

TABLE XIV

FNOC Temperature Profile for 1200 GMT, November 9, 1982 at
latitude 44°N, longitude 141°W

<u>Standard level (mb)</u>	<u>Temperature (°K)</u>
100	212.
150	214.
200	216.8
250	221.8
300	229.7
400	244.6
500	254.3
700	267.7
850	275.5
1000	283.4
1010 (SFC)	289.7

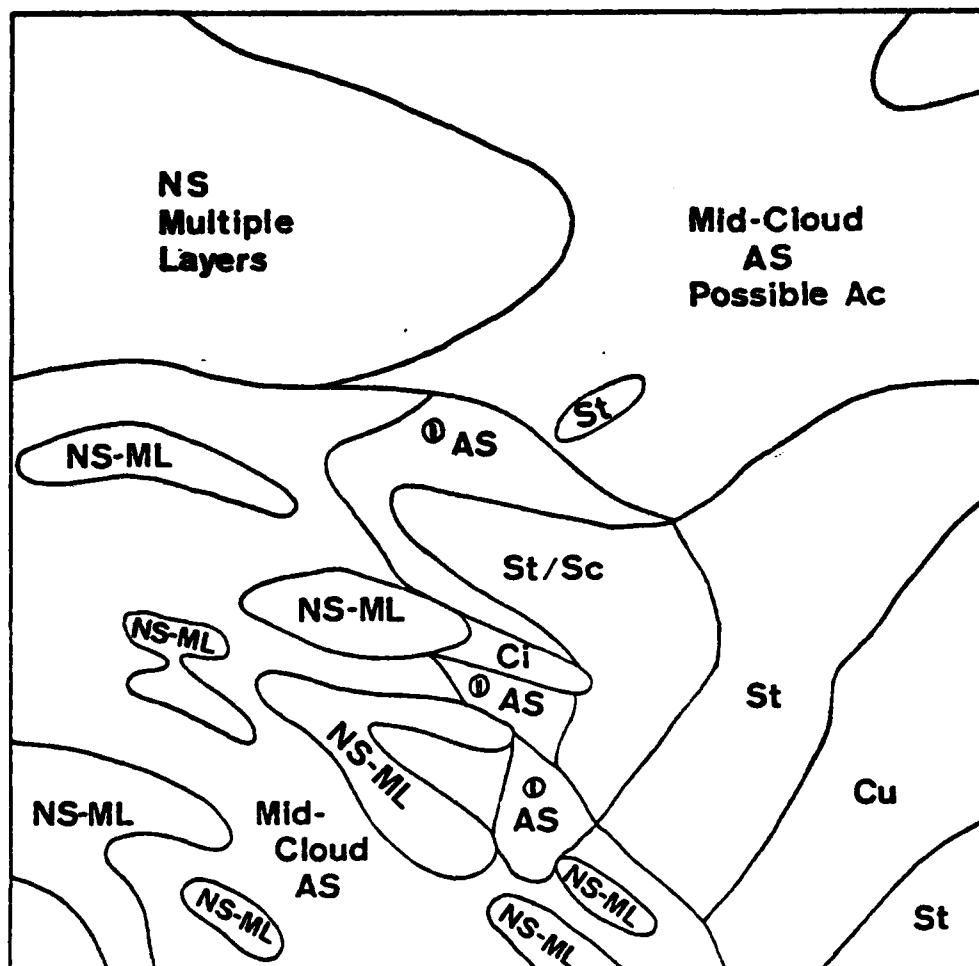


Figure 37. Manual Cloud Analysis of Fig. 35 and 36 (see Table XV for the symbol definitions).

TABLE XV
Definitions of Symbols Used in Fig. 37

Nimbostratus - Multiple layers	NS-ML
Altostratus	AS
Alto cumulus	AC
Cirrus	Ci
Cumulus	Cu
Stratus	St
Stratocumulus	SC
Broken	⦶

TABLE XVI
Standard Deviation (SIGi) Values Used for Run 1 and 2 (see Table XII for how they are used)

<u>SIG (i)</u>	<u>Test 1</u>	<u>Test 2</u>
SIG 1	4	2.5
SIG 2	20	20
SIG 3	3	1.5

D. RESULTS

The following subsections discuss the results of the two computer runs as compared to the manual analysis. The results are discussed by the type of product and run number;

where the products are cloud type, precipitation, cloud amount, cloud top temperature and height, and texture (standard deviation).

1. Run 1

a. Cloud Typing

The overall general patterns of the cloud types (see Fig. 38) compared well to the manual analysis (see Fig. 37). The observed cloud structure is most easily discussed by considering the images as four quadrants; northeast (NE), northwest (NW), southwest (SW), and southeast (SE) with north being the Top of the image.

The NE quadrant has mid-level clouds such as altostratus (see Fig. 37). The SPADS cloud model did well here indicating predominately mid-level clouds (see Fig. 38). The model also matched the manual analysis in the NW quadrant. This area has high cloud tops of nimbostratus and embedded cumulonimbus.

The SW quadrant has a mixture of mid-level and multi-layered thick clouds and again the cloud model is in agreement with the manual analysis (see Fig. 37 and 38). The objective analysis shows more detail than the manual analysis because the computer program is working pixel by

pixel while the manual analysis can only resolve groups of pixel defining cloud areas.

In the SE quadrant, the SPADS cloud model could not resolve the difference between low-level (stratus) and mid-level clouds. The boundary between these is located on the upper border of the SE quadrant. Another discrimination problem is between stratus and cumulus in the lower right quadrant. The amount of cumulus humulus that seems apparent in the visual satellite picture (see Fig. 36) and the manual analysis (see Fig. 37) did not appear in the computer analysis (see Fig. 38). This problem is related to the texture threshold tests, as both stratus and cumulus humulus have the same cloud type thresholds.

b. Precipitation

The patterns of rain intensity (see Fig. 39) in the NW and SW quadrants are based on the premise that the thicker and colder, therefore brighter, clouds (compare Fig. 39 to Fig. 35 and 36) have a greater probability of rain and a higher intensity of rain. Along with this, is the knowledge that the approximate threshold for rain clouds is colder than -22°C (Liljas, 1981a; Barrett and Martin, 1981). Both computer runs gave the same agreement with the

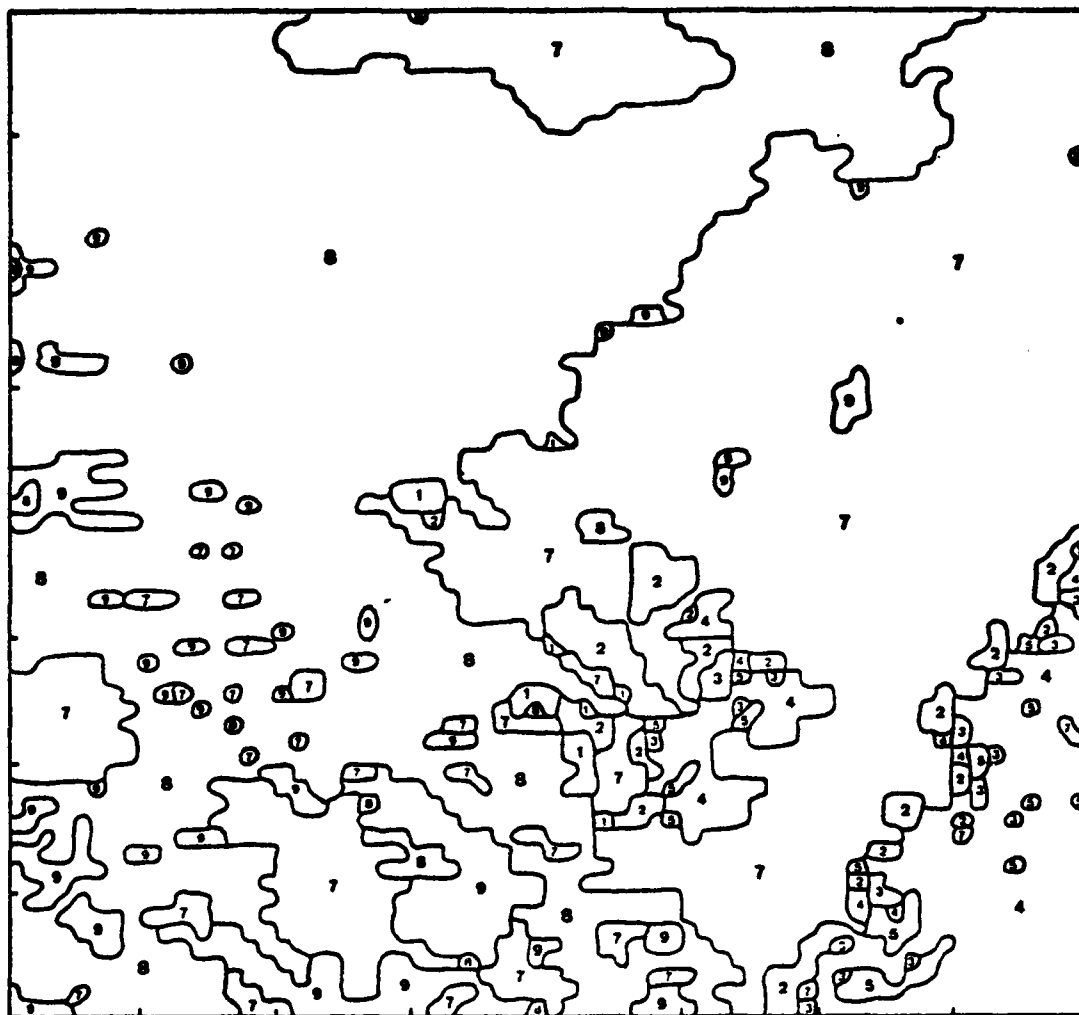



Figure 38. Cloud Types as Analyzed by the SPADS Cloud Model in Run 1 (see Table XII for numeric definitions).

manual analysis because the areas of rain clouds did not change. At this time, no surface data are available for ground-truth verification of the rain patterns.

c. Cloud Amount

The cloud amount for the first run was 100% for the entire analysis area. The visual, IR, and manual pictures all showed clear and scattered cloud areas in the SE quadrant. In the manual analysis (see Fig. 37), this quadrant has these sections marked Cu, St/Sc, and  As (see Table XV for symbol definitions). Further research into the cloud threshold for GOES satellite imagery, combined with analysis of the high resolution visual data used in this test, suggested a better cloud threshold value would be 20 visual counts (Muench and Keegan, 1979, and see discussion in Section C). The results from using this threshold are discussed in the Run 2 section.

d. Cloud Top Temperatures and Heights

The cloud top temperatures (see Fig. 40) and heights (see Fig. 41) look reasonable for the cloud types identified. The NE quadrant had temperatures ranging from 260 to 250 K and a height of approximately 500 mb, these matching the type of mid-level cloud. The NW quadrant

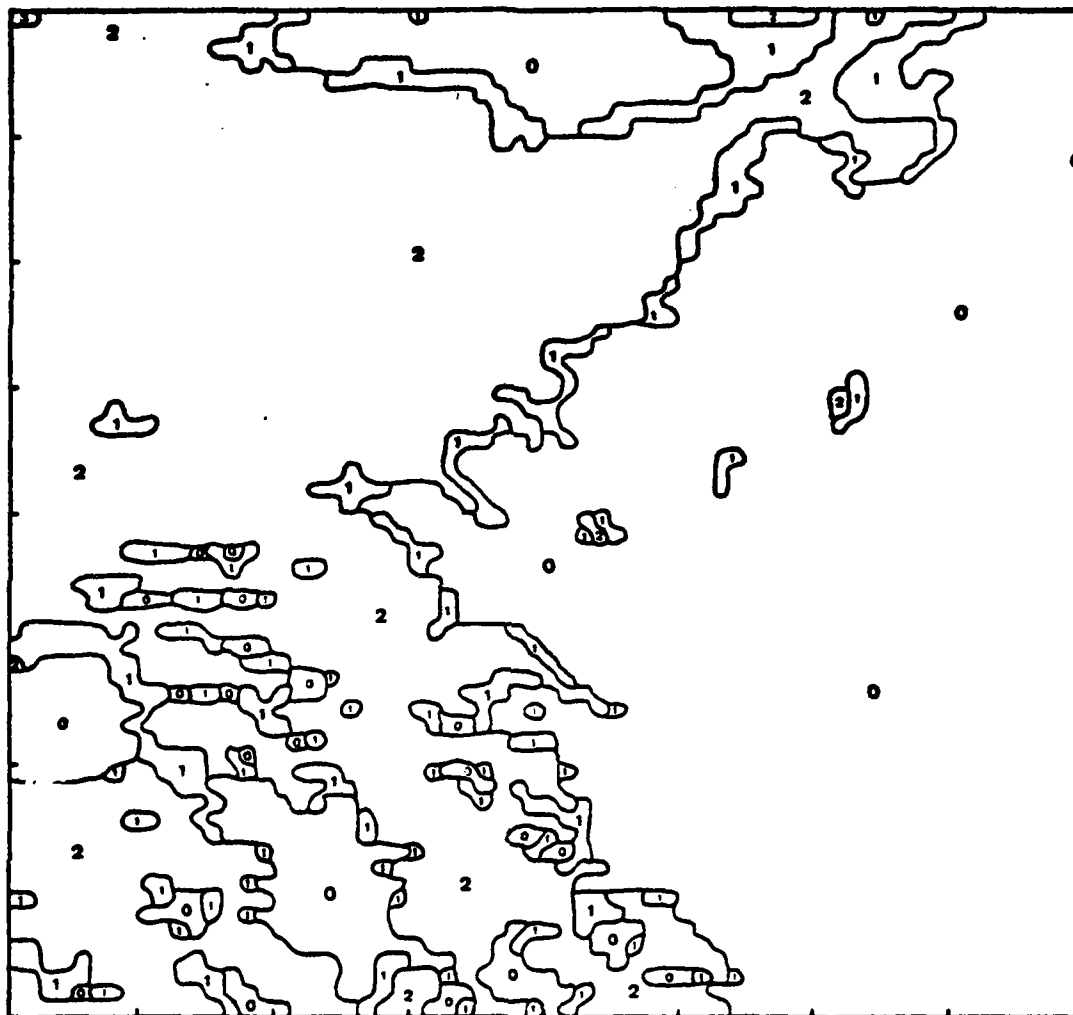


Figure 39. Qualitative Precipitation Intensity from Run 1 of the SPADS Cloud Model (see Table XIII for numeric definitions).

clouds are mostly nimbostratus with high-level, cold cloud tops. The height is approximately 300 mb and the temperature is 230 K. Again, agreement is good. The mixed clouds in the SW quadrant also have mixed height (mid-level and high-level) and temperatures which compare well (see Fig. 40 and 41)

The SE quadrant's heights, ranging from 850 to 700 mb, define the area reasonably well (see Fig. 41). The division for the low and mid-level clouds (see Fig. 37) appears as the 700 mb contour line (see Fig. 40). The cloud temperature field (see Fig. 40) defines the division of low and mid-level clouds less clearly, but partly cloudy areas (275 K contour) are indicated. The cirrus and altostratus clouds are too cold and high, as compared to the FNOC temperature profile. This error appears to be in the application of the bispectral radiance equation (Eq. 4, Table IV) from Reynolds and Vonder Haar (1979) in partly cloudy regions. The coefficients in that equation depend strongly on the radiance calibration of the radiometer used. The assumed calibration coefficients used in this study are clearly inadequate and must be improved through empirical validation of GOES VISSR calibration using ground truth data.

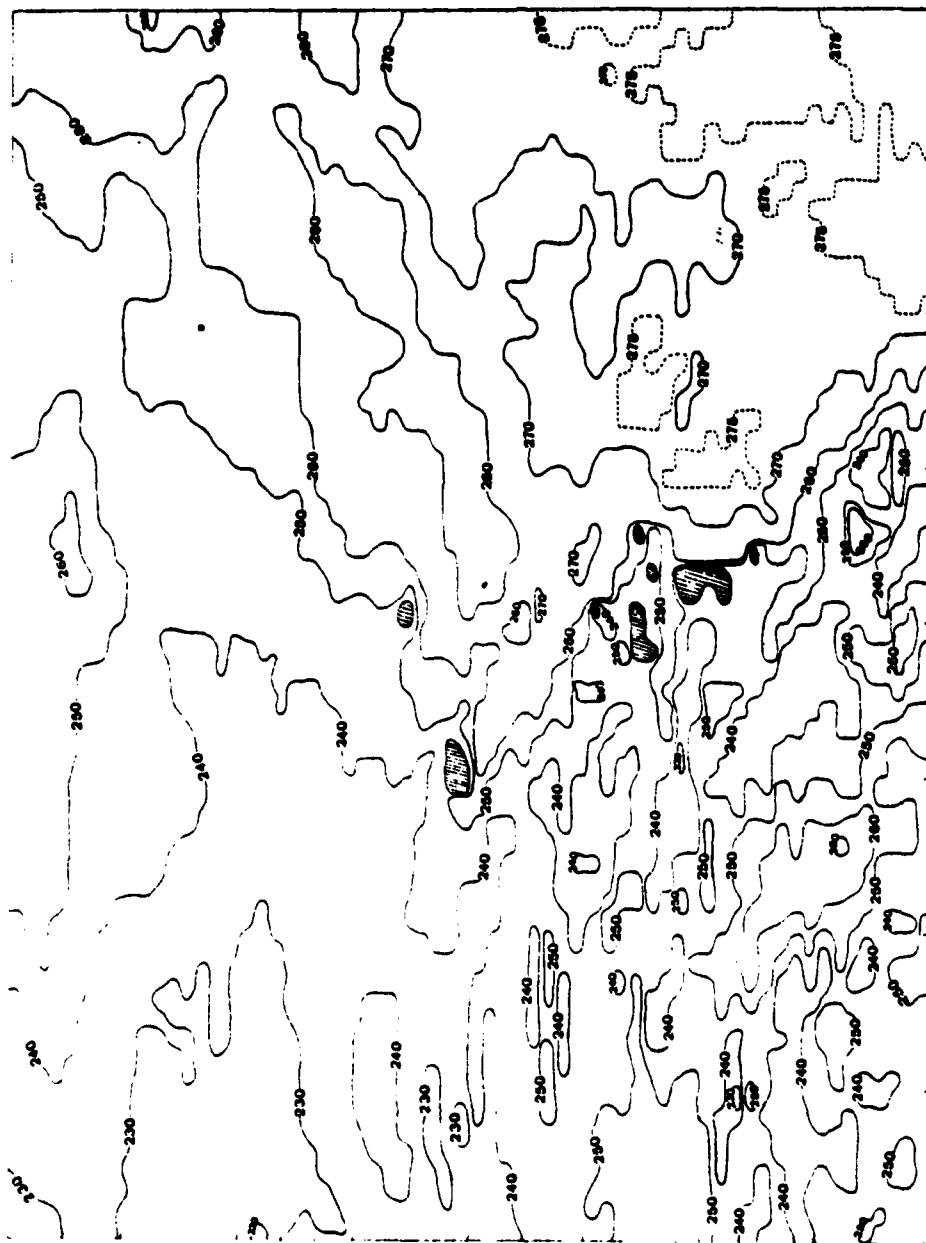


Figure 40. Cloud Top Temperature (K) from Run 1 of the SPADS Cloud Model.

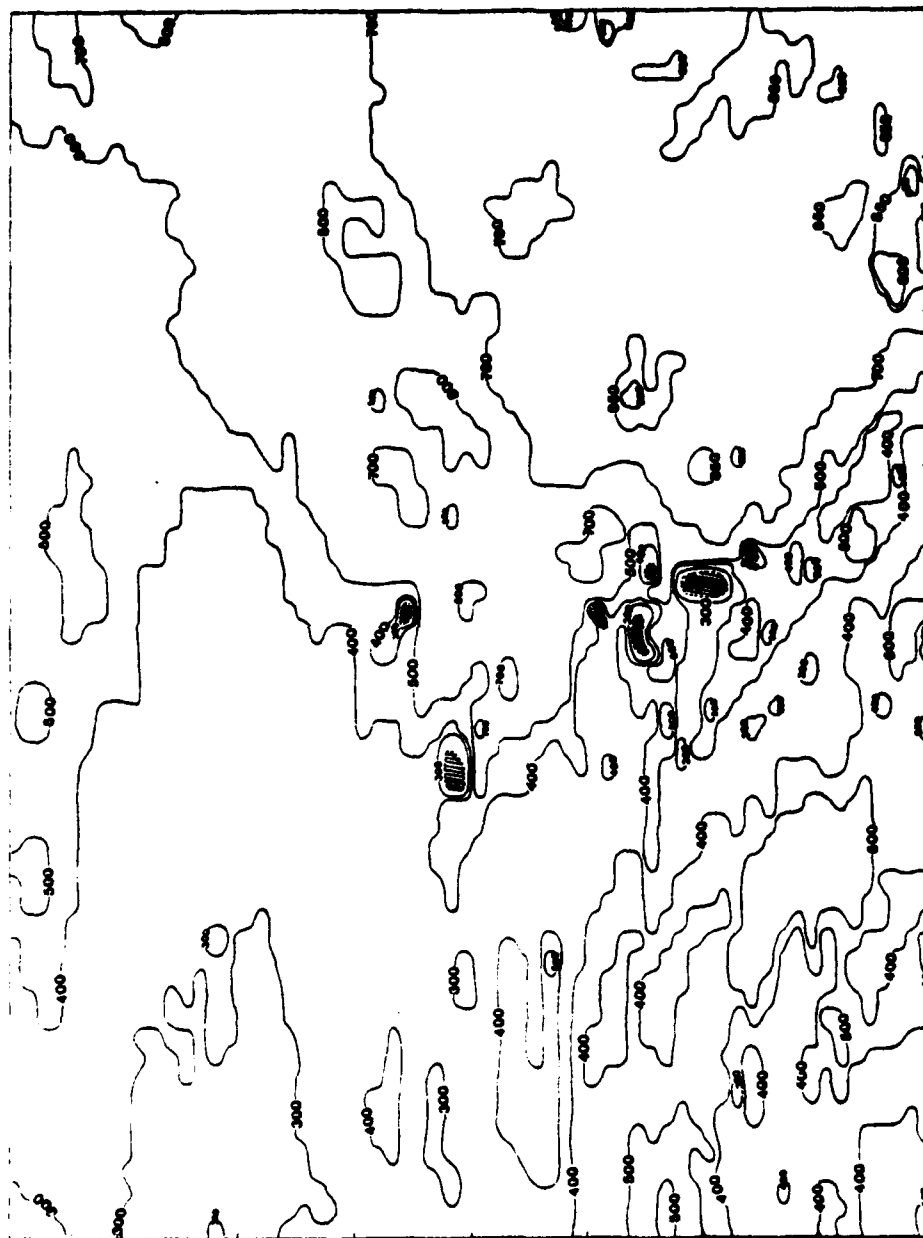


Figure 41. Cloud Top Heights (mb) from Run 1 of the SPADS Cloud Model.

e. Cloud Texture (Standard Deviation)

The cloud texture (standard deviation) calculation results are presented in Fig. 42. Overall, they show an expected pattern; mixed and broken cloud areas (in the SW and SE quadrants) have the highest variation and uniform stratus type cloud cover areas (in the NW and NE quadrants) have the smallest variation (compare Fig. 36 and 42). The highest deviations (approximately 4.0) were located in the SE quadrant in the areas discussed previously under cloud amount. After contouring, there appeared to be a definite boundary between the highly variable region (SE quadrant) and the nearly uniform areas (NE quadrant, see Fig. 42). The SE quadrant had been manually typed as cumulus, with broken areas, and stratus/stratocumulus clouds (see Fig. 37). After evaluation, the standard deviation threshold value for discerning cumulus humulus was adjusted along with the value for altostratus. There did not appear to be obvious patterns of different size cumulus congestus and therefore this standard deviation threshold was not adjusted. The standard deviation definitely shows promise in discriminating between cumuloform and stratus cloud types.

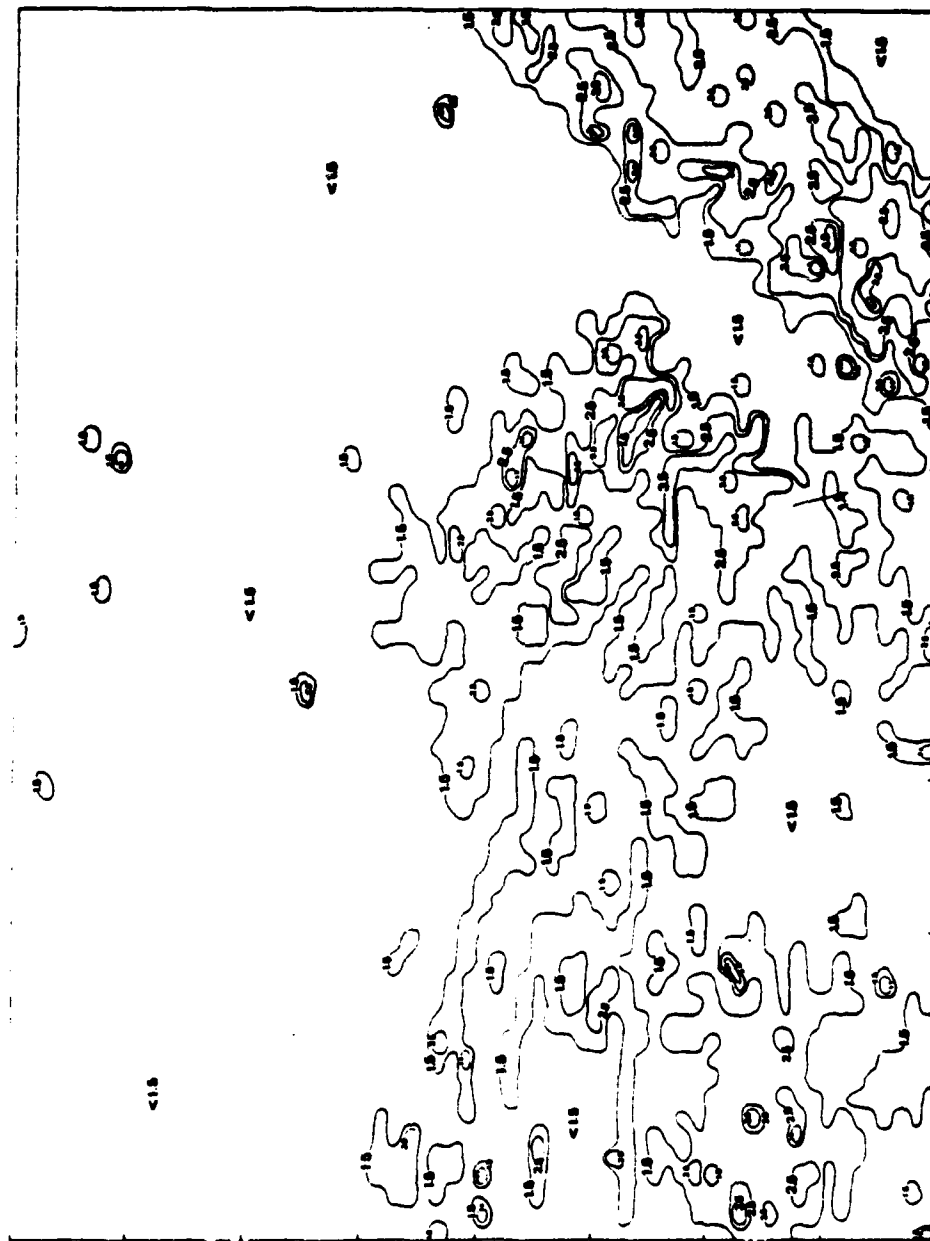


Figure 42. Cloud Texture (Standard Deviation of the Digital Counts) from Run 1 of the SPADS Cloud Model.

2. Run 2

The results from the second run are presented below with the revised cloud and standard deviation thresholds. Only regions where changes from Run 1 occurred are discussed in detail.

a. Cloud Typing

The cloud typing results were changed somewhat because of the new cloud threshold and standard deviation thresholds (see Fig. 43) especially in the lower right quadrant. More cumulus humulus and altostatus types were delineated and the patterns appear closer to those in the manual analysis.

b. Cloud Amount

The cloud amount patterns (see Fig. 44) are more in line with the manual analysis and what can clearly be seen on the satellite images. It appears that the cloud threshold of 20 is better, but this may require additional study.

c. Cloud Top Temperature and Height

The problem in obtaining the correct cloud top temperature and height in a partly cloudy situation using a bispectral technique still remained. This problem stems from uncertainty in calibration of the GOES VISSR. The VISSR

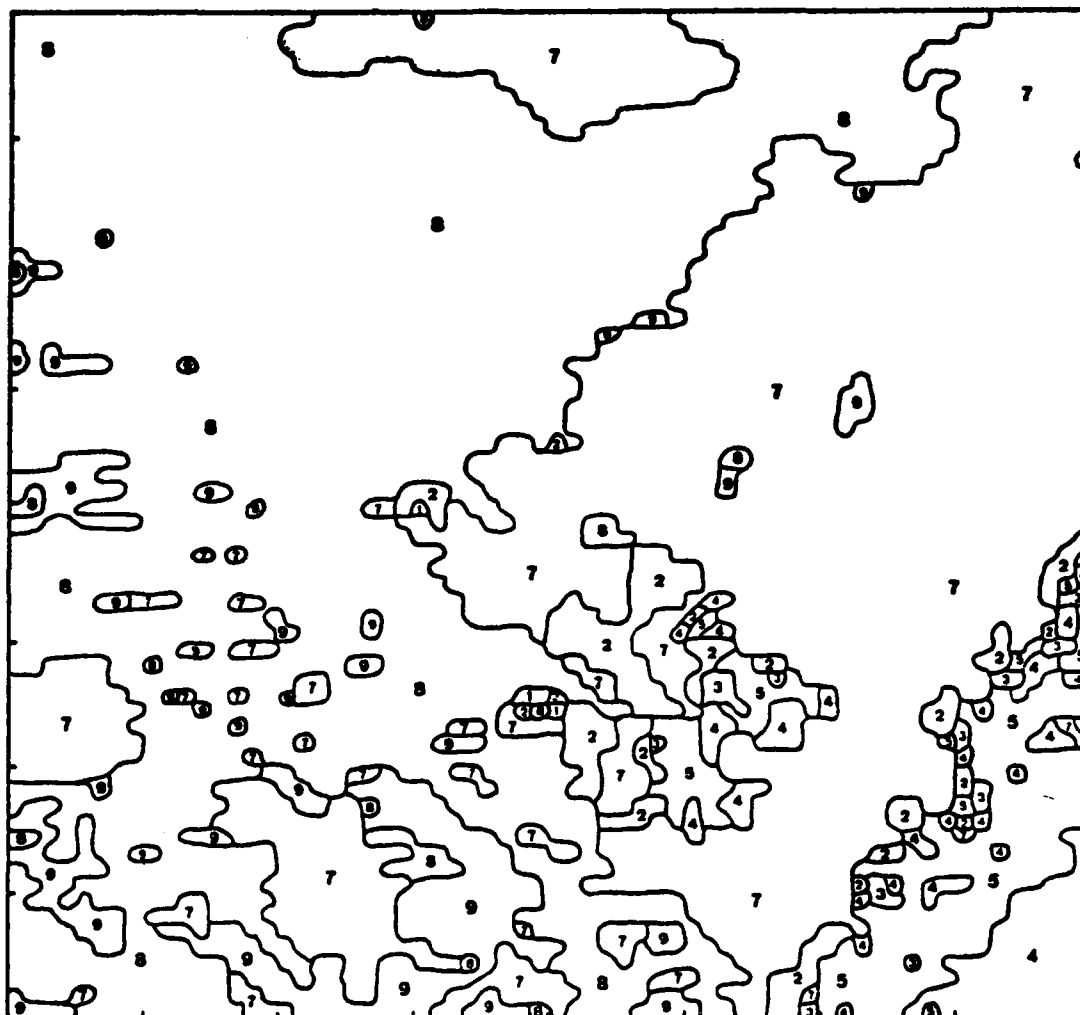


Figure 43. Cloud Types as Analyzed by the SPADS Cloud Model, Run 2 (see Table XII for numeric definitions).

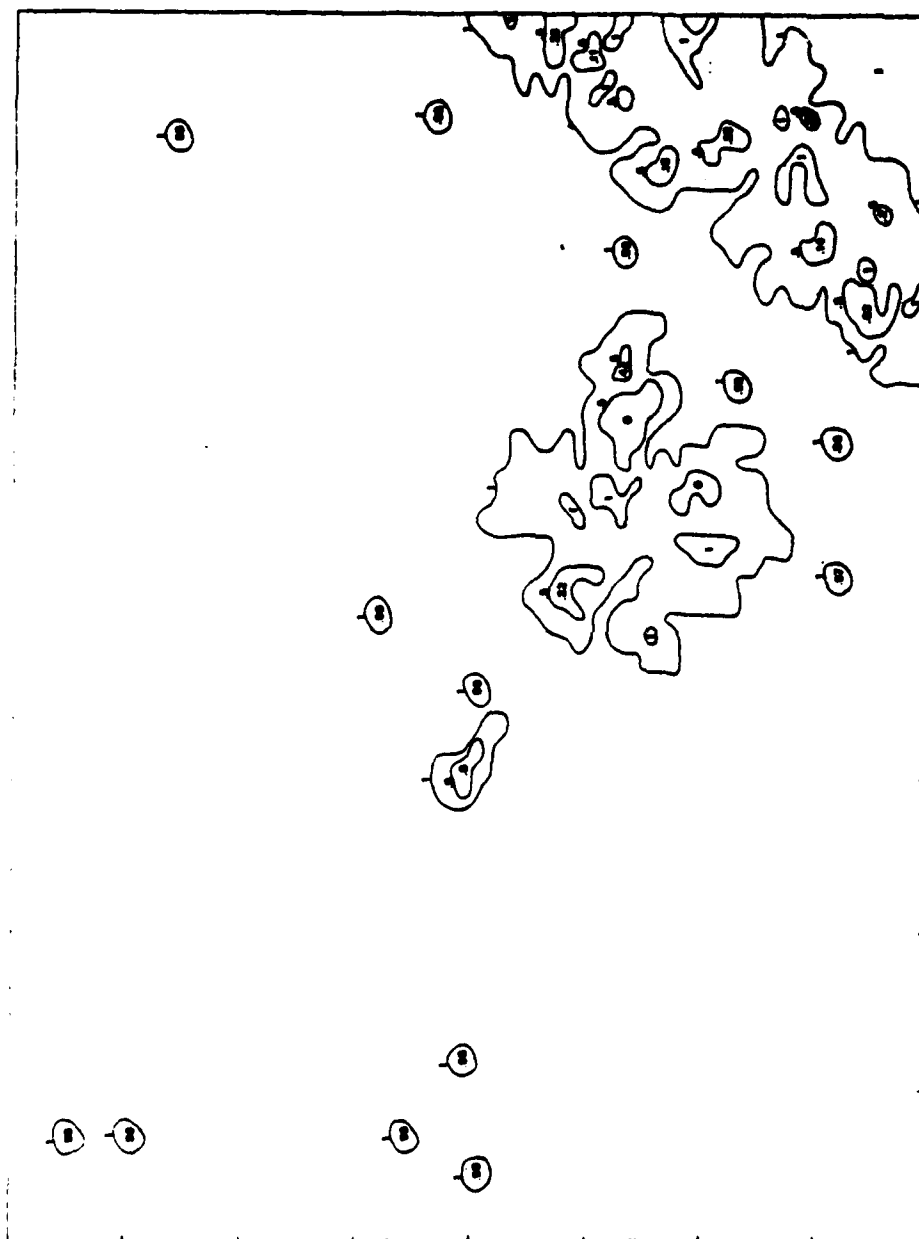


Figure 44. Cloud Amount (in 100ths) from Run 2 of the SPADS Cloud Model (the number in the enclosed areas represents the lowest cloud amount for the area).

infrared channel is not actively calibrated and extensive ground truth is required to accurately interpret its data in terms of temperatures (Maul, 1981). In the present program, temperature calibration would enter into the coefficients of the cloud height Eq. 4 (Table IV) and directly into the cloud top temperatures. Time was not available in this study to make this adjustment.

V. SUMMARY

A. DISCUSSION

This chapter summarizes the thesis accomplishments, the problems encountered, and suggestions for future research.

1. Accomplishments

The first accomplishment was to complete an overview of cloud and precipitation studies with an emphasis given to those using an interactive computer system. Next, useful techniques and ideas were selected from these studies and used to design the SPADS cloud and precipitation model. This SPADS Cloud Model was then coded and established on the SPADS system. Finally, two test runs on a test case were completed with good success.

Within an hour, detailed information was produced by the SPADS Cloud Model through concurrent analysis of high resolution visual and infrared digital satellite data. Over a maritime region, the SPADS Cloud Model estimated various cloud types, precipitation intensity, cloud amounts, and cloud top temperatures and heights.

2. Problems

Several problems were encountered. The cloud amount threshold needed adjustment and two tests of different thresholds were accomplished. The threshold of 20 was satisfactory but further verification is suggested.

Another area of concern is the threshold values for the texture tests. Two thresholds were adjusted in the tests but all three need further refinement. The separation test (the least square fit equations) for cirrus and altostratus could not be substantiated in this data set and will also need verification in future runs.

An additional problem is in the cloud top temperature and height calculations. As discussed before, the temperatures are too cold and the heights too high in certain partly cloudy areas. The bispectral equation to obtain these values needs further study.

All three of these problems are related, at least in part, to the problem of inter-calibration of AVHRR and GOES VISSR visible and infrared data.

3. Recommendations

The following are recommendations and suggestions for additional research. The SPADS Cloud Model should be:

- a. converted to use temperatures for infrared thresholds and albedoes for visual thresholds to allow easier conversion between different satellites (polar and geostationary) and seasons (this will require development and addition of sensor calibration tables and modules to the SPADS Cloud Model).
- b. converted to a variable resolution so that larger areas could be analyzed in the same time frame but also keep the high resolution capability.
- c. tested and verified in various regions by using surface observations, rawinsondes, aircraft platform observations, ship observations, radar, and, if available, the U.S. Air Force 3DNEPH cloud analysis.

Digital satellite data are currently underutilized, except perhaps for sea surface temperature and temperature sounding applications. Most visual and infrared satellite data are treated as images and are still analyzed manually. Now, with the development of SPADS and similar systems, new satellite products can be produced in regional forecast sites based on digital satellite data. This thesis illustrates the detailed analysis of the digital satellite information that can be received by the user in a short (1-2 hours) time frame. Specifically, this work was directed to using the SPADS computer system toward process satellite visual and infrared digital data and to produce cloud and precipitation information. As SPADS is placed in the field

forecast sites, this information will, for the first time, be made available in an operational setting instead of being available only to meteorologists at the major satellite centers. In the future, this and other applications will substantially aid the operational forecaster.

LIST OF REFERENCES

Austin, G.L. and Lovejoy, S., 1981: A combined visible and IR technique for the estimation of rain amounts from GOES data. In, D. Atlas and O.W. Thieme (editors), Precipitation Measurements from Space, Workshop Report, October 1981, NASA, Goddard Space Flight Center, Greenbelt, Md., D141-144.

Barrett, E.C., 1981: The Bristol Method of satellite-improved rainfall monitoring. In, D. Atlas and O.W. Thieme (editors), Precipitation Measurements from Space, Workshop Report, October 1981, Goddard Space Flight Center, Greenbelt, Md., D159-169.

Barrett, E.C. and R. Harris, 1977: Satellite infrared nephelanalysis. Met. Mag., 106, 11-24.

Barrett, E.C. and D. Martin, 1981: The Use of Satellite Data Rainfall Monitoring. Academic Press, London, 340pp.

Fye, F.K., 1978: The AFGWC automated cloud analysis model. AFGWC Technical Memorandum 78-102, H.Q. Air Force Global Weather Central, Offutt AFB, Nebraska, 97pp.

Fye, F.K. and G.L. Logan, 1977: AFGWC satellite-based analysis and prediction programs. Proceedings of the 7th Technical Exchange Conference, El Paso, Texas, 30 Nov.-3 Dec. 1976, 113-121.

Griffith, C.G. and W.L. Woodley, 1981: The estimation of convective precipitation from GOES imagery with the Griffith/Woodley technique. In, D. Atlas and O.W. Thieme (editors), Precipitation Measurements from Space, Workshop Report, October 1981, NASA Goddard Space Flight Center, Greenbelt, Md., D154-158.

Griffith, C.G., W.L. Woodley, P.G. Grube, D.W. Martin, J. Stout and D.N. Sikdun, 1978: Rain estimation from geosynchronous satellite imager-visible and infrared studies. Mon. Wea. Rev., 106, 1153-1171.

Harris, R. and E.C. Barrett, 1975: An improved satellite nephelanalysis. Met. Mag., 104, 9-16.

Harris, R. and E.C. Barrett, 1978: Toward an objective nephelanalysis. J. Appl. Meteorol., 17, 1258-1266.

Liljas, E., 1981a: Analysis of cloud and precipitation through an automated classification of AVHRR data. RMK 32, SMHI (in Swedish), 33pp.

Liljas, E., 1981b: Automated techniques for satellite imager analysis. Proc. IAMAPS Symposium, Hamburg, 25-28 Aug. 1981, 331-339.

Lovejoy, S. and G.L. Austin, 1979: The delineation of rain areas from visible and IR satellite data for GATE and mid-latitudes. Atmos-Ocean, 17, 77-92.

Maul, G.A., 1981: Application of GOES visible-infrared data to quantifying mesoscale ocean surface temperatures. J. Geophys. Res., 86, 8007-8021.

Muench, H.S. and T.J. Keegan, 1979: Development of techniques to specify cloudiness and rainfall rate using GOES imagery data. AFGL-TR-79-0255, AD A084, 757pp.

Platt, C.M.R., 1981: Two dimensional histogram of GMS-1 satellite visible albedo and infrared temperature for selected cloud systems. Division of Atmospheric Physics Tech. Paper no. 40, Commonwealth Scientific and Industrial Research Organization, Australia, 43pp.

Reynolds, D.W. and T.H. Vonder Haar, 1977: A bispectral method for cloud parameter determination. Mon. Wea. Rev., 105, 446-457.

Simpson, J. and V. Wiggert, 1969: Models of precipitating cumulus towers. Mon. Wea. Rev., 97, 471-489.

Stout, J., D.W. Martin and S.N. Sikdar, 1979: Estimating GATE rainfall from geostationary satellite images. Mon. Wea. Rev., 107, 585-598.

Wylie, D.P., 1979: An application of a geostationary satellite rain estimation technique to an extratropical area. J. Appl. Meteorol., 18, 1640-1648.

APPENDIX A

SPADS CLOUD MODEL COMPUTER PROGRAM

```

C      CLOD -- IS DRIVER/MAIN PROGRAM

C      THIS PROGRAM ANALYZES VIS AND IR TOGETHER TO DERIVE TYPES OF
C      CLOUDS, CLOUD HEIGHTS, CLOUD AMOUNT, CLOUD TOP TEMPERATURE,
C      AND RELATIVE INTENSITY OF RAIN.
C      PROGRAMMED BY LT. C. NELSON
C      INITIALIZATION
C
COMMON/A/ML(128),CIRRUS,K,K1,ISEL
COMMON/B/CTYPE(64),PRCIPI(64),MSAVG(64),M
COMMON/C/SIGMA(64),SIG1,SIG2,SIG3
COMMON/D/HEIGHT(64),CTEMP(64),ACDAVG(64),E1,E2,ALAT,ALON,J1,
*TLV(11),E3
COMMON/F/ZP,XCEN,YCEN,FLIP,A1,BASLON,LVL(11)
COMMON/G/STDP(11)
REAL ML,MS2(8,8),MSAVG,SIGMA,E1,E2,E,ACLD,ACDAVG,AMCLD,SUM,SUMSIG,
*HEIGHT,N,CTEMP,SIG1,SIG2,SIG3
INTEGER CTYPE,CIRRUS,PRCIPI,M,O,P,L,PCLD1,PCLD2,O,ISEL,MS(256,3),
*VISFN(7),IRFN(7),MS1(8)

C
      I1=1
      ISEL=0
      M=0
      N=0.0
      E1=0.9
      E2=0.55
      E3=0.0
      SUM=0.0
      SUMSIG=0.0
      AMCLD=0.0
      CIRRUS=0
      ACLD=0.0
      P=64
      SIG1=2.5
      SIG2=20.0
      SIG3=1.5
      PCLD1=20.0
      O=512

```

C
C
C

MENU

```
TYPE "<15>"
TYPE "THIS PROGRAM IDENTIFIES CLOUD TYPES"
TYPE "ADDITIONAL CLOUD DATA CAN ALSO BE OBTAINED"
TYPE "THESE ARE - "
TYPE "0 NO ADDITIONAL INFORMATION"
TYPE "1 PRECIPITATION INTENSITY"
TYPE "2 CLOUD TOP TEMPERATURE"
TYPE "3 CLOUD TOP HEIGHT"
TYPE "4 ALL OF THE ABOVE"
TYPE "8 EXIT PROGRAM"
ACCEPT "ENTER REQUEST= ",ISEL
IF(ISEL.EQ.8)GO TO 80
IF(ISEL.EQ.0.OR.ISEL.EQ.1)GO TO 181
CALL OPEN(4,"TLVN.0",1,IER)
IF(IER.EQ.1)GO TO 170
TYPE "TLV FILE OPEN ERROR, RC= ",IER
170 CALL RDBLK(4,1,MS,1,IER)
IF(IER.EQ.1)GO TO 180
TYPE "TLV FILE READ ERROR, RC= ",IER
GO TO 70
180 DO 1 I=1,11
    TLV(I)=FLOAT(MS(I))/100.0
    1 CONTINUE
    WRITE(12,826)(TLV(L),L=1,11)
826 FORMAT(2Y,11F6.2)
    2 FORMAT(S13)
181 TYPE "<15>"
    ACCEPT "ENTER IR FILENAME"
    READ(11,2)IRFN(1)
    CALL OPEN(2,IRFN,1,IER)
    IF(IER.EQ.1)GO TO 190
    TYPE "IR FILE - OPEN ERROR, RC= ",IER
    ACCEPT "TRY AGAIN?",IX
    IF(IX.EQ.1)GO TO 181
    IF(IX.EQ.0)GO TO 70
190 ACCEPT "ENTER VIS FILENAME"
    READ(11,2)VISFN(1)
```

```

CALL OPEN(1,VISFN,1,IER)
IF(IER.EQ.1)GO TO 200
TYPE "VIS FILE - OPEN ERROR, RC= ",IER
ACCEPT "TRY AGAIN?",IX
IF(IX.EQ.1)GO TO 190
GO TO 69

C
C OPEN FILES FOR STORAGE OF CALCULATED VALUES
C
200 CALL OPEN(5,"CALC1D.0",3,IER)
IF(IER.EQ.1)GO TO 201
TYPE "DATA 1 FILE OPEN ERROR, RC= ",IER
GO TO 69
201 CALL OPEN(7,"CALC2D.0",3,IER)
IF(IER.EQ.1)GO TO 202
TYPE "DATA 2 FILE OPEN ERROR, RC= ",IER
GO TO 69

C
C DO LOOP TO CALL IN SERIES OF DATA
C BLOCKS RUN FROM 0 TO 511
C LOOP STARTS AT 192,192 FOR IR TO MATCH VIS (COLLOCATED CENTER
C POINT). IR IS 2 MILE THEREFORE NEED TO USE EVERY OTHER VALUE
C
202 I3=0
I2=0
DO 32 I1=1,128,2
I3=(I1-1)+191
I2=1+I2
DO 6 I=1,P
HEIGHT(I)=0.0
PRCIPI(I)=0.0
ACDAVG(I)=0.0
SIGMA(I)=0.0
CTYPE(I)=0
CTEMP(I)=0.0
6 CONTINUE

C
C DRIVER MODULE WHICH WILL PREPARE VISUAL DATA TO BE USED IN OTHER
C MODULES. THE AVERAGE VISUAL BRIGHTNESS, THE STANDARD DEVIATION OF
C VISUAL BRIGHTNESS, AND THE CLOUD AMOUNT IN 8X8 GRID SETS WILL BE

```

```

C      DETERMINED.
C      IR DIGITAL VALUE FILE
C
      CALL RDBLK(2,I3,MS(1,1),1,IER)
      IF(IER.EQ.1)GO TO 203
      TYPE "IR FILE - READ ERROR, RC= ",IER
      GO TO 69
203 CALL UPK(MS(96,1),MS(1,2),128)
      DO 100 I=1,128
      ML(I)=FLOAT(MS(I,2))
100 CONTINUE
      K1=0
      J1=(I2-1)*3
      CALL RDBLK(1,J1,MS,3,IER)
      IF(IER.EQ.1)GO TO 204
      TYPE "VISUAL FILE READ ERROR, RC= ",IER
      GO TO 69
204 CONTINUE
      DO 30 K2=1,128,2
      K1=K1+1
      K=K2+1
C
C      THIS LOOP PROCESSES VISUAL DATA BY 8X8 GRID
C
      DO 8 I=1,3
      MS1(I)=0.0
      DO 7 J2=1,3
      MS2(I,J2)=0.0
7 CONTINUE
3 CONTINUE
      L1=(K1-1)*4+1
      DO 11 Q=1,3
      CALL UPK(MS(L1,Q),MS1,3)
      DO 10 L=1,3
      MS2(L,Q)=FLOAT(MS1(L))
10 CONTINUE
11 CONTINUE
      N1=8
      DO 13 L=1,3
      DO 12 Q=1,N1

```

```

N=N+1.0
SUM=SUM+MS2(L,Q)
SUMSIG=SUMSIG+(MS2(L,Q))**2.0
IF(MS2(L,Q).GE.PCLD1)ACLD=1.0
IF(MS2(L,Q).LT.PCLD1)ACLD=0.0
AMCLD=ACLD+AMCLD
12 CONTINUE
13 CONTINUE
SIGMA(K1)=SQRT((N*SUMSIG-SUM**2.0)/(N*(N-1.0)))
MSAVG(K1)=SUM/N
CALL CLOUD
ACDAVG(K1)=AMCLD/N
IF(CTYPE(K1).EQ.8.OR.CTYPE(K1).EQ.9)E3=1.0
IF(ISEL.EQ.0.OR.ISEL.EQ.1)GO TO 18
CALL TEMPT
IF(ISEL.EQ.8)GO TO 69
13 CIRRUS=0
N=0.0
ACLD=0.0
AMCLD=0.0
SUM=0.0
SUMSIG=0.0
E3=0.0
30 CONTINUE
C
C STORE ALL VALUES
C VALUES ARE STORED IN CALC1 FILE -- CTYPE,PRCIPI,CTEMP,
C HEIGHT(1-256 WD)
C VALUES IN CALC2 -- MSAVG,SIGMA,ACDAVG,0(1-256 WD)
C
DO 23 I=1,64
MS(I,1)=CTYPE(I)
J=I+64
MS(J,1)=PRCIPI(I)
K5=J+64
MS(K5,1)=IFIX(CTEMP(I)+.5)
K4=K5+64
MS(K4,1)=IFIX(HEIGHT(I)+.5)
MS(I,2)=IFIX(MSAVG(I)+.5)
MS(J,2)=IFIX(100.0*SIGMA(I)+.5)

```

```

      MS(K5,2)=IFIX(100.0*ACDAVG(I)+.5)
      MS(K4,2)=0
23  CONTINUE
      K7=I2-1
      CALL WRBLK(5,K7,MS(1,1),1,IER)
      IF(IER.EQ.1)GO TO 22
      TYPE "WRITE ERROR 5 RE= ",IER
      GO TO 69
22  CALL WRBLK(7,K7,MS(1,2),1,IER)
      IF(IER.EQ.1)GO TO 26
      TYPE "WRITE ERROR 7 RC= ",IER
      GO TO 69
26  WRITE(12,27)(HEIGHT(I),I=1,64)
      WRITE(12,24)(SIGMA(I),I=1,64)
      WRITE(12,27)(CTEMP(I),I=1,64)
      WRITE(12,24)(MSAVG(I),I=1,64)
      WRITE(12,24)(ACDAVG(I),I=1,64)
      WRITE(12,25)(CTYPE(I),I=1,64)
      WRITE(12,25)(PRCIPI(I),I=1,64)
      WRITE(12,27)(ML(I),I=2,128,2)
24  FORMAT(/,4(/,16(1X,F7.4)))
25  FORMAT(/,64I2)
27  FORMAT(/,4(/,16(1X,F7.2)))
      ACCEPT "CONTINUE?",ISTP
      IF(ISTP.EQ.1)GO TO 69
32  CONTINUE
69  CALL CLOSE(1,IER)
70  CALL CLOSE(2,IER)
      CALL CLOSE(4,IER)
      CALL CLOSE(5,IER)
      CALL CLOSE(7,IER)
30  STOP
      END

```

SUBROUTINE CLOUD

```
C
C   CLOUD TYPING MODULE, ALSO THE PRECIPITATION MODULE IS CALLED
C   FROM HERE WHEN PRECIPITATION CLOUDS ARE IDENTIFIED.
C
COMMON/A/ML(128),CIRRUS,K,K1,ISEL
COMMON/B/CTYPE(64),PRCIPI(64),MSAVG(64),M
REAL ML,MSAVG,HEIGHT,CTEMP,SIG,SIG1,SIG2,SIG3
INTEGER I,CTYPE,PRCIPI,CIRRUS,ISEL
C
C   THESE ARE LILJAS CONVERTED GOES THRESHOLDS
C
H2= 84.0
H3=100.0
H4=118.0
H5=159.0
H6=255.0
C
C   THE FOLLOWING IF STATEMENTS CHECK BOTH IR (ML) AND VIS (MSAVG)
C   VALUES AGAINST THRESHOLDS TO DETERMINE CLOUD TYPE. THE
C   STANDARD DEVIATION (SIG) OF THE 8X8 VISUAL GRID IS USED.
C
C   TYPE 1 AND 2 --- CIRRUS/ALTOSTRATUS
IF(ML(K).GT.H4.AND.ML(K).LE.H6.AND.MSAVG(K1).GT.5.0.AND.
*MSAVG(K1).LE.23.0)GO TO 700
C   TYPE 3 --- FOG/STRATUS/CUMULUS HUMULUS
IF(ML(K).GT.H2.AND.ML(K).LE.H4.AND.MSAVG(K1).GT.13.0.AND.
*MSAVG(K1).LE.20.0)GO TO 900
C   TYPE 4 AND 5 --- THICK FOG/STRATOCUMULUS/CUMULUS HUMULUS
IF(ML(K).GT.H3.AND.ML(K).LE.H4.AND.MSAVG(K1).GT.20.0.AND.
*MSAVG(K1).LE.36.0)GO TO 600
GO TO 601
600 M=1
GO TO 800
C   TYPE 6 AND 7 --- SMALL/LARGE CUMULUS CONGESTUS
601 IF(ML(K).GT.H4.AND.ML(K).LE.H5.AND.MSAVG(K1).GT.23.0.AND.
*MSAVG(K1).LE.39.0)GO TO 605
GO TO 606
605 M=2
GO TO 800
```

```

C      TYPE 8 ---- NIMBOSTRATUS (MULTI-LAYERED)
606 IF(ML(K).GT.H5.AND.ML(K).LE.H6.AND.MSAVG(K1).GT.23.0.AND.
      *MSAVG(K1).LE.31.0)GO TO 910
C      TYPE 9 ---- CUMULONIMBUS
      IF(ML(K).GT.H5.AND.ML(K).LE.H6.AND.MSAVG(K1).GT.31.0)
      *GO TO 915
      CTYPE(K1)=0
      GO TO 38
C      CALL STDDEV MODULE TO FURTHER DISCRIMINATE CLOUD TYPES
700 M=3
800 CALL STDDEV
      GO TO 38
C      LABEL TYPES
900 M=4
      GO TO 800
      38 PRICI(K1)=0
      GO TO 40
910 CTYPE(K1)=8
      GO TO 920
915 CTYPE(K1)=9
C      BOTH 8 AND 9 TYPES ARE CONSIDERED RAIN CLOUDS, SO CALL
C      PRECIP MODULE.
920 IF(ISEL.EQ.0.OR.ISEL.EQ.2.OR.ISEL.EQ.3)GO TO 40
      CALL PRECIP
40 RETURN
END

```

SUBROUTINE STDDEV

```

C
C STANDARD DEVIATION TEST MODULE HELPS DISCRIMINATE FURTHER THE
C TYPE OF CLOUDS. ALSO IT SETS CIRRUS FLAG FOR USE IN THE TEMHT
C MODULE.
C
COMMON/A/ML(128),CIRRUS,K,K1,ISEL
COMMON/B/CTYPE(64),PRCIPI(64),MSAVG(64),M
COMMON/C/SIGMA(64),SIG1,SIG2,SIG3
REAL ML,MSAVG,HEIGHT,CTEMP,SIG,Y,SIG1,SIG2,SIG3
INTEGER CTYPE,PRCIPI,CIRRUS,I,M
C
IF(M.EQ.4)GO TO 818
IF(M.EQ.1)GO TO 810
IF(M.EQ.2)GO TO 813
C CIRRUS VS ALTOSTRATUS, FIRST TEST
C THIS EQUATION IS FOR LILJAS CONVERTED GOES THRESHOLDS

$$Y=158.094-6.6076*MSAVG(K1)+4.159*MSAVG(K1)**2.0$$

IF(Y.LE.ML(K))GO TO 814
C SECOND TEST FOR CI/AS
C THIS EQUATION IS FOR LILJAS CONVERTED GOES THRESHOLDS

$$Y=115.24+0.5246*MSAVG(K1)+0.0395*MSAVG(K1)**2.0$$

IF(Y.GE.ML(K))GO TO 816
C THIRD TEST FOR CI/AS
IF(SIGMA(K1).GT.SIG3)GO TO 814
GO TO 816
810 IF(SIGMA(K1).LT.SIG1)GO TO 811
C TYPE 5 — CUMULUS HUMULUS
CTYPE(K1)=5
GO TO 820
C TYPE 4 — THICK FOG/STRATOCUMULUS
811 CTYPE(K1)=4
GO TO 820
813 IF(SIGMA(K1).LT.SIG2)GO TO 817
CTYPE(K1)=6
C TYPE 6 — SMALL CUMULUS CONGESTUS
GO TO 820
C TYPE 1 — CIRRUS
814 CTYPE(K1)=1
CIRRUS=1

```

```

      GO TO 820
C     TYPE 2 — ALTOSTRATUS
816  CTYPE(K1)=2
      GO TO 820
C     TYPE 7 — CUMULUS CONGESTUS - LARGE
817  CTYPE(K1)=7
      GO TO 820
818  IF(SIGMA(K1).LT.SIG1)GO TO 819
C     TYPE 5 — CUMULUS HUMULUS
      CTYPE(K1)=5
      GO TO 820
C     TYPE 3 — FOG/STRATUS
819  CTYPE(K1)=3
820  RETURN
      END

```

SUBROUTINE PRECIP

C
C THIS MODULE IDENTIFIES PRECIPITATION INTENSITY AREAS
C 1=LIGHT, 2=MODERATE, 3=HEAVY, AND 0=NO RAIN.
C
COMMON/A/ML(128),CIRRUS,K,K1,ISEL
COMMON/B/CTYPE(64),PRCIPI(64),MSAVG(64),M
REAL ML,HEIGHT,CTEMP,MSAVG
INTEGER K,CIRRUS,PRCIPI,CTYPE,SUM1
C
C THESE ARE LILJAS CONVERTED GOES THRESHOLDS
C
I1=184
I2=195
I3=224
C
C ADD IR (ML) AND AVERAGE VISUAL (MSAVG), THIS SUM WILL BE TESTED
C FOR INTENSITY OF RAIN.

SUM1=ML(K)+MSAVG(K1)
IF(SUM1.GE.I1.AND.SUM1.LE.I2)GO TO 43
IF(SUM1.GT.I2.AND.SUM1.LE.I3)GO TO 44
IF(SUM1.GT.I3)GO TO 45
PRCIPI(K1)=0
GO TO 49
43 PRCIPI(K1)=1
GO TO 49
44 PRCIPI(K1)=2
GO TO 49
45 PRCIPI(K1)=3
49 RETURN
END

```

SUBROUTINE TEMHT
C
C THIS SUBROUTINE CALCULATES THE CLOUD TOP TEMPERATURE (CTEMP)
C USING THE IR RADIANCE FOR THE SURFACE (NCLR), THE AMOUNT OF CLOUD
C (ACDAVG), EMISSIVITY (E), AND THE MEASURED IR RADIANCE FROM THE
C SATELLITE (ML). CTEMP IS THEN CORRELATED TO AN AREA
C REPRESENTATIVE UPPER AIR SOUNDING (UALV) TO DETERMINE THE CLOUD
C TOP HEIGHT (HEIGHT).
C
COMMON/A/ML(128),CIRRUS,K,K1,ISEL
COMMON/D/HEIGHT(64),CTEMP(64),ACDAVG(64),E1,E2,ALAT,ALON,J1,
*TLV(11),E3
COMMON/G/STDP(11)
REAL ML,HEIGHT,CTEMP,E1,E2,NCLR,NCLD,ACDAVG,E,SIG1,SIG2,SIG3,
*TLV,STDP
INTEGER I,CTYPE,PRCIPI,CIRRUS
DATA STDP/1010.0,1000.0,850.0,700.0,500.0,400.0,300.0,250.0,200.0,
*150.0,100.0/
E=0.0
C CHECK TO SEE IF THERE ARE ANY CLOUDS, IF NOT SKIP TO END
IF(ACDAVG(K1).LT.0.1)GO TO 61
C CONVERT SURFACE TEMPERATURE (TSFC) TO NCLR
IF(TLV(1).GE.242.0)NCLR=2.0*(331.0-TLV(1))
IF(TLV(1).LT.242.0)NCLR=420.0-TLV(1)
C IS CIRRUS FLAG SET? IF YES, USE E2 FOR E. IF NOT, USE E1 FOR E.
IF(CIRRUS.EQ.1)GO TO 850
C IS THE CB OR NS CLOUD FLAG SET? IF YES USE E3 FOR E1.
IF(E3.EQ.1.0)GO TO 849
E=E1
GO TO 851
849 E=E3
GO TO 851
850 E=E2
C COMPUTE CLOUD RADIANCE
851 NCLD=ML(K)-NCLR/(E*ACDAVG(K1))+NCLR
C CONVERT TO CTEMP
IF(NCLD.LE.178.0)CTEMP(K1)=331.0-NCLD*0.5
IF(NCLD.GT.178.0)CTEMP(K1)=420.0-NCLD
WRITE(12,353)NCLR,NCLD
353 FORMAT(/1X,5(1H*,E15.3),"NCLR,NCLD")

```

```

IF(ISEL.EQ.2)GO TO 60
C
C INTERPOLATE UPPER AIR SOUNDING TO CONTINUOUS CURVE OF TEMP
C VERSUS HEIGHT, THEN COMPARE TO CTEMP TILL GET MATCH. CHECK
C FROM TOP DOWN. THEN USE MATCH TO SELECT CORRECT HEIGHT FOR
C CLOUD TOP.
C
DO 812 IB=2,11
IA=13-IB
IF(IA.EQ.11.AND.TLV(11).GT.CTEMP(K1))GO TO 816
IF(TLV(IA).LT.CTEMP(K1))GO TO 813
IF(TLV(IA).EQ.CTEMP(K1))GO TO 814
812 CONTINUE
813 IF(IA.EQ.2)IA=3
RHG=EXP(ALOG(STDP(IA+1))-(ALOG(STDP(IA+1))-ALOG(STDP(IA)))*
*(TLV(IA+1)-CTEMP(K1))/(TLV(IA+1)-TLV(IA)))
GO TO 815
816 TYPE "TEMPERATURE IS ABOVE 100 MB"
ACCEPT "CONTINUE?",ICONT
IF(ICONT.EQ.0)ISEL=8
814 RHG=STDP(IA)
815 HEIGHT(K1)=RHG+0.5
60 RETURN
61 CTEMP(K1)=TLV(1)
HEIGHT(K1)=STDP(1)
RETURN
END

```

INITIAL DISTRIBUTION LIST

	No. Copies
1. Defense Technical Information Center Cameron Station Alexandria, VA 22314	2
2. Library, Code 0142 Naval Postgraduate School Monterey, CA 93940	2
3. Professor Robert J. Renard, Code 63R1 Department of Meteorology Naval Postgraduate School Monterey, CA 93940	1
4. Professor Christopher N. K. Mooers, Code 68 Department of Oceanography Naval Postgraduate School Monterey, CA 93940	1
5. Assistant Professor Carlyle H. Wash, Code 63Wy Department of Meteorology Naval Postgraduate School Monterey, CA 93940	9
6. Assistant Professor James L. Mueller, Code 68My Department of Oceanography Naval Postgraduate School Monterey, CA 93940	1
7. Lt. Cynthia Ann Nelson Department of Oceanography U.S. Naval Academy Annapolis, MD 21402	1
8. Director Naval Oceanography Division Naval Observatory 34th and Massachusetts Avenue NW Washington, D.C. 20390	1
9. Commander Naval Oceanography Command NSTL Station Bay St. Louis, MS 39522	1
10. Commanding Officer Naval Oceanographic Office NSTL Station Bay St. Louis, MS 39522	1

11. Commanding Officer
Fleet Numerical Oceanography Center
Monterey, CA 93940 1
12. Commanding Officer
Naval Ocean Research and Development
Activity
NSTL Station
Bay St. Louis, MS 39522 1
13. Commanding Officer
Naval Environmental Prediction Research
Facility
Monterey, CA 93940 1
14. CDR Don Hinsman
Naval Environmental Prediction Research
Facility
Monterey, CA 93940 1
15. Chairman, Oceanography Department
U.S. Naval Academy
Annapolis, MD 21402 1
16. Chief of Naval Research
800 N. Quincy Street
Arlington, VA 22217 1
17. Chief of Naval Research (Code 480)
Naval Ocean Research and Development
Activity
NSTL Station
Bay St. Louis, MS 39522 1
18. Commander
Oceanographic Systems Pacific
Box 1390
Pearl Harbor, HI 96860 1
19. Commanding Officer
Naval Eastern Oceanography Center
Naval Air Station
Norfolk, VA 23511 1
20. Mr. Larry Breaker, Code 68
Department of Oceanography
Naval Postgraduate School
Monterey, CA 93940 1

FILMED

5-83

DTIC